2010

Interface Characterization of Metal-Thermoplastic Composites

Carol Ochoa Putman
University of Alabama at Birmingham

INTERFACE CHARACTERIZATION OF METAL-THERMOPLASTIC COMPOSITES

by

CAROL OCHOA PUTMAN

UDAY K. VAIDYA, COMMITTEE CHAIR
DERRICK DEAN
SELVUM PILLAY
NASIM UDDIN
GARRY W. WARREN

A DISSERTATION

Submitted to the graduate faculty of The University of Alabama at Birmingham,
in partial fulfillment of the requirements for the degree of
Doctor of Philosophy

BIRMINGHAM, ALABAMA

2010

INTERFACE CHARACTERIZATION OF
METAL-THERMOPLASTIC COMPOSITES

CAROL OCHOA PUTMAN

MATERIALS SCIENCE AND ENGINEERING

ABSTRACT

Hybrid materials featuring thermoplastic polymer composites in conjunction with metals can be used as structural materials in military and commercial transport vehicles and for protection of buildings and infrastructure. Constituent thermoplastics and metals have distinct advantages as protective materials; however, metals on their own are heavy; hence, hybrid materials offer an option as lighter materials. Since the optimal performance of a composite strongly depends on the behavior of the interface, the present study focuses on understanding the mechanisms of mechanical and chemical bonding as well as the effect of thermal stresses at the interface of metal-thermoplastic composites. The mechanical interactions between a thermoplastic polymer and steel cord have been studied with a goal to improve interfacial shear strength and cohesive strength. Steel cord was combined with thermoplastics to evaluate the parameters that affect mechanical bonding via pull-out tests and friction coefficient tests. The test parameters have been correlated to interfacial shear strength using an experimental and modeling approach.

This work also establishes the basis that polar groups and free radicals improve adhesion between thermoplastics and metallic surfaces. Chemical adhesion between the steel cord and thermoplastic polymer was investigated. Plasma-activated chemical vapor deposition is used to impart silicon, carbon and hydrogen radicals to the metal surface.

Thermoplastic polymers with chemical modification were used to investigate the effect of polar groups (-NH, -CO= and -OH) and its influence on the surface energy and adhesion properties.

The influence of thermal stresses at the interface is investigated by finite element model (FEM). The analysis takes into consideration the difference in coefficients of thermal expansion between the fiber and the matrix in a steel cord thermoplastic composite and its effect during the cool down from processing temperature to room temperature. As temperature changes during cooling down, thermal stresses are induced at the matrix-fiber interface. The study investigated the correlation of interfacial strength to the residual thermal stresses. The overall study provides a basis to determine the limiting bond strength that establishes continuity of the interface between the two phases, i.e. the steel cord and thermoplastic polymer composites.

DEDICATION

This work is dedicated to Jacob, my wonderful husband, and our little baby Daniel. They bring me unbelievable happiness and give me courage and energy to live everyday beyond expectations.

ACKNOWLEDGEMENTS

This work would have not been possible without the support of people, research laboratories and institutions.

First, I would like to thank my advisor, Dr. Uday K. Vaidya, for his guidance, wisdom, encouraging words and confidence in me that allow me to finish this work. I would also like to thank the remaining members of my committee for their valuable time, support and contributions to this research. I also want to thank Dr. Derrick Dean, Dr. Alan Eberhardt, Dr. Robin Foley from the University of Alabama at Birmingham and Dr Emmanuel Waddell from the University of Alabama in Huntsville for allowing me to work in their labs and receive the support of their students. In addition, I want to express my gratitude to my past and current colleagues and friends in the composites research group, who were always willing to help and discuss solutions. Also I want to thank Jennifer Greer, my English teacher for her kindness, patience and advice to make me a better writer.

I would like to gratefully acknowledge the received support from the Department of Energy (DOE) Graduate Automotive Technology Education (GATE) program and National Science Foundation NSF-EPSCor.

Special thanks to my parents and family for their love, encouragement and understanding. Above all, I want to thank God for being my rock.

TABLE OF CONTENTS

LIST OF TABLES

NUMERICAL ANALYSIS OF THERMAL STRESSES IN A METAL-THERMOPLASTIC COMPOSITE

LIST OF FIGURES

Figure *Page*

INTERFACIAL SHEAR STRENGTH IN A METAL-THERMOPLASTIC COMPOSITE

MECHANISMS OF INTERFACIAL ADHESION IN METAL-THERMOPLASTIC POLYMER COMPOISTES_EFFECT OF CHEMICAL TREATMENT

NUMERICAL ANALYSIS OF THERMAL STRESSES IN A METAL-

THERMOPLASTIC COMPOSITE

INTRODUCTION

Polymer composite materials have been studied extensively in an effort to implement their potential advantages of light weight, high fracture toughness, high temperature resistance, repairability and ease of manufacture [1]. In general, polymer composites consist of two phases - high strength/stiffness reinforcing fibers embedded in a thermoplastic or thermoset polymer matrix [2]. The composite structure of both materials results in enhancement of properties not achievable with the constituents alone. Compared to thermosets, composites fabricated from thermoplastic materials typically provide longer shelf life, higher strain-to-failure, faster consolidation and retain the ability to be repaired, reshaped and re-used. Therefore, thermoplastic composites are increasingly gaining importance as substitute materials for metals in applications within the aerospace, automotive, marine, sporting goods and electronic industries.

A specific type of polymer composite material is called steel reinforced polymer (SRP). This composite involves the use of steel cords as reinforcement element. The first well-known application of SRPs was in steel-belted tires, in which the steel cords increase the tire's performance in terms of mechanical and fatigue properties, and triple its wear in miles over older bias-ply tires [3]. Other applications have used unidirectional steel cords embedded within a thermoset matrix for strengthening civil structures and bonding to concrete structures to improve flexural capacity in concrete beams [4-9]. SRPs are being analyzed for blast resistant applications. The inherent ductility of the reinforcement, the endurance properties and light weight characteristics make SRPs attractive for this application. [10-11]

However, as in many polymer composite systems, SRPs frequently suffer from a lack of adequate fiber-matrix adhesion. The problem can be addressed by appropriate design of the fiber-matrix interface as well as optimization of composite fabrication procedures. Since the optimum performance of a composite strongly depends on the behavior at the interface, the present work deals with study of the interface between a thermoplastic material and dissimilar materials such as steel fibers. First, the control of the degree of bonding between the thermoplastic polymer matrix and steel reinforcement is undertaken. Then, the understanding of the different levels of bond strength and the response of the interface under specific loading scenarios are analyzed in this work.

According to Cerny [12], there are two principal bonding types in fiber thermoplastic composites, namely mechanical and chemical. The mechanical bond can be explained by the mechanism of friction and engagement of the polymer to the metallic surface. The chemical bond relates to intermolecular forces that cause chemical linkage(s) between components at the interface. In general, polyolefins including PP have poor adhesion to the substrate due to non-polar properties and saturated chains that make the sharing of electrons difficult. Consequently, the chemical bonding between metal and polymer such as PP and steel is complex to reach. Hence, imparting polarity to the polymer surface could provide an avenue to achieve enhanced adhesive bonding due to molecular interactions [13, 14].

OBJECTIVES

The primary objective of this study is to understand, characterize and tailor the load transfer in the interface between steel reinforcement and thermoplastic polymers.

The specific objectives of the research are to:

1. Determine mechanical bond between thermoplastic polymer and steel reinforcement and parameterize the effect of physical properties of the fiber and matrix.
2. Investigate the chemical bond between steel and thermoplastic polymer such as PP by reactive sites and chemical treatment of the surfaces.
3. Evaluate the thermal effect at the interface between thermoplastic polymer composites containing steel reinforcement.
4. Develop an efficient and accurate finite element model to determine the interfacial behavior between PP and steel reinforcement.

An interface is a region where the fiber and matrix phases are chemically and/or mechanically combined and discontinuity of parameters occur [15]. It is well known that material properties such as elastic modulus, stiffness, strength and coefficient of thermal expansion affect the final performance of the composite. Because the optimum performance of a composite strongly depends on the behavior of the interface, the present work will focus on techniques to tailor the mechanical as well as chemical bonding between PP and steel reinforcement. In situations of dynamic loads such as from impact and blast load threats, the controlled opening of the interface can provide a mechanism for energy

absorption, without rupturing or breaking the reinforcing fibers. The effect of temperature at the interface will also be considered in this study. When the composite is exposed to temperature, the bond strength can be adversely affected and the mechanical performance of the composite could be drastically affected.

This work limits its results to the interface interaction of steel with the specific polymers in the study. Even though the values obtained through the work have no dependency on geometry factors, the work focuses on the intrinsic parameters between polymeric matrix and steel reinforcement. Furthermore, the methodology adopted to characterize the interface can be extrapolated to a specific metal-thermoplastic composite.

BACKGROUND

It has been observed that a strong interfacial bond will result in improved interlaminar shear strength, delamination resistance, fatigue and corrosion resistance in a polymer matrix composite [15]. By definition, an interface is a boundary demarcating distinct phases namely fiber, matrix, or coating layer as seen in Figure 1. The goal for structural polymer composites is to enhance fiber-matrix interfacial bonding.

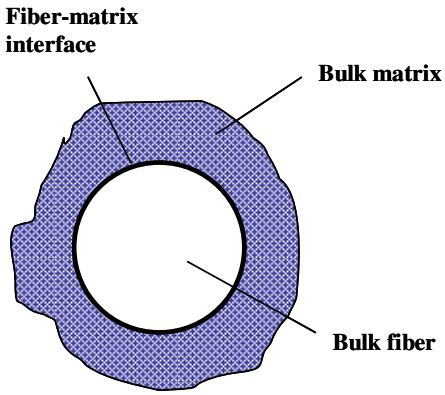

Fig. 1. Schematic illustration of fiber-matrix interface.

Surface treatments including mechanical and chemical methods have been adopted to improve interfacial bonding, and several numerical models have been developed to understand the parameters that affect the integrity of the interface. Among different experimental tests, the single fiber pull-out and three-point bend loading have been considered to be useful because of their simplicity in characterizing interlaminar properties [13]. In addition, pull-out test has been numerically modeled to describe the stages of failure at the interface. Kocak and Ebbott [3, 16] proposed a model to characterize the

crack propagation due to fatigue along the interface in a cord-rubber composite. Meo [17] developed a finite element model (FEM) to simulate the spontaneous pull-out of a steel pin through the thickness from a polymer composite. The Meo model implements frictional contact between the fiber-matrix interface, assuming a constant friction coefficient along the fiber-matrix interface in the axial direction. The model considers isotropic materials and deformation with a fully and partially bonded interface plus frictional sliding. Zhang and Yuan [18, 19] consider a variable friction coefficient, the value of which has dependence on the pull-out rate for the two cases studied, i.e. fully bonded and fully debonded.

As in Meo's model [17] and Zhang and Yuan [18,19] consider interface debonding and sliding as being the stages of failure with the difference that the phenomenon of stick and slip is a decreasing exponential function of the pull-out rate. Hutchinson and Jensen [20] analyzed the debonding of a fiber embedded in a brittle matrix. They considered two boundary conditions: one an isolated fiber-matrix unit cell and the other a matrix containing an array of unidirectional fibers. In the latter, both fiber and matrix were considered to be isotropic with similar modulus and Poisson's ratio, which constitute a modeling limitation for composites with significant differences in elastic properties as the case of steel cord embedded in PP. Pidaparti [21, 22] developed a three-dimensional micromechanical model to describe the load deformation characteristics of cord rubber composites. He investigated the influence of the cord shape on the interface stress distribution, assuming a fully bonded interface and then a non-sliding interface.

Previous research shows that the use of finite element analysis (FEA) is a useful technique for describing the mechanical behavior at the interface in a composite material.

The present work extends the use of FE modeling to characterize the interface between steel cord and the surrounding thermoplastic polymer. The study focuses on the stress distribution, interface debonding and frictional sliding aspects of the interface. The proposed model employs surface-to-surface contact elements to define the interface, which is developed as a rigid-to-flexible contact problem. In the first case to impart loading, a single steel cord is subjected to pull-out from a PP matrix. The pull-out force generates the interface stresses necessary to characterize the interface strength. In addition to the elastic load transfer in the perfectly bonded interface, the model also considers load transfer in a partially bonded interface. The model further accounts for the sliding of the cord reinforcement when it is fully debonded from the matrix, a behavior that is governed by Coulomb's friction law [13]. The model analyzes the influence of specific geometry and size of the cord as well as the effect of matrix elastic properties in both material cases, i.e. isotropic and anisotropic. This approach will demonstrate the possibility to predict the limiting bond strength that establishes continuity of the interface between the two phases of the steel cord and thermoplastic PP matrix.

To understand the fiber-matrix interface, research efforts have been directed towards mechanical and chemical bonding mechanisms. Some of the adhesion mechanisms through which the surface treatments promote interfacial bonding consider improvement in wettability, creation or addition of chemical groups and variation in surface topography [15]. Thermoplastic composite materials, unlike thermosetting polymer composites, frequently suffer from a lack of fiber-matrix adhesion. This is typically remedied using fiber surface modification. Chemical modification or the addition of a compatible phase (i.e. adhesives) bridging the fiber and matrix phases has been successfully applied to im-

proving the interfacial characteristics of many polymer composite systems [15]. Huang and Dhramarajan [4, 14, 24] analyzed the effect of maleic anhydride modifier to impart polarity to a polyolefin surface, improving the adhesive bonding with aluminum and glass surfaces. Cai [25] demonstrated that grafting of PP with acrylic acid (AA) not only improves the impact strength of PP but also the adhesion to polar substrates; however, the industrial application is limited because of the total treatment cost. Zhang [26] implemented oxidation etches on carbon fibers to increase the shear strength with epoxy matrix with the compromise of decreasing in tensile strength. Ishida [27] used silane coupling agents between glass and polymer matrices, and reactive amine groups between aramid fibers and epoxy resin to create covalent and hydrogen bonds at the interface. Kim [28] studied the effect of fiber-matrix interface and the influence of silane agents on intermolecular fracture and the impact performance of woven-glass fabric composites. A brittle interface causes unstable crack propagation and low fracture toughness values. The use of silane surface modifiers resulted in improved impact performance. Cerny and Molitor [12, 29] investigated the use of adhesives as intermediate layers to promote a durable polymer composite-metal bond, using titanium alloy and fiber glass fiber composite as substrate. Previous research suggests that it is possible to improve the adhesive bonding between steel and thermoplastic polymers due to surface treatment or chemical modifiers that allow diffusion across the interface. The understanding of the bonding between metals and polymers will enhance potential applications in thermal and electrical functions and corrosion resistance mechanisms [30-32].

Mechanical Bonding in a Metal-Thermoplastic Composite

The combination of steel reinforcement and thermoplastic polymer creates a composite with synergy of constituents, i.e. stiff reinforcement in a fairly ductile matrix. Numerical and experimental studies have been carried by several researchers to investigate the mechanical behavior of epoxies and rubber reinforced with steel, but there is limited work that considers the combination of thermoplastics with steel [33, 34]. Steel wires have been used with epoxy resin in structural applications [4] and enhancement of mechanical properties has been reported as illustrated in Table 1. The tensile modulus, tensile strength and compression modulus of a SRP has been compared to neat epoxy resin in Table 1. It can be seen that significant improvement in the stiffness and strength is obtained by reinforcing the polymer with steel fibers.

Table 1. Mechanical properties of steel reinforced polymer (SRP) versus neat polymer.

Material	Tensile Modulus (GPa)	Compressive Modulus (GPa)	Tensile Strength (MPa)
Neat Epoxy resin	3.06	3.00	54
SRP	5.86	8.55	15

For the case illustrated in Table 1, the performance of the composite is favorable when using steel cord reinforcement, but the studies have not considered the effects of replacing epoxy resin with thermoplastic polymers such as PP. The different degrees of surface roughness alter the characteristics of the interface. According to Ramani [35], the roughness of the metallic surface increases polymer penetration and, consequently, increases the bond strength at the interface. He also concluded that processing conditions, including temperature and pressure, can influence the penetration of the polymer in the

metal surface [17]. Figure 2 illustrates the desired cohesive failure at the interface when steel surface is graft blasted with aluminum oxide to create roughness and tested to obtain peel strength in contact with polycarbonate. After the surface treatment and injection of polymer on the surface, the peel strength was estimated to be 20.4 MPa compared to 10 MPa for a non-treatment metal surface.

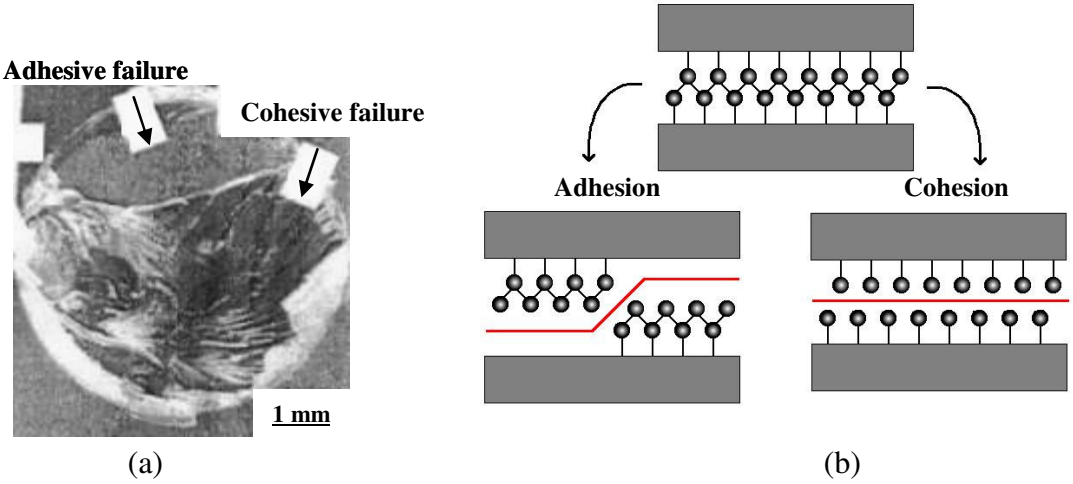

Fig. 2. Cohesive and adhesive failure (a) Cohesive and adhesive failure mode of steel to polycarbonate. (b) Adhesive bonding phases; the red line indicates the location of the fracture.

For the purposes of describing the mechanical bonding at the interface in a metal-thermoplastic composite, the shear strength criterion [28, 35] is implemented to correlate the experimental data with a numerical model. In this criterion, failure occurs when the interface shear stress exceeds the interface shear bond strength. In order to characterize the interface shear bond strength, three-point loading and pull-out tests are conducted using samples of steel cords embedded in a PP matrix. With the goal of modeling, the first approach was to reproduce the three-point loading test and compare with the load displacement curve obtained from the experiment [35]. The simulation considered three sce-

narios: (1) perfectly bonded; (2) elastic deformation with a partially debonded interface and (3) elastic deformation plus frictional sliding where the fiber is fully debonded from the matrix. The last scenario is the most general case defined with specific contact and friction parameters.

Finite Element Model (FEM)

The FE model considers the basic Coulomb friction law to describe the mechanical bonding at the interface of the steel and the PP as given by Equation 1. The two contacting surfaces (PP and steel) withstand shear stresses up to a certain magnitude across their interface before they start sliding relative to each other; this stage is called debonding. The Coulomb friction model defines an equivalent shear stress, at which sliding on the surface begins as a fraction of the contact pressure. Once the shear stress is exceeded, the two surfaces slide against each other; this stage is called slipping. The stress distribution along the interface constitutes a complex interaction of the fiber axial stress, matrix axial stress and interface shear stress, as shown in a simplified representation in Figure 3.

The first part of Equation 1 provides sliding resistance at the interface, even with zero normal stress. The second part of Equation 1 indicates that any contraction of the matrix on the reinforced cords would result in interlocking or enhanced mechanical bonding. The coefficient of friction and sliding resistance are inputs to the FE model and have been adopted from literature [17, 36-38]. For the fully bonded case, the friction coefficient is μ=1, while for the partially bonded case the friction coefficient is μ= 0.5 and μ=0.3 for rough and weak interfaces, respectively. The value for cohesive bonding is assumed to be 10 MPa.

$\tau_i = \tau_o + \mu(\sigma_n)$ Eq. (1)

τ_i : adhesion bond strength

τ_o : cohesive bond strength

μ : coefficient of friction

σ_n: normal stress due to the contact pressure

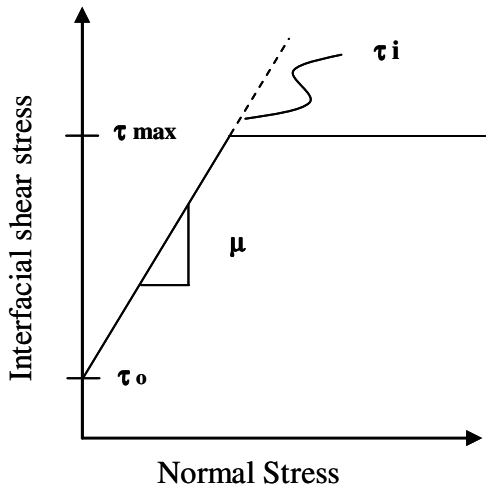

Fig. 3. Coulomb friction model used to characterize the mechanical bonding at the interface.

Contact Algorithm. The definition of initial contact was an important aspect of the FE model. For modeling the interface between the steel and the thermoplastic, the penalty method was used as the contact algorithm [39]. This method uses a contact "spring" to establish a relationship between the two contact surfaces with a contact stiffness k. The amount of penetration between the contact and target surfaces depends on the normal stiffness, and the amount of slip in sticking contact depends on tangential stiffness. Higher stiffness values decrease the amount of penetration/slip. Hence, the model considers high stiffness to produce a small penetration slip, but low enough to obtain adequate convergence.

To define the contact stiffness and the allowable penetration, the model considers normal penalty stiffness, penetration tolerance factor, static-dynamic ratio, and contact opening stiffness. Describing each term briefly, penalty stiffness refers to the amount of penetration between contact and target surfaces. Penetration tolerance factor determines the penetration of each element in ratio of its thickness. Static dynamic ratio specifies the

ratio of static to dynamic coefficients of friction, which allow the model to have the friction coefficient value dependent of the velocity for the surfaces in contact. Contact opening stiffness refers to the weak or strong spring effect between the contact surfaces. To determine the contact detection, the model uses Gaussian integration in which the contact surface (polymer) is constrained against penetration into the target surface (steel). However, in principle, the target surface can penetrate into the contact surface.

For the type of interface, i.e. weak or strong, the model was updated with specific contact behavior of unilateral contact, rough frictional contact, or fully bonded contact. In the first case, normal pressure was considered equal to zero if the separation occurs; the second case corresponds to an infinite friction coefficient where there is no sliding; and in the third case, the target and contact surfaces remain bonded.

Element Type and Mesh. Both the steel reinforcement and the polymeric matrix are built using 3D elements in ANSYS 8.0 (SOLID185) with 8 nodes and three degrees of freedom for each. The mesh was mapped as hexagonal elements. For the interface, the CONTA174 element was used. These elements have 8 degrees of freedom and are used to define surface-to-surface contact. The interface is generated as rigid-to-flexible contact. The contact surface is associated with the polymeric matrix and the target surface with the steel cord.

Failure Mode under Three-Point Bend Load

For a specimen of PP reinforced with steel cords, the failure tend to be dominated by interfacial debonding between the steel cords and the matrix as can be seen in Figure 4. The weak interface between the thermoplastic PP and steel fibers limits the possibility

to transfer load through the thickness; therefore, the material fails along the interface. The steps of failure are shown in Figure 4. The composite starts to fail by compressive failure under buckling through the polymeric matrix (a). Further debonding occurs (b) at the interface. The steel cords slip when the interfacial stress exceeds the interfacial strength (c), and finally when there is loss in contact friction, both surfaces separate completely from each other (d).

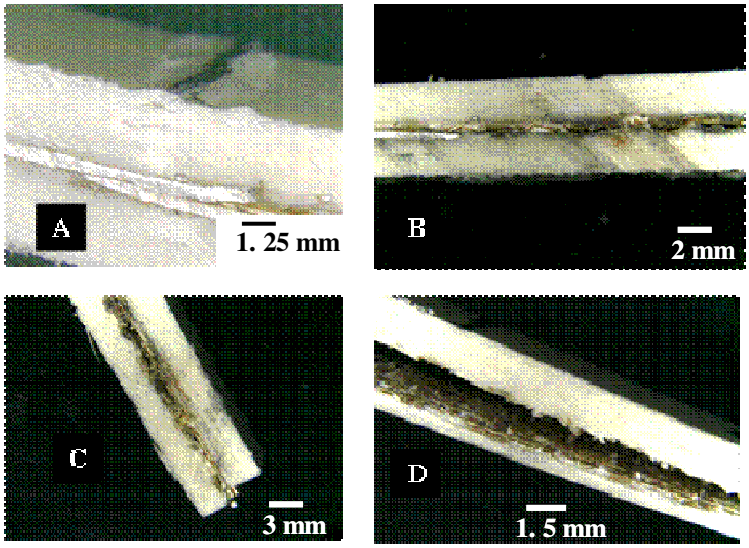

Fig. 4. Failure sequence for flexure loading of a metal-thermoplastic composite.
(a) Buckling of the matrix (b) Debonding along the interface
(c) Cord slipping and (d) Interface opening.

Microstructure of Polypropylene-Steel Cord Composite

A weak interface is observed in Figure 5 for PP reinforced with steel cords. The weak interface can be explained by the lower degree of physical interlocking between the PP and the steel cord due to the relatively low surface energy of this polymer according to the values shown in Table 2 [40-41]. Figure 5 represents the interface between PP and steel for a single cord and for common arrangement of steel cords. The diameter of each cord is 1.016 mm. The microstructure suggests that surface abrasion of the steel fibers

can enhance the roughness, and hence mechanical bonding; or a surface coating to achieve improved chemical bonding.

Table 2. Solid surface energies for common polymers [40-41].

Material	Surface Energy (mN/ m)
Polytetrafluoroethylene (PTFE/Teflon)	20
Polypropylene (PP)	30
Polyethylene (PE)	35
Polystyrene (PS)	38
Styrene butadiene rubber (SBR)	48

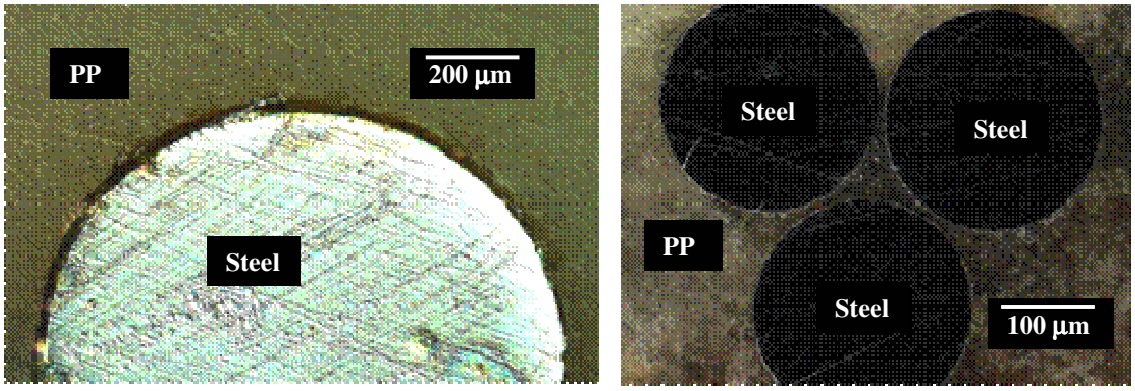

Fig. 5. Interface between PP and steel cord. (Left) Single cord, (Right); Configuration of steel cord rope.

Effect of Chemical Treatment on Fiber Matrix Interfacial Adhesion

The possibility of developing an improved fiber-matrix interfacial adhesion can result in composites with superior properties such as interlaminar shear strength, delamination resistance, and fatigue and corrosion resistance. In general, polyolefins such as PP have poor adhesion to the substrate due to non-polar properties and saturated chains that makes the sharing of electrons difficult. One approach to enhance the interface is the use of chemical surface modifiers to promote free-radical evolution and cross linking to in-

crease compatibility with polar substrates such as metals [25]. The present work investigates the use of chemical modifiers to PP that provide polarity to the surface and improve adhesion with metallic surfaces [14, 42]. Styrene maleic anhydride (SMA) was used as a modifier for PP. The grafting of SMA on PP improves the adhesion by increasing its surface energy [43]. Further, PP with butane co-polymer (PPB) reacts with SMA to form (PPB-g-SMA) and creates a link between oriented PP and polar substrates. PPB has good solubility in polar solvents, which are suitable for the grafting of SMA. Thus, PPB-g-SMA can be used as an adherent film between oriented PP and polar metallic surfaces. The study explores the possibility to achieve enhanced chemical bonding between surfaces that feature difference in polarity by the creation of reactive sites, carboxylic groups (-C=O) and sulfur radicals, on the PP backbone as show in Figure 6.

The degree of grafting on the PP is determined by Fourier Transform Infrared Spectroscopy (FTIR). The spectra is used to determine the absorption of carboxylic group as well as the sulfur element. The increment in surface energy is determined by function of the contact angle. Figure 7 illustrates that surface energy has direct relationship with the amount of polar groups at the surface of a grafted PP. Higher surface energy at the PP reveals superior interface adhesion with aluminum foil, which is measured by peel strength test [24]. Table 3 shows other mechanical properties of a composite made by grafted PP with acrylic acid (AA) and bonded to aluminum [25]. This establishes the basis that polar groups improve adhesion between polyolefins and metallic surfaces.

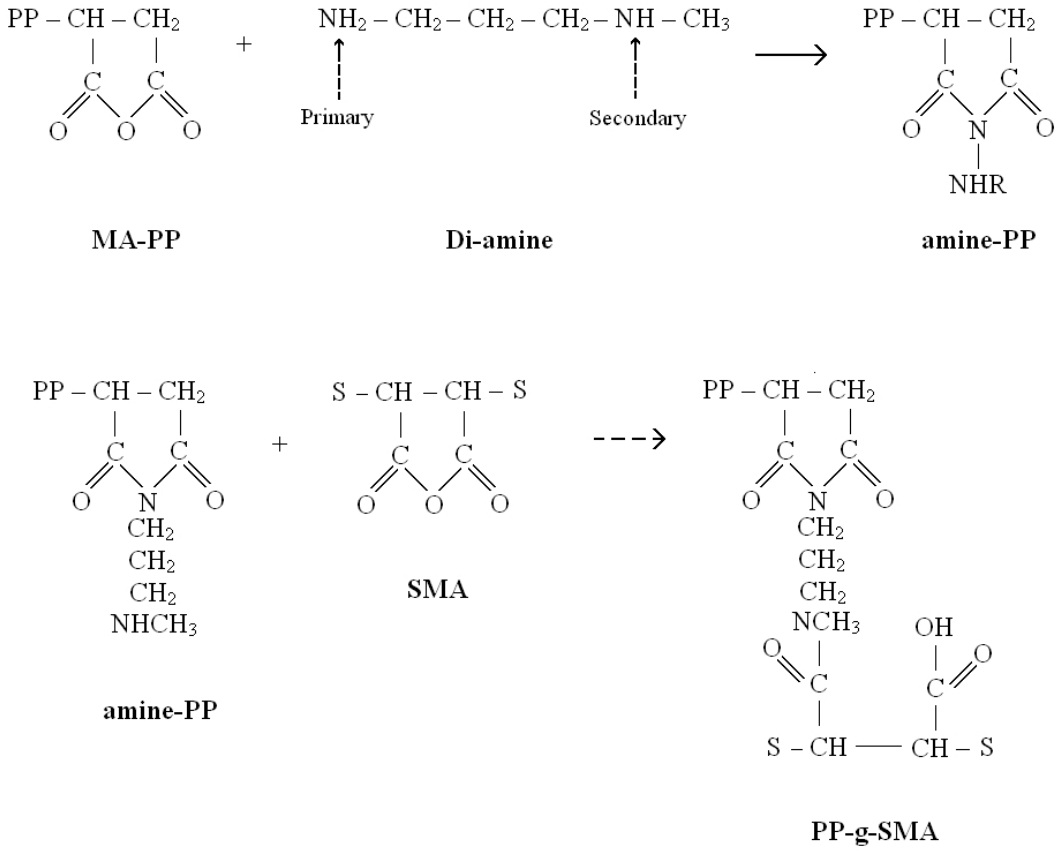

Fig 6. Chemical reaction between styrene maleic anhydride and PP co-polymer [24].

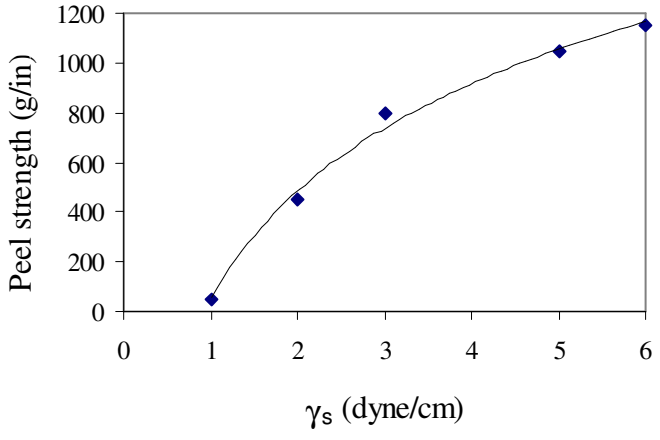

Fig. 7. Relationship between the peel strength of PP and aluminum adhered with propylene-butene co-polymer grafted with styrene maleic anhydride (PPB-g-SMA) as a function of surface energy [14].

Table 3. Mechanical properties and adhesion of neat PP and grafted PP [25].

Material	Tensile Strength (MPa)	Elongation to break (%)	Notched impact strength (kJ/m^2)	Peel Strength (kN/m)
Neat PP	26.6	220.7	17.3	0
PP with 0.8% (AA) *	28.4	149.8	30.1	5.07

*At 0.47% of grafting degree.

Scanning electron microscopy (SEM) analysis is used to characterize the failure mode under peel strength test. The failure of bonded surfaces takes place under three different modes: (1) separation by cohesion, when the failure occurs in the molecules of the adhesive; (2) failure by adhesion, when the failure occurs at the interface between adhesive and substrate; and (3) substrate failure, when the failure occurs first at the substrate prior to the failure at the interface or in the adhesive, as seen in Figure 8.

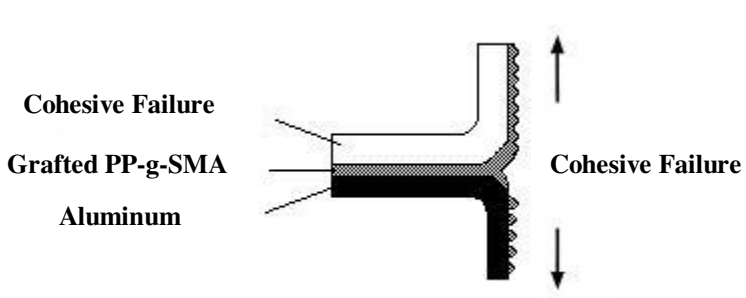

Fig. 8. Schematic representation of cohesive failure at the interface between PP and aluminum substrate using a co-polymer with grafted polar groups as coupling agent.

Temperature Distribution on a Metal-Thermoplastic Composite

The thermal distribution at the interface is investigated to determine practical applications of thermoplastics with steel cord reinforcement. The main concern with temperature is the generation of residual stresses at the interface due to the mismatch in coef-

ficient of thermal expansion (CTE) between the reinforcement fiber and the matrix. Thermal stability is influenced primarily by the strength of the chemical bonds. Numerous models have been studied to understand the effect of CTE in the composite. Jamshidi [44] studied the cord/rubber interface at elevated temperatures. He concluded that increase in temperature causes bond breakage at the interface of nylon 6 cord with rubber compound and also established an optimal temperature and time of curing to achieve the maximum adhesive strength. Rosso [45] implemented the use of an FEM to analyze the effect of thermal stresses in the response of carbon fiber composite under tensile load. In this approach, the material was treated as linear elastic with temperature-dependent properties. The location of the high stress concentration was found at the outer edge at the interface between fiber and matrix. A numerical modeling study of the effect of temperature is conducted. FEM is developed to evaluate the generation of thermal stresses at the interface. The FE model will allow predicting critical points at the interface due to thermal stresses.

The determination of temperature distribution at the metal-thermoplastic composite provides guidance to potential thermal applications of this material. The thermal conductivity of the composite is determined with the aid of numerical analysis. A basic model is shown in Figure 9, where heat is applied to the steel layer from one side (referred to as front side in the figure); as a result the gradient of temperature is displayed for the metal-thermoplastic composite. Thermal properties of steel and PP as well as the properties of other materials that could be used to enhance thermal and structural applications of metal to thermoplastic composites are shown in Table 4.

FEM considers fully bonded condition (perfect interface) and can be used for either thermal analysis or thermal plus structural analysis. The use of contact elements at the interface not only allows the model to update typical conditions of heat transfer such as conduction, convection and radiation but also heat generation due to frictional sliding.

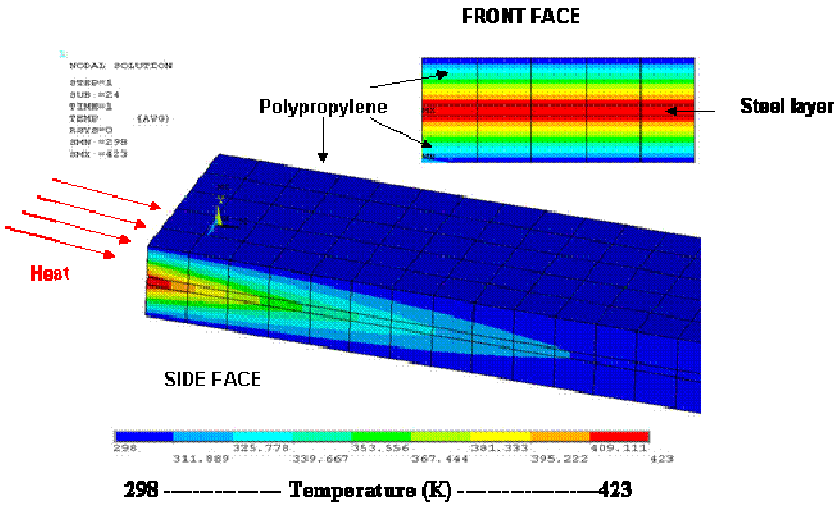

Fig 9. Finite Element Method to evaluate thermal conductivity of steel embedded in PP matrix.

Table 4. Thermal properties of some common materials used for structural composites [47].

Material	Thermal Conductivity @ 20°C (W/m-K)	CTE (μm/m-°C)	Melting Point (°C)
Stainless Steel (0.15%C)	21	16.6	1421
Polypropylene	0.12	5.2	180
S2-Glass	1.45	1.6	1725
Aluminum	210	24.0	660

Experimental Techniques

Table 5 shows the experimental techniques used in this study to characterize the interface on a metal-thermoplastic composite. Experiments involve the determination of

cohesive strength, shear strength, flexural strength, pull-out force, friction coefficient, contact angle, surface energy and presence of reactive and polar groups by IR spectra and X ray diffraction at the interface for a metal-thermoplastic composite.

Table 5. Experimental techniques used in the study to characterize the interface.

Technique	Purpose
Cohesive strength	Bond strength generally involves determining the stress required to rupture a bond formed by an adhesive between two metal blocks. In this case, PP is between two metal surfaces. The test may compare the fractured surface to failure analysis within the adhesive interface region. [ASTM D952 or Butt strap tensile lap shear test].
Shear strength	Shear testing is performed to determine the shear strength of the composite. It measures the maximum shear stress that may be sustained before a material will rupture [ASTM D3165/66].
Friction coefficient	Friction coefficient is an important parameter for the value of maximum shear stress as can be seen in the Figure 3. The contacting points under interfacial tangential force cause them to deform elastically and store potential energy to initiate the interfacial sliding. When the applied forces exceed the static friction force, sliding occurs. To be more accurate the FE model will require both types of friction coefficient, static and dynamic. Static friction is the force that holds back a stationary object up to the point that it just starts to move. It is calculated by finding the initial peak force required to move the sled and dividing the value by the weight of the sled. Kinetic friction is the force holding back regular motion. This kinetic friction coefficient concerns the force restricting the movement of an object that is sliding on a relatively smooth, hard surface. It is calculated by finding the average load during the test and dividing this by the weight of the sled, which holds the other material. The static peak force should not be included in the average force. [ASTM D1894].
Three-point bend test	This test evaluates the mechanical response of the composite under tensile, compressive and shear stresses simultaneously. Also relates the force-at-failure to interfacial shear stress [ASTM D790].

Pull-out test	The integrity of a high performance of the composite is highly dependent on the adhesion in this case of the steel to the polymer matrix. Frictional forces between the steel cord and the PP matrix play an important role in the behavior of the ultimate strength of the composite. The test will allow measuring the force required to pull-out an individual cord from the matrix that is tightly gripped and pre-tensioned in the direction perpendicular to the cord pull-out.
Lap shear test	Peel strength is generally used to measure the adhesive bond strength of a material, typically and adhesive. Peel strength is the average load per unit width of bond line required to separate bonded materials where the angle of separation is 180-degrees. [ASTM D903, D3807].
Contact angle and surface energy	The contact angle can be measured using ASTM D5946 and ASTM D5725 at room temperature. Water and ethylene glycol can be used as reference liquids. Once the contact angle is obtained the surface energy can be calculated used a mathematical relationship.
FT-IR infrared spectroscopy	This test determines functional groups on the polymer through surface reflectance.
X-ray spectroscopy	This test determines chemical elements on the steel modified surface.
SEM	This test characterizes topography at the interface and type of failure under peel stress load.

Data Analysis

The experimental design has been chosen to determine the influence of the variables listed in Table 6 on the mechanical and thermal conductivity properties for composite with thermoplastic matrix and steel cords reinforcement. To have statistically significant results, the experimental strategy will be a 2^3 factorial design [48]. This plan aids in studying the interaction between different factors at two levels with respect to the response variable, as seen in Figure 10. Table 7 enumerates the factors that will be ana-

lyzed to characterize the bond strength between metal to thermoplastic composite. The results for the factorial experiment will indicate the effect of each factor and the effect of the interaction between them.

Table 6. Factors and levels for the experimental design.

Case	Factor and purpose	Level 1	Level 2
Metal to Thermo-plastic: flat surfaces	x: Polymer Surface: to analyze surface energy	Neat polymer	Grafted polymer (polar sites)
	y: Metal Surface: to analyze roughness	fine roughness	coarse roughness
	z: Temperature: to analyze thermal stresses	Low Temperature gradient	High temperature gradient

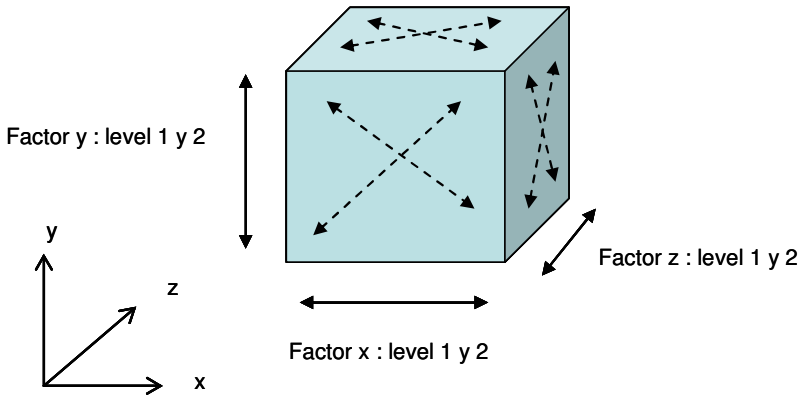

Fig. 10. Geometric interaction of the adopted experimental design.

Organization of Work

This work has been organized into three manuscripts, which report findings for each of the objectives mentioned above.

Manuscript 1 describes the correlation of friction coefficient, matrix stiffness, initial adhesive bond and pull-out force for the interfacial shear stress for a composite material involving different thermoplastic polymers with steel cord reinforcement. Then, using FEA, the interface between the steel cord and thermoplastic materials is characterized. FEA focuses on the stress distribution, interface debonding and frictional sliding of the interface under flexural load. This approach demonstrates the possibility of predicting the limiting bond strength that establishes continuity of the interface between the steel and thermoplastic matrix and provides a basis for parameters that could improve mechanical bonding.

Manuscript 2 describes the effect of surface treatment to improve the adhesion of thermoplastic polymers to steel reinforced surfaces. Plasma treatment is used to add reactive molecules (Si, H and C) on the surface of steel, and maleic anhydride is used to add carbonyl groups (–C=O) on PP with the purpose to create reactive sites that promotes bonds between surfaces. Furthermore, this study analyzes the adhesion of steel with not only PP but also with soft thermoplastic polyurethane (TPU). In addition, this study also analyzed PP modified by maleic anhydride (PP-MA) and a new generation of nanofullerene epoxy resin with the objective to investigate mechanisms of bonding and ways to enhance the bond at the interface between metal-polymer surfaces. Single lap shear joint testing was then used to assess interfacial adhesion for the different cases in the study. This work establishes the basis to promote adhesion between polymer and metal surfaces by the addition of chemical functional groups and elements that attach between the metal and polymer surfaces to create a stronger interface.

Manuscript 3 describes a transient thermal analysis using FEA to examine the interface effect on a metal-thermoplastic composite. The FEA is developed at two scales: one at a micro scale and the other at a macro scale. The micro scale model considers the effect of interface bond strength, mismatch in coefficients of thermal expansion, thermal conductivities and stiffness to predict the temperature gradient and thermal stresses and in strains along the interface of a cylindrical cord embedded in a polymeric matrix. The macro scale model focuses on temperature gradients across the interface and generation of thermal stresses consistent with a cool-down process. Additionally, this model uses a coupled thermal-mechanical load to evaluate the effect of residual thermal stresses on the mechanical performance of the composite. This is accomplished by simulating a three-point-bend test with the induced thermal stresses. Both models consider surface-to-surface contact elements along the interface to study the effect of weak, medium and strong bonding between cord and matrix on the generation of thermal stresses. The FEA results in a non-linear thermal strain distribution in the polymeric matrix around the metal cord. Physical parameters, such as the difference in coefficient of thermal expansion and thermal conductivity as well as the bond strength are evaluated to predict residual stresses along the matrix-cord interface.

INTERFACIAL SHEAR STRENGTH IN A METAL-THERMOPLASTIC COMPOSITE

CAROL OCHOA PUTMAN, UDAY K. VAIDYA

Submitted to Polymer Composites

Format adapted for dissertation

ABSTRACT

Hybrid materials featuring thermoplastic polymer composites in conjunction with steel cords are being considered as structural materials in infrastructure, transportation and military applications. The present study focuses on understanding the mechanical performance of metal cord-thermoplastic composites. Since the optimal performance of a composite strongly depends on the behavior of the interface, finite element modeling has been adopted to characterize the interface between steel fibers and thermoplastic composite material. The mechanical interactions between thermoplastics and steel have been studied with a goal to improve interfacial shear strength and cohesive strength. Steel cord was combined with nylon 6, polypropylene, soft thermoplastic polyurethane and hard thermoplastic polyurethane to find the parameters that affect mechanical bonding via pull-out tests and friction coefficient tests. The test parameters have been correlated to interfacial shear strength using both experimental and modeling approach.

Keywords: Friction coefficient, pull-out test, Finite Element Analysis (FEA), Interface Analysis.

1. INTRODUCTION

The study of steel cords reinforcement in polymer composites is of growing interest in structural materials. During the last 50 years, cord reinforced composites have constituted a growing number of structural, military, automotive and aerospace applications. These materials are constructed of steel cord embedded in a polymer matrix, for which the combination of the constituent materials produces superior mechanical properties [1]. The first well-known application of steel cord reinforcement was in steel-belted tires, in which the steel cords increased the tire's performance in terms on fatigue properties, and improved its wear resistance in miles over older bias-ply tires [2].

Metal-polymer (or fiber reinforced) composites offer promising new options in shock absorption and explosion resistance structures. High interlaminar strength, greater ductile behavior, higher capability of energy absorption, and higher impact resistance are required in these applications [3-4]. Since the optimal performance of a composite strongly depends on the type of constituent materials and their compatibility, careful selection of the cord and matrix combination is essential.

The key to the selection process is an understanding of the metal-composite (or polymer) interface. High strength or high toughness can be achieved by modifying interface properties [4]. Experimental and numerical methods have been developed to understand the effect of interface on the mechanical behavior of composites. Single fiber pull-out and push-out test [5-9], interfacial shear stress and bending test [5-6, 10] have been considered useful to quantitatively determine the interfacial strength.

The present work establishes the correlation of friction coefficient and pull-out force to the value of interfacial shear stress for a composite material involving different

thermoplastic polymers with steel cord reinforcement. Then, using finite element analysis (FEA), the interface between the steel cord and thermoplastic materials is characterized. FEA focuses on the stress distribution, interface debonding and frictional sliding aspects of the interface under flexural load. The FEA model employs surface-to-surface contact elements to define the interface, which is developed as a rigid-to-flexible contact problem [11]. The numerical approach uses the same specimen dimension span support and load as the experiment. The interfacial behavior in the model is governed by Coulomb's friction law [5, 12]. Both experimental and FEA results show a correlation between interfacial parameters to improve the mechanical behavior in a metal-thermoplastic composite. This approach demonstrates the possibility of predicting the limiting bond strength that establishes continuity of the interface between the steel and thermoplastic matrix and provides a basis for parameters that could improve mechanical bonding. Furthermore, it is deduced that the integrity of a steel reinforced thermoplastic composite is heavily dependent on the adhesion at the interface.

2. METHODOLOGY

The properties of a composite material are a function of the constituent fiber/matrix and the interface [6]. The effect of bulk properties of composites has been investigated by several researchers [6-9]; however, the interactions at the interface between matrix and fibers are less understood. There is very limited literature that addresses the interaction of a metal surface with a thermoplastic matrix.

This study is based on the Coulomb friction law [5, 12] which indicates that any contraction of the matrix on the fiber will result in gripping of the fiber by the matrix.

The mechanical interaction at the interface is related to the interlocking effect between two surfaces. To implement the Coulomb friction law, the experimental values of friction coefficient, interfacial shear stress and cohesive bonding have to be determined. Thus, we focus on experimental techniques to find these values, as well as their interaction that influences lower or higher interfacial shear stresses leading to interfacial failure. Four thermoplastic polymers were employed in this study: polypropylene (PP), soft and hard thermoplastic polyurethane (soft TPU and hard TPU respectively) and nylon 6 (PA6), for which the values for elastic modulus are 1.6, 0.006, 1.65 and 3.0 GPa, respectively. These polymers were investigated in combination with ultra-high strength steel cords [13]. The rationale for choosing these thermoplastic material systems was to cover a range of properties including stiffness, Poisson's ratio, viscoelastic properties, cost and availability.

The ASTM G99-05 standard was adopted to determine the friction coefficient between the thermoplastic matrix and the steel cord. The conditions for pin to disk were established [14-16]. Different path patterns of the contact as well as different velocity values were analyzed for all the systems until the proper path conditions were determined to estimate the static and dynamic friction coefficient. The characteristics of the test are explained by Schmitz [14].

A pull-out test was developed to obtain the values of interfacial shear strength and shear resistance (cohesive strength) of a steel cord embedded in a thermoplastic matrix for all four polymer systems. The fabrication of the pull-out test samples and testing conditions is described later. The same displacement rate was used for the friction coefficient test and pull-out test, since the friction coefficient has velocity dependence [15]. In addi-

tion to the pull-out test, microstructure has been studied to investigate the interaction between the fiber and the matrix of the different systems.

The interfacial behavior was also investigated by finite element modeling. A pull-out model using contact elements at the interface was developed to reproduce the experimental force versus displacement curve. Contact elements were based on the shear strength criterion which defines interfacial failure when the interface shear stress exceeds the interface shear strength. Both experimental and numerical curves were compared for the different thermoplastic resin systems. The model was applied to develop a parametric study to investigate the influence of matrix stiffness, friction coefficient and cohesive bond at the interface to generate variables of interfacial stresses. A prediction of the interfacial bond between the steel cord and a specific thermoplastic matrix creates the potential for optimizing the design of cord reinforced materials.

2.1 Coulomb Friction Model

The failure of a metal cord-thermoplastic composite is highly influenced by frictional conditions at the interface. The Coulomb friction law describes the interaction at the interface after debonding [12]. Using this law, two contacting surfaces (polymer and steel) can support shear stresses up to certain magnitude across their interface before they start sliding relative to each other, corresponding to the debonding stage. The Coulomb friction model defines an equivalent shear stress, at which sliding on the surface begins as a fraction of the contact pressure. Once the shear stress is exceeded, the two surfaces will slide relative to each other. This stage is called ‘slipping’. The shear stress is given by Equation 1:

$$\tau = \frac{P}{A} = \tau_0 + \mu(\sigma) \qquad \text{Eq. (1)}$$

The stress distribution along the interface (τ) constitutes an interaction of the fiber axial stress (τ_o) and compressive perpendicular stress (σ) acting on the fiber caused by the perpendicular load (P) and the friction coefficient (μ) between both materials through the sliding area (A) is shown in Figure 1.

2.2 Friction Coefficient Test

2.2.1 Sample Preparation

Thermoplastic polymer pins were made by extrusion-compression molding using cylindrical molds of 3/8" diameter with a tip of 3/16". All samples were sanded by an 800 grit sand paper and cleaned with methanol to remove contamination. Samples were maintained at a control temperature of 90 ^{0}C to avoid moisture absorption. The surface of the samples was wiped with alcohol prior to each test.

2.2.2 Testing Parameters

The static and dynamic coefficients of friction were determined for cold-rolled low carbon steel (AISI/SAE 1018) against four different thermoplastics surfaces, PP, PA6, hard TPU and soft TPU in an AMTI OrthoPOD six station pin on disk friction and wear testing machine (Figure 2) [14,16].

The friction coefficient was established at a constant force of 10 N and velocity of 0.1 mm/s for a semi-circular path to determine the dynamic friction coefficient, and linear path to estimate the static friction coefficient with a total path distance of 25 mm. The horizontal (F_x and F_y) and vertical (F_z) force components at the pin-disk interface were

measured simultaneously by three separate triaxial load cells. The friction coefficient (μ) for each sample was determined by using Equation 2.

$$\mu = \frac{\sqrt{\sum F_x^2 + \sum F_y^2}}{\sum F_z} \qquad \text{Eq. (2)}$$

To obtain the static friction coefficient the first peak of the force-time curve of the linear path was used (Figure 3). Dynamic friction coefficient is obtained according to ASTM G99-05, and it is calculated as the average of all points along the semi-circular path (Figure 4).

2.3 Pull-out Test

Single fiber pull-out test is devised to measure interfacial characteristics [17-19]. Two specific values are obtained from the load versus displacement curve. The first corresponds to the peak load value, which is related to the bond strength between the cord and the matrix. Thus, the peak load corresponds to the total debonding of the interface between the thermoplastic polymer and the steel cord, the decrease in load at the curve (Figure 5) corresponds to the frictional sliding at the interface; the steady decrease in the load is attributed to the decreasing area of the interface as the fiber is pulled out. The second value corresponds to the interfacial shear strength, which can be determined by the slope of the force versus embedded length curve. This value is dominated by friction and the different Poisson's contractions of the fiber and matrix resulting in radial compressive stress at the interface (Figure 6). According to this method the shear force acting along the cord/matrix interface is linear, the higher for the soft TPU and steel cord sys-

tem, followed by hard TPU, PA6 and PP respectively. Additional analysis of the curves will be described in Section 3.

2.3.1 Sample Preparation

To fabricate samples for the pull-out test, single 3XS configuration steel cords were confined at the ends with thermoplastic polymer tabs, leaving the center region of the cord uncovered by the use of specific designed molds for compression molding (Figure 7). The 3XS steel cord (1 mm diameter) is made from ultra-high strength by twisting three identical filament wires together and one single filament over-wrapping the bundle [15, 19]. Properties of the cord and the used polymer properties are provided in Table 1.

The steel cord is embedded in polymer at both sides along 40 mm each, and it is free over a distance of 80 mm. The mold that constrains the shape of the polymer has a rectangular shape of 40 x 15 x 5 mm according to Figure 8. For each polymer (PP, PA6, soft and hard TPU) at least 10 samples were fabricated by compressive molding.

The applied temperature was increased to the melting point of the polymer as a pressure of 160 psi was applied to mold each sample. Samples were demolded after cooling down to 120 ^{0}C, then tested under longitudinal load in a Mechanical Testing System (MTS Systems Corp., Eden Prairie, MN, USA) under a displacement rate of 0.1 mm/s.

2.3 Contact Algorithm in Finite Element Model

The definition of initial contact was an important aspect of building the finite element model. For both models, i.e. three-point bend flexure and pull-out, the Penalty method (KEYOPT (2) =1 ANSYS 11.0) was used as the contact algorithm to set the contact properties. This method uses a contact “spring” to establish a relationship between

the two contact surfaces with a contact stiffness k. The amount of penetration between the contact and target surfaces depends on the normal stiffness, and the amount of slip in sticking contact depends on tangential stiffness. Higher stiffness values decrease the amount of penetration/slip. Hence, the model considers high stiffness to produce small penetration slip, but low enough to obtain adequate convergence. To define the contact stiffness and the allowable penetration, the model considers normal penalty stiffness, penetration tolerance factor, static dynamic ratio, and contact opening stiffness. To determine the contact detection, the model uses Gaussian integration, in which the contact surface (polymer) is constrained against penetration into the target surface (steel). However, the target surface in principle can penetrate into the contact surface.

2.4 Scanning Electron Microscope (SEM)

The pull-out samples were analyzed after pull-out testing using a Philips SEM 515 scanning electron microscope which employs a field emission gun. A sample was coated with a thin layer of gold-palladium to minimize charging and the microscope was operated between 20-25 kV.

3. RESULTS AND DISCUSSION

3.1 Pull-out Curves

Figure 9 represents the pull-out curves from the experiment. Three stages of pull-out are observed, namely elastic stress response, partial debonding and frictional pull-out. As shown in Fig 9 (a-c), there are two characteristic force values that demarcate the different stages; the critical load (P_c) is the initial pull-out force causing debonding which

demarcates the end of elastic zone, and the peak load (P_p), the highest pull-out failure load which indicates the point of total debonding, and the beginning of the frictional sliding zone.

In the elastic zone, the cord and the matrix are perfectly bonded. There is adequate stress transfer from the fiber to the matrix, thus the initial slope of the force displacement curve is sharp, and the area under the stress-strain curve is dominated by the properties of the cord. The critical load is directly proportional to the shear yield strength of the polymer as seen in Table 2. As the shear yield strength increases, for example PP (10 MPa) to TPU (25 MPa), the critical and peak load increases accordingly.

The second stage involves partial bonding, where part of the stress is transferred in an elastic manner but is less than the perfectly bonded case. The slope of the curve decreases but exhibits an increasing trend. The partial bonding stage takes place until reaching the highest peak load and the fiber and the matrix is totally debonded. The stress is transferred only by friction past this point, thus the force decreases as the fiber is progressively pulled out. Thus, a lower critical load and peak load signify weaker interfacial adhesion. Considering this, with steel reinforcement, PP exhibits the lowest mechanical performance followed by PA6 and the TPU.

Figure 10 shows the values of interfacial shear strength and debonding strength as a result of pulling out a steel cord from the different thermoplastic materials. The best case corresponds to the soft TPU in combination with steel cords with the higher interfacial shear strength and good bond strength in comparison to the hard TPU, PA6 and PP. The combination of PP and steel cord exhibited the lowest values of interfacial shear and bonding strength. The value of interfacial shear strength correlates directly to the friction

coefficient as shown in Figure 11. Thus, higher friction coefficient provides higher value of interfacial shear strength. The increase in value of dynamic friction coefficient from 0.3 to 0.5 increases the value of interfacial shear strength almost four times, to reach a value of approximately 26 MPa for the TPU-steel cord composite. The weak interface can be explained by the lower degree of physical interlocking between PP and the steel cord due to the relatively low surface energy (20 mN/m) of this polymer according to the values provided in Table 3 [20-21]. These results suggest that steel cord reinforcement works better with some polymers but not all from a mechanical adhesion standpoint.

3.2 Finite Element Analysis to Reproduce Pull-out Experiment

FEA was used to reproduce the experimental curves for pull-out of a steel cord from the thermoplastic matrices. A quad-symmetrical model was used to reproduce the experimental pull-out test (Figure 12), because a cylindrical cord is embedded in the thermoplastic matrix. An axial displacement was applied on one face of the cord while recording the pull-out force. The coefficient of friction and bond strength obtained by experimental data and properties of the matrix, namely the elastic modulus and Poisson's ratio, were input for the different polymers. Both the steel cord and the polymer matrix were built using 3D elements in ANSYS 8.0 (SOLID185) with 8 degrees of freedom for each. The mesh was mapped by hexagonal elements. For the interface, CONTACT 174 element was used. These elements have 8 degrees of freedom and are used to define surface-to-surface contact between the cord and the matrix. The contact surface is associated with the polymer and the target surface with the steel cord.

With the use of contact elements in the finite element model, the sequence of failure at the interface was determined (Figure 13). Figure 13 (a-b) considers the best performing (TPU-steel cord) to the worst (PP-steel cord) cases tested. Prior to loading, the surfaces are in perfect contact. Once the load is imposed three states can be observed, namely - sliding, sticking and opening. The distribution of these states across the surface leads to the debonding. The contact state can be used to predict a strong or weak interface. A strong interface is mainly composed of a sticking area, contact elements penetrate into the target surface with high degree of mechanical bonding on the surface. The sticking area (red color) indicates enhanced mechanical bonding.

Figure 13 (c-d) represents the stress distribution across the interface on both polymer matrix and steel cord surfaces with maximum stresses values of 0.94 MPa on the PP matrix and almost insignificant of 17 Pa on the steel cord. The stresses on the polymer surface are radial and can be explained by the deformation of the matrix due to the axial load applied to the cord during the pull-out process. Higher matrix deformation is observed for polymers with low stiffness (i.e. PP), thus higher matrix deformation generates higher interfacial stresses. On the other hand, the stress generated at the surface of the cord is parallel to the direction of the applied force; and because the stiffness of the material is much higher than the matrix, the deformation is insignificant in comparison with the deformation of the polymer.

The FEA results show that interfacial friction provides additional resistance to debonding and frictional sliding. With increase in interfacial friction, an increased force is required to pull-out the cord. Thus, for μ=0.3 the debonding load reaches 150 N and for μ=0.5 the same value increase to 750 N. Figure 14 shows two regions in each curve dur-

ing the pull-out process: the bonded region corresponding to elastic deformation (interface is fully bonded) and a frictional sliding region where the fiber is debonding from the matrix and the frictional force supports the interface joint. The effect of the matrix is also observed from Figure 14. Improved interfacial bonding with the steel cord results in higher peak load, thus, the steel cord bonding to the TPU is the best, followed by PA6 and then PP. FEA indicated that the effect of changing the friction coefficient on the model has a bigger effect on the maximum pull-out force than the effect of changing matrix stiffness as input value.

The pull-out behavior of steel cords from thermoplastic matrix is seen to follow the Coulomb friction model. The model explains the effect of shear resistance, friction coefficient and matrix stiffness to the shear stresses along the interface between the matrix and the cord.

Figure 15 compares the pull-out curves obtained by the experimental data and the FEA. The model captures the elastic and debonded zone but not the intermediate zone when there is partial bonding between the cord and the matrix. The debonding peak (maximum) appears to be premature in the finite element curves. Despite this, the values for the peak force are in close agreement between the model and experiment. The experimental debonding load for PP was 140N versus the FEA of 150N with 6% of discrepancy. For PA6, the debonding load was 270N versus 310N and for soft TPU was 650N versus 750N by the model with 13% in difference. The discrepancy between the model and the experiments can be attributed to the material interfaces and local variations that are not considered in the model. Furthermore, elasto-plastic behavior is not included in the model, which affects behavior in the case of soft TPU. Other similarities in both

the experiment and the FEA curves correspond to the slopes before (elastic zone) and after the debonding load (sliding zone) for all three cases.

According to the model adopted by Equation 1 to characterize the interface, three parameters can affect the value of interfacial shear strength: the cohesive (bond strength), the friction coefficient and the matrix stiffness (given by the relationship $\sigma = \varepsilon E$). The effect of these parameters on the interfacial shear strength has been analyzed using 2^3 factorial statistical design [22]. Experimental results have been chosen to determine the influence of coefficient of friction, matrix stiffness and cohesive (bond) strength on the value of interfacial shear strength between thermoplastics and metal surfaces (Table 4, 5). This statistical design plan analyzes the interaction between the different factors at two levels with respect to the response variable (Figure 16). The results of the factorial analysis indicate the effect of each factor and the effect of the interaction between them.

In general, both experimental and numerical (FEA) approaches showed that the friction coefficient was a major factor in increasing the shear strength. Approximately 80% of the shear strength is due to the value of friction coefficient between the material of cord and the matrix. The matrix stiffness contributes to less than 5%, and less than 1% of contribution relates to the initial cohesive (bond) strength. The interaction between matrix stiffness and friction coefficient plays a significant role resisting 12% of the shear. Finally the cohesive bond seems to be an independent parameter with respect to the response variable of interfacial shear strength (Table 6).

3.3 Microstructure after Pull-out Test

The failure processes were examined using scanning electron microscopy. Clean fiber pull-out was observed for the PP and PA6 matrices, whereas shrinkage was observed in the case of polyurethane matrices (Figure 17). Shrinkage may indicate the creation of cross links between the polymer matrix and the cord, while a clean pull-out surface is an indication of poor adhesion between the surfaces and limited mechanical bond during the pull-out process. The microstructure suggests that surface abrasion of the steel cord would enhance mechanical bonding, or alternatively a surface coating or treatment can provide improved mechanical bonding.

Figure 18 shows the interface between cord and matrix for the case of the hard TPU matrix, the adhesion of the resin to the surface of the matrix is poor, the pull-out of the cord is clean, and, no adhesion of polymer is observed around the surface of the metallic cord. The asperity on the surface polymer surrounding the metallic cord may be due to the kink band formation due to the difference in coefficient of thermal expansion during the cool down process.

4. CONCLUSIONS

The interfacial strength between a steel cord and a thermoplastic polymer is significantly influenced by the friction coefficient, matrix stiffness and cohesive bond. The interfacial shear strength between steel cords and thermoplastic polymers is guided by several contributing factors, of which approximately 83.5% was attributed to the friction coefficient, 3% to matrix stiffness, and only 0.5% due to the initial cohesive bond. The interaction between friction coefficient and matrix stiffness plays a significant role with

13% of contribution. No significant interaction between other parameters and the cohesive bond strength was observed.

The experimental studies indicated that PP on steel showed the lowest coefficient of friction, followed by PA6, hard TPU and soft TPU. Similar correlation was observed for the cohesive bond. Thus, an optimum value of interfacial shear strength is suggested for soft TPU with steel cords. The value of interfacial shear strength correlates directly to the friction coefficient; thus, the increase in value of dynamic friction coefficient from 0.3 to 0.5 increases the value of interfacial shear strength almost four times.

Finite element analysis (FEA) was an effective tool to simulate contact problems by the implementation of a frictional model. This approach is based on the simple case of Coulomb friction law to describe the mechanical bonding isolated from other interactions. The FEA captures the peak load for the pull-out process. Both experimental and numerical values are close enough with a discrepancy less than 10%. The debonding load to pull-out the steel cord from PP is 140N from experimental measurements versus 150N for the FEA; for PA6, it is 270N versus 310N and for TPU 650N versus 750N.

ACKNOWLEDGEMENT

Support provided by the Department of Energy (DOE) Graduate Automotive Technology Education (GATE) program is gratefully acknowledged.

REFERENCES

[1] Kocak S, Pidavarti V. Three-dimensional micromechanical modeling of cord-rubber composites. *Mechanics of Composite Materials and Structures,* 7 (2000).

[2] Ebbot T.G. An application of finite element-based fracture mechanics analysis to cord-rubber structures. *Tire Science and Technology,* 24 (1996).

[3] Sun T, Jih C.J. Quasi static modeling of delamination crack propagation in laminates subjected to low velocity impact. *Composites Science and Technology,* 54 (1995).

[4] Srinisavan K. et al. Characterization of damage modes in impacted thermoset and thermoplastic composites. *Reinforced Plastics and Composites,* 11 (1992).

[5] Chawla K. Composite Materials: Science and Engineering. Second edition, Springer Publisher, New York (2001).

[6] Kim J.K, Mai Y.W. Engineered Interfaces in Fiber Reinforced Composites. Elsevier Sciences Publisher, New York (1998).

[7] Ishida H, Koenig J.L. FTIR characterization of the reaction at the silane/matrix resin interphase of composite materials. *Colloid and Interface Science*, 15 (1986).

[8] Suresh S, Needleman A. Symposium on Interfacial Phenomena in Composites: Processing, Characterization, and Mechanical Properties. RI, Newport (1988).

[9] Jiand KR, Penn LS. Improved analysis and experimental evaluation of the single filament pull-out test. *Composites Science and Technology,* 27 (1992).

[10] Furukawa Y, Hatta H, Kogo Y. Interfacial shear strength of C/C composites. *Carbon,* 41 (2003).

[11] Ansys Contact Technology Guide. ANSYS 10.0 version, (2005).

[12] Branstetter J, Kromp K, Peterlik H, Weiss R. Effect of surface roughness on friction in fibre-bundle pull-out test. *Composites Science and Technology,* 11 (2005).

[13] Hardwire LLC. Cord types. Retrieved http://www.hardwirellc.com/cord_types.html

[14] Schmitz T et al. The difficulty of measuring low friction: Uncertainty Analysis for friction coefficient measurements. *Tribology,* 27 (2005).

[15] Hampe A. Marotzeke C. Experimental results of a pull-out test performed with single and multi fiber samples. *Adhesion,* 14 (2002).

[16] Hill M. et al. Tribological evaluation of nanostructures diamond coatings and CoCr against ultra-high molecular weight polyethylene. *Biomedical Materials B: Application of Biomaterials,* 9 (2008).

[17] So C.L, Young R.J. Interfacial failure in poly(p-phenylene benzoic)/epoxy single fiber pull-out specimens.*Composites: Part A*, 10 (2001).

[18] Zhamu A, Zhong W.H, Stone J.J. Experimental study on adhesion property of UHMWPE fibe/nano-epoxy by fiber bundle pull-out test. *Composites Science and Technology,* 14 (2006).

[19] Mega T, Hasewak K, Kawabe H. Ultra high-strength steel sheets for bodies, reinforcement parts, and seat frame parts of automobile: ultra high-strength steel sheets seading to great improvement in crashworthiness. JFE GIHO, (2004).

[20] Solid surface energy data (SFE) for common polymers. Retrieved from http://www.surface-tension.de/solid-surface-energy.htm. (2007).

[21] Diversified Enterprises, Solid surfaces energies. Retrieved from http://www.accudynetest.com/ surface_energy_materials.html. (2005).

[22] Montgomery Douglas C. Design and Analysis of Experiments. 5th Ed, New York, Prentice Hall, (2001).

Table 1. Properties of polymers and steel cord.

Material	Elastic Modulus (GPa)	Tensile Strength (MPa)	Density (g/cm^3)
Polypropylene	1.60	37	0.91
Hard polyurethane	1.65	50	1.23
Soft polyurethane	$6.0x10^{-3}$	35	1.16
Nylon 6	3.0	79	1.14
Steel cord	16.4	370	7.87

Table 2. Shear yield strength of the matrix and the critical loading.

Material	Shear Yield Strength (MPa)	Critical Load (N)	Peak Load (N)
Polypropylene	10	85	140
Nylon 6	15	215	270
Polyurethane	25	370	630

Table 3. Solid surface energies for common polymers [20-21].

Material	Surface Energy (mN/ m)
Polytetrafluoroethylene (PTFE/Teflon)	20
Polypropylene (PP)	30
Polyethylene (PE)	35
Polystyrene (PS)	38
Styrene butadiene rubber (SBR)	48

Table 4. Factors and levels for the statistical analysis on the parameters affecting the interfacial shear strength between the thermoplastic polymer and steel cord.

Response variable	Factor	Level 1	Level 2
Steel to thermo-plastic interfacial shear strength	x: Friction coefficient	Low =0.3	High=0.5
	y: Matrix Stiffness	Low=6 MPa	High=3 GPa
	z: Cohesive Bond	Low =1 MPa	High= 5 MPa

Table 5. Interfacial shear strength values for the combination of levels.

Friction coef-ficient (x)	Matrix Stiffness (y)	Cohesive Bond (z)	Average Interfacial Shear Strength (MPa)	Samples (n)
low	low	low	5.4	3
high	low	low	24.8	3
low	high	low	13.3	3
high	high	low	21.5	3
low	low	high	5.8	3
high	low	high	25.8	3
low	high	high	14.3	3
high	high	high	23.3	3

Table 6. Statistical results of influence of variables on interfacial shear strength.

Factor	Estimated Effect	Sum of squares	Shear Contribution
x	14.16	1202.33	83.5 %
y	2.68	43.17	3.0%
z	1.04	6.48	0.5%
xy	-5.57	186.43	13%
xz	0.36	0.76	0.0%
yz	0.31	0.57	0.0%
xyz	0.03	0.01	0.0%

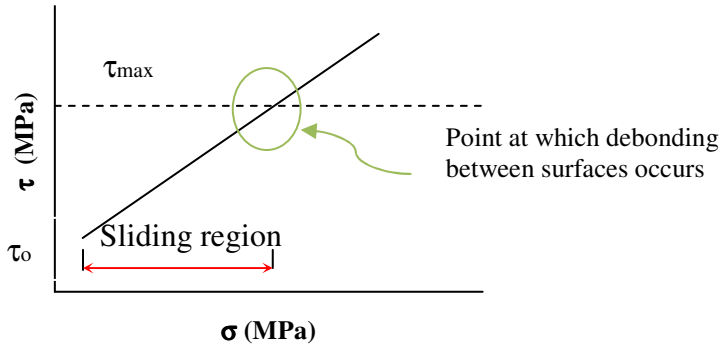

Fig. 1. Frictional shear stresses (τ) dependence on compressive stress (σ) due to the effect of Poisson's contractions of fiber and matrix.

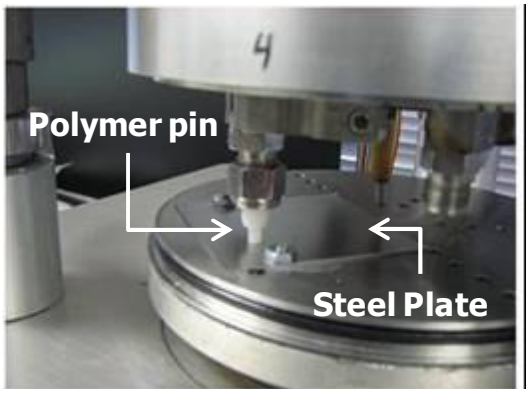

Fig. 2. Pin on disk friction test.

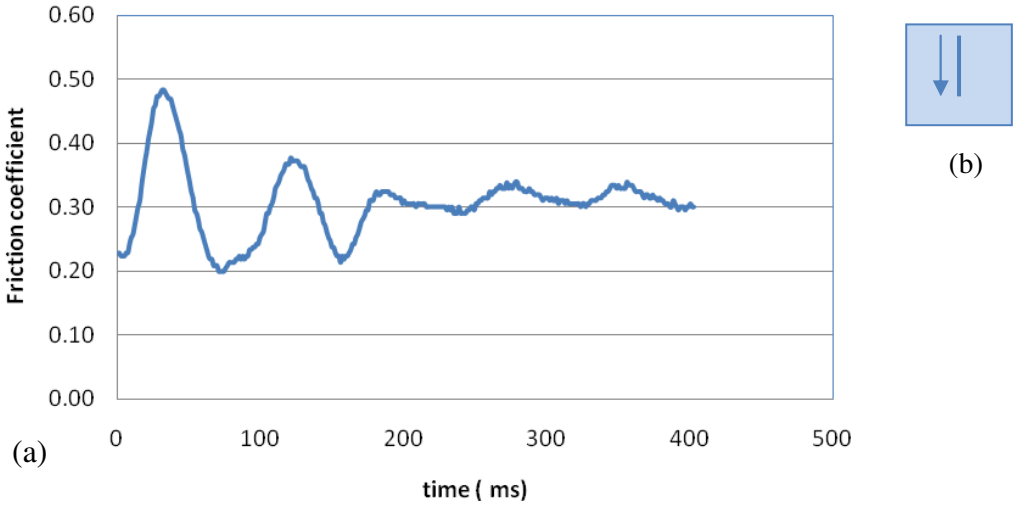

Fig. 3. (a) Friction coefficient data points for linear path of PA6 pin against steel disk, (b) the path is a straight line of 25 mm at sample rate of 1200 points/s with duration of 4 s over one loop count.

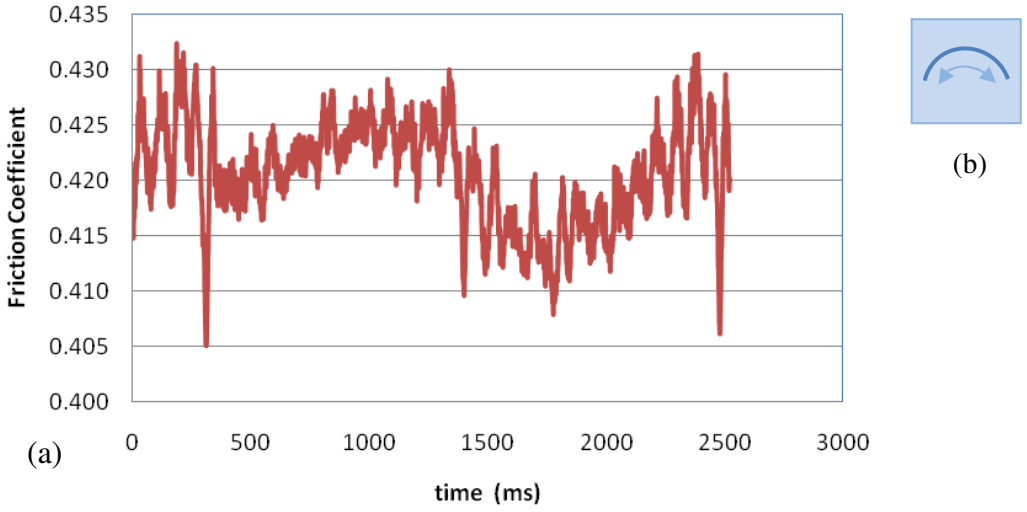

Fig. 4. (a) Friction coefficient data points for semicircular path of hard TPU pin against steel disk, (b) the path is semi-circular with 25.4 mm in radius at sample rate of 1200 points/s. The period per loop is 1500 ms over 2 loop counts.

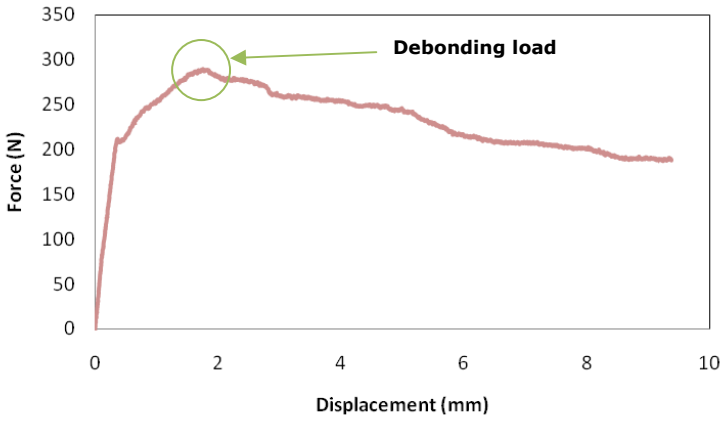

Fig. 5. Force-displacement curve for PA6 matrix and steel cord during pull-out test.

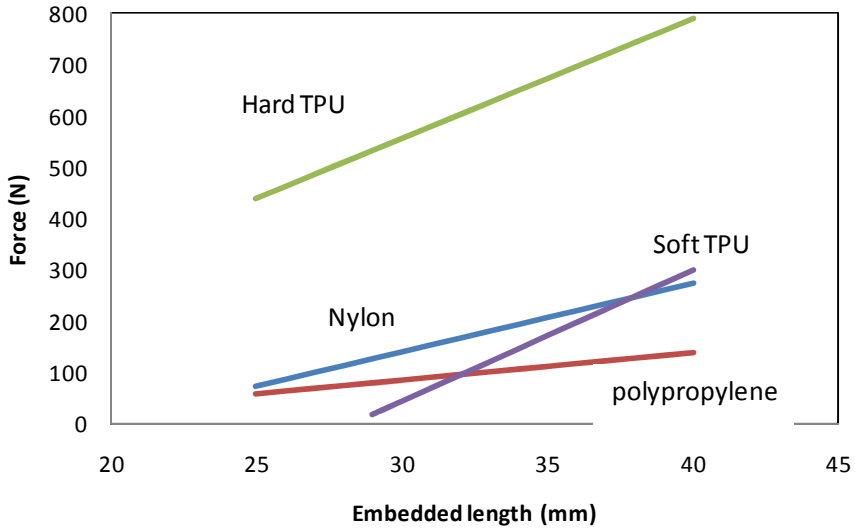

Fig. 6. Force require to pull-out a steel cord from a thermoplastic matrix as a function of embedded cord length.

Fig. 7. Pull-out sample during testing.

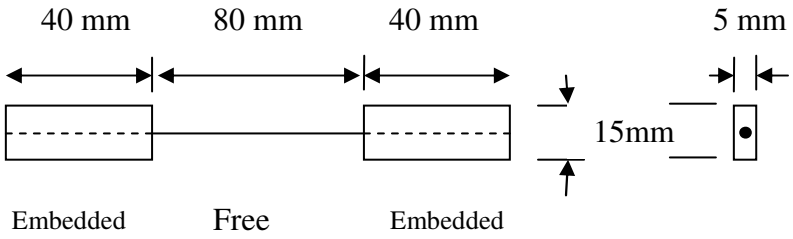

Fig. 8. Schematic representation for a pull-out sample.

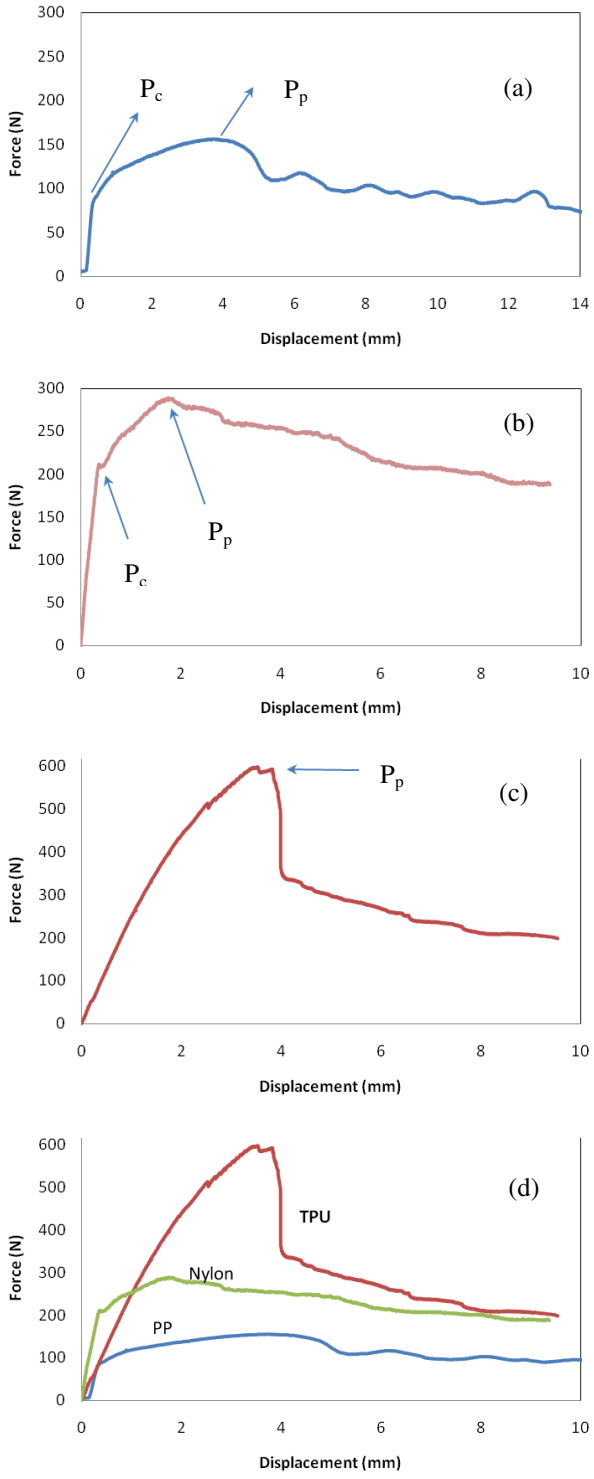

Fig. 9. Pull-out curves indicating critical load (P_c) and peak load (P_p), for (a) PP matrix and single steel cord, (b) nylon matrix and single steel cord, (c) thermoplastic polyurethane and single steel cord, and (d) comparison of different systems.

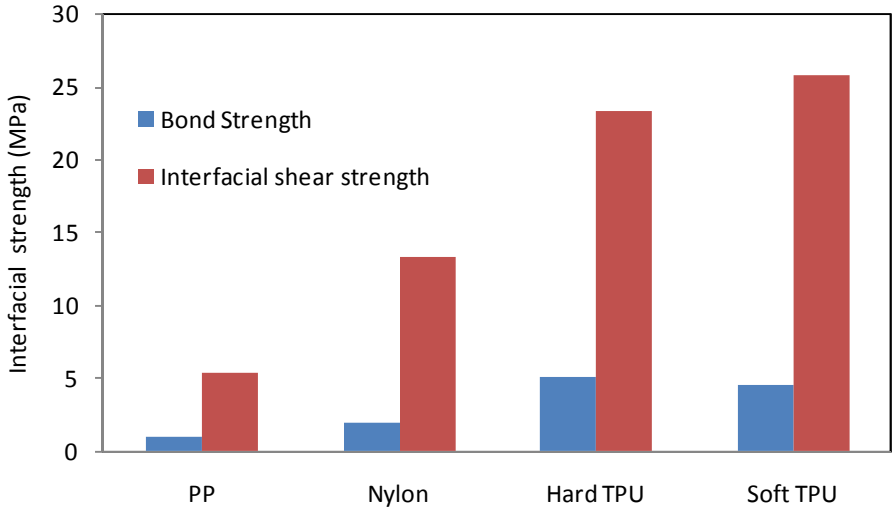

Fig. 10. Cohesive strength and interfacial shear strength for 3XS-steel cord/thermoplastic matrix.

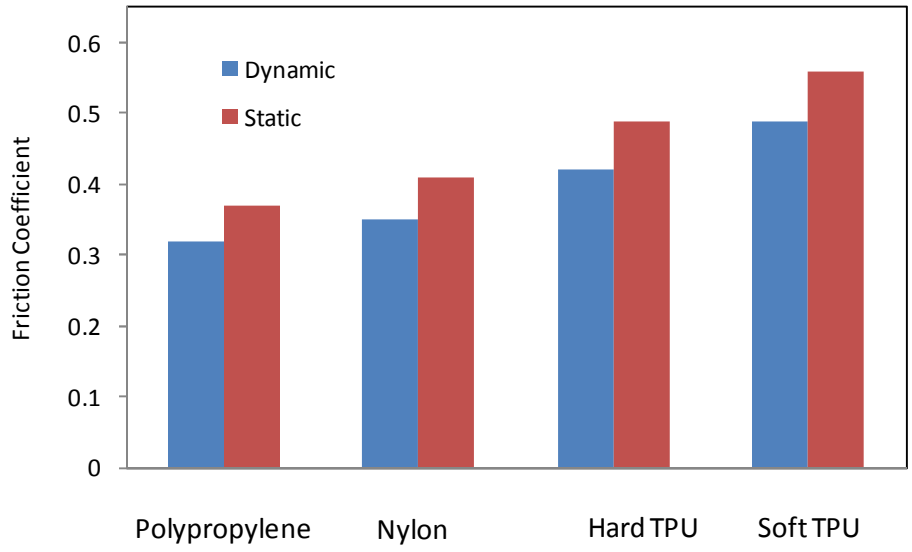

Fig. 11. Friction coefficient between a thermoplastic matrix and low carbon steel.

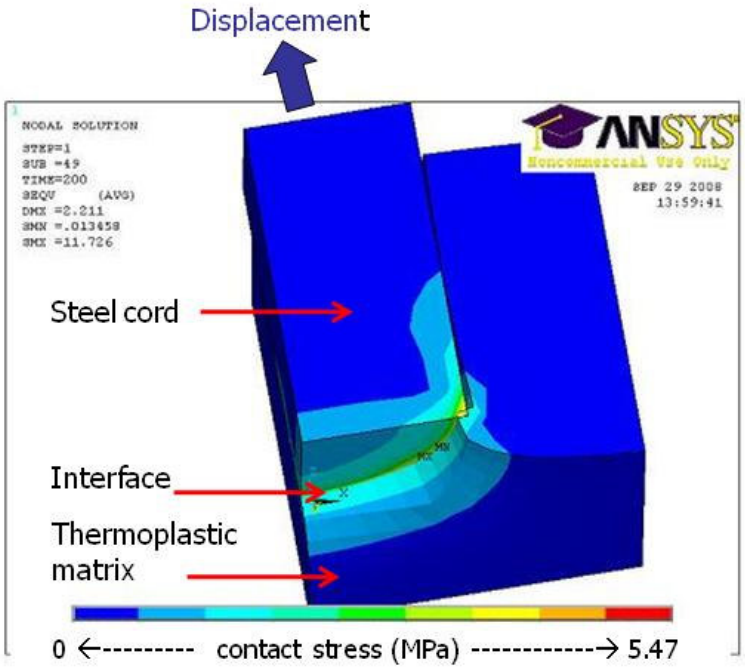

Fig. 12. Quad-symmetrical model for the pull-out process of a steel cord from the thermoplastic polyurethane (TPU) polymer.

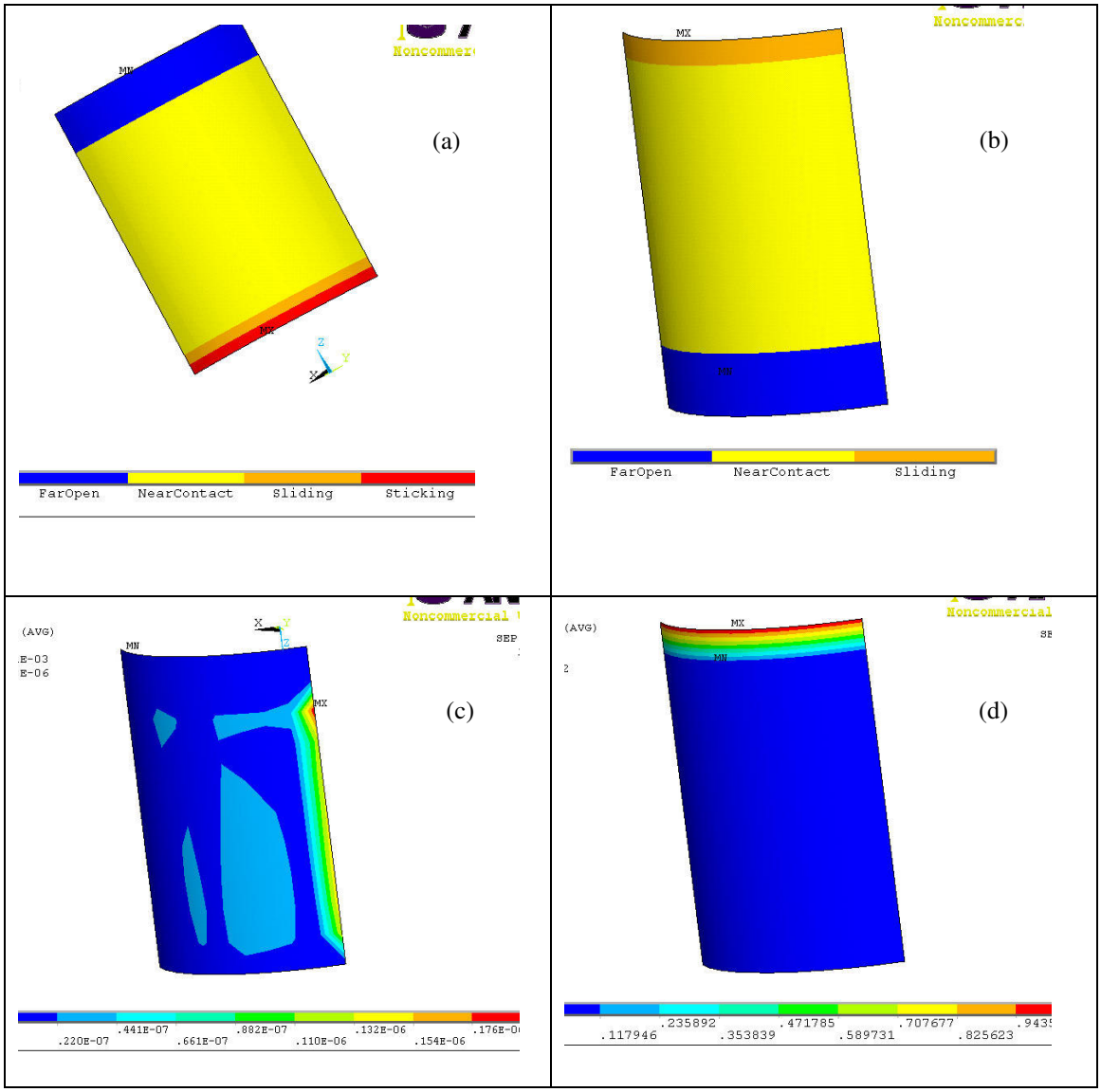

Fig. 13. Contact elements describing the interface behavior for the pull-out process: (a) Contact condition for soft TPU surface for soft TPU/steel cord. (b) Contact condition for PP surface for PP/Steel cord. (c) Stress distribution on steel surface after pull-out force for PP/steel cord. (d) Stress distribution on PP surface after pull-out force for PP/steel cord.

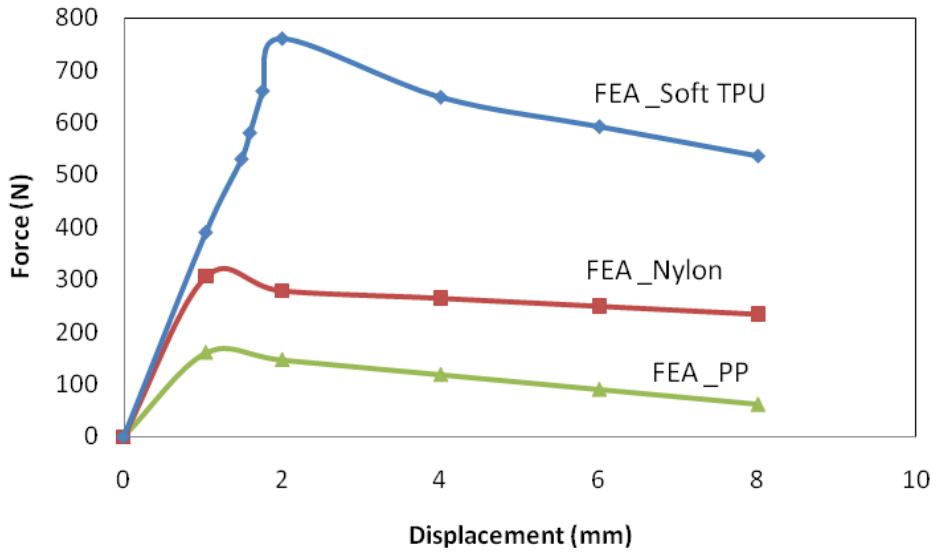

Fig. 14. Pull-out curve using FEA for a steel cord embedded in a thermoplastic Matrix.

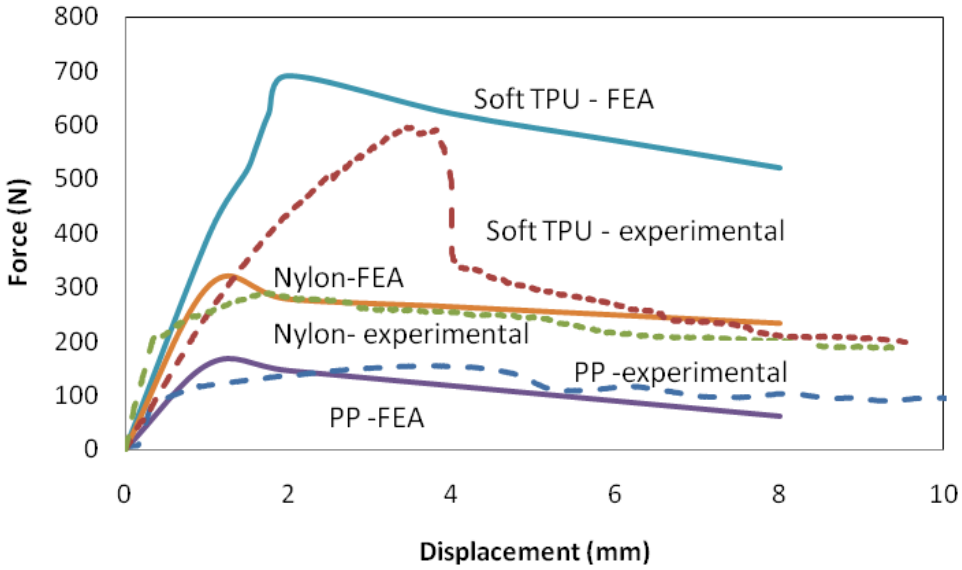

Fig. 15. Comparison of FEA and experimental results for a steel cord embedded in thermoplastic matrix.

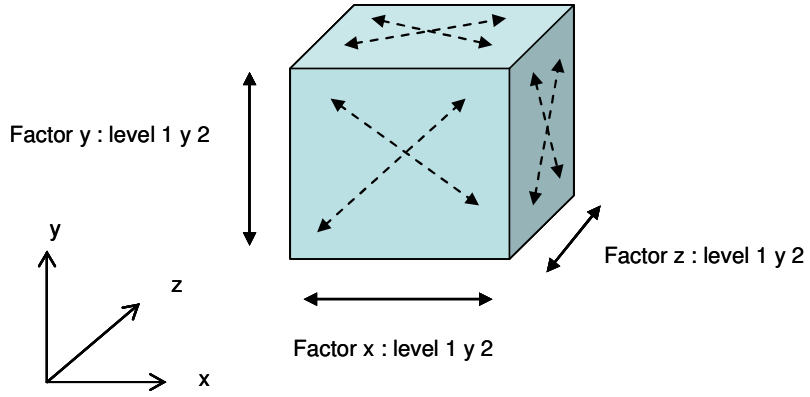

Fig. 16. Geometric interaction for the statistical analysis.

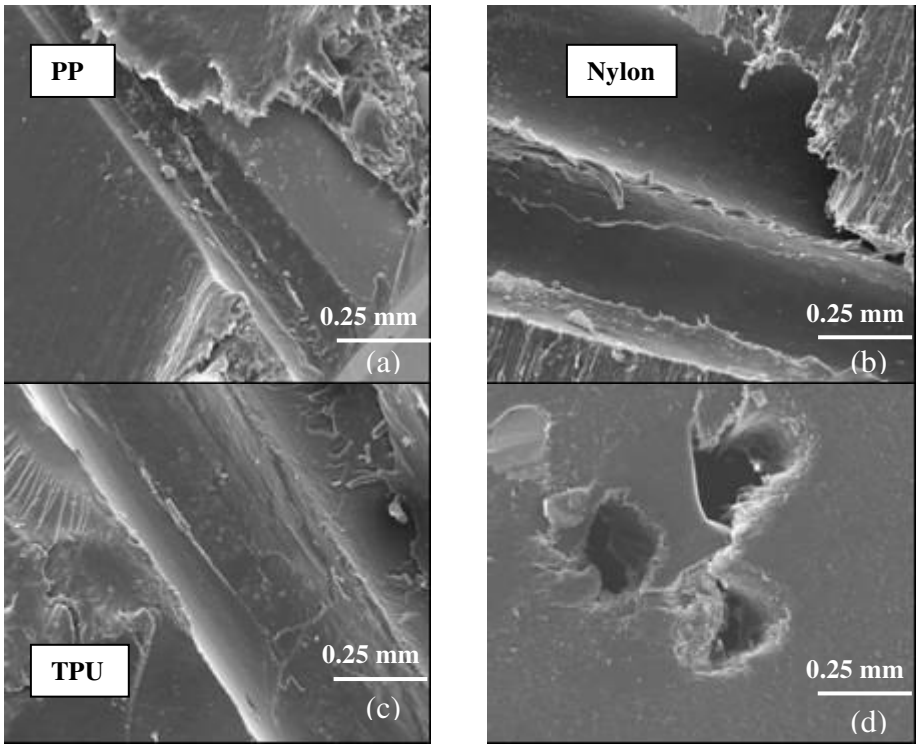

Fig. 17. SEM surface morphology after pull-out of steel cord from different thermoplastics, 150X.(a) PP matrix, (b) nylon matrix, (c) hard TPU, (d) cross section area left from 3XS steel cord.

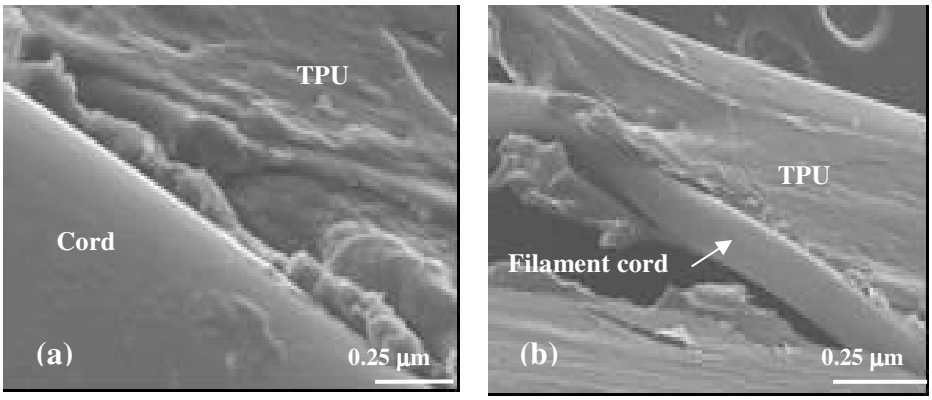

Fig. 18. (a) Interface of hard TPU and steel cord, 1200X, (b) Steel wrapped cord and hard TPU, 300X

MECHANISMS OF INTERFACIAL ADHESION IN METAL-THERMOPLASTIC POLYMER COMPOSITES - EFFECT OF CHEMICAL TREATMENT

CAROL OCHOA PUTMAN, UDAY K. VAIDYA

Submitted to Composites Part A: Applied Science and Manufacturing

Format adapted for dissertation

ABSTRACT

Hybrid materials featuring thermoplastic polymer composites in conjunction with metals can be used as structural materials in military and commercial transport vehicles and for protection of buildings and infrastructure. Constituent thermoplastics and metals have distinct advantages as protective materials; however, metals on their own are heavy. Hence, hybrid materials offer an option as lighter materials. This study investigates the chemical interaction between steel and thermoplastic polymer by reactive adhesives and chemical treatment of surfaces. Adhesion between polymers and steel has been studied by chemical surface treatment. Modification of the surface to create greater surface area, in addition to imparting free radical surface effects to create new surface bonds with introduced chemical functionalities, are the primary approaches for maximizing interfacial adhesion. Plasma-activated chemical vapor deposition (PACVD) is used to impart silicon, carbon and hydrogen radicals to the metal surface. Thermoplastic polymers with chemical modification were used to investigate the effect of polar groups (-NH, -CO= and -OH) and its influence on the surface energy and adhesion properties. In addition, a new alternative is analyzed to improve adhesion by embedding fullerene particles in a thermoset resin. Thus, this study focuses on the effect of surface treatments to improve adhesion between dissimilar materials such organic polymers with metal reinforcement materials. The degree of modification on the polymers is determined by Fourier Transform Infrared Spectroscopy (FTIR) for the absorption of polar groups. Plasma coating is analyzed by Scanning Electron Microscopy and Energy Dispersive Spectrometry (EDS/SEM). The increment in surface energy is determined by function of the contact angle. Surface energy has a direct relationship with the amount of polar groups on the

surface of a modified polymer and free radicals on the metal surface. Higher surface energy correlates with superior interface adhesion. This work establishes the basis that polar groups and free radicals improve adhesion between polymeric (thermoplastics) and metallic surfaces.

Keywords**:** Thermoplastic composites, Metal-Thermoplastic, Adhesion, Protection

1. INTRODUCTION

Thermoplastic composites which have high strength and low weight are becoming more prevalent in automobile, aerospace, medical and electronic applications. The growing demand for high performance thermoplastic-metallic composites has been challenged by the problem of the lack of adhesion between fiber and matrix. Adhesion problems have been addressed by surface treatment [1]. Some of the adhesive mechanisms through which the surface treatments promote interfacial bonding include improvement of wettability, addition of chemical groups and variation of surface topography [2]. Chemical modification of the surface has been successfully applied to increase surface area in addition to imparting free radical surface effects to promote surface bonding. Thus, Huang [3], Funasaka [4] and Dhramarajan [5] analyzed the effect of maleic anhydride modifier to impart polarity to a polyolefin surface, improving the adhesive bonding with aluminum and glass surfaces. Cai [6] demonstrated that grafting of PP with acrylic acid (AA) not only improves the impact strength of PP but also the adhesion to polar substrates; however, the industrial application is limited because of the total treatment cost. Zhang [7] implemented oxidation etches on carbon fibers to increase the shear strength with epoxy matrix with the compromise of decreasing the tensile strength. Ishida [8] used silane coupling agents between glass and polymer matrices, and reactive amine groups between aramid fibers and epoxy resin to create covalent and hydrogen bonds at the interface. Kim [9] studied the effect of fiber-matrix interface and the influence of silane agents on intermolecular fracture and the impact performance of woven-glass fabric composites. A brittle interface causes unstable crack propagation and low fracture toughness values. The use of silane surface modifiers resulted in improved impact performance. Cerny and Mo-

litor [10, 11] investigated the use of adhesives as intermediate layers to promote a durable polymer composite-metal bond, using titanium alloy and fiberglass composite as substrates. Itoi and Yamada [12] studied the effect of carbon fiber surface modification by oxidation with nitric acid and hydrogen peroxide on adhesion with polyethernitrile. Laminates made with treated fibers showed improvement on interlaminar shear strength and transverse flexural strength**.** Byung-Jae Park [13] analyzed the anodic oxidation treatment of carbon fibers to determine the effect on their interlaminar shear strength for epoxy resin matrix composites. Sodium bicarbonate electrolyte was recommended as an effective electrolyte for changing surface functionalities and improving interfacial adhesion between carbon fibers and epoxy-resin matrix. Chen [14] found that carboxymethylation, a polar group introduction on Kevlar fibers, is useful to increase fiber/matrix adhesion with poly (methyl methacrylate) matrix. Thus, previous research suggests that it is possible to improve the adhesive bonding between dissimilar materials across the interface.

This paper studies the effect of surface treatment to improve the adhesion of thermoplastic polymers to steel reinforced surfaces. Plasma treatment is used to add reactive molecules (Si, H and C) on the surface of steel, maleic anhydride is used to add carbonyl groups (–C=O) on PP with the purpose to create reactive sites that promotes bonds between surfaces. Furthermore, this study analyzes the adhesion of steel with not only PP but also with soft thermoplastic polyurethane (TPU), PP modified by maleic anhydride (PP-MA) and a new generation of nano-fullerene epoxy resin with the objective to find mechanisms of bonding and finally enhance the bond at the interface between metal-polymer surfaces. Single lap shear joint testing was then used to assess interfacial adhe-

sion for the different cases in the study. This work establishes the basis to promote adhesion between polymer and metal surfaces by the addition of chemical functional groups and elements that attach between the metal and polymer surfaces to create a stronger interface.

2. MATRERIALS & METHODS

2.1 Materials

The materials used and select properties are summarized in Table 1.

2.2 Contact Angle Test

The determination of contact angle on the different surfaces was performed using 100μL of distilled water. Each surface was dried at 90^{o}C and cleaned with methanol before the test to avoid contamination interference. The contact angle values were estimated by analyzing an image of a water droplet using a Reme Hart Goniometer (model 100-00115) with a Sony CCD B/W digital camera module (model XCD-X700 with dire-I 3.0 software). The apparatus was used to visualize the tangent (right and left) of the drop and the three-phase points. For each material, five drops of water were placed along the surface to obtain the average of ten readings for each sample. A standard deviation between measurements less than 3% was the higher limit to accept the value. Others parameters followed the ASTM D5946 and ASTM D5725.

2.3 Lap Shear Strength Test

Lap shear strength tests were performed to analyze the effect of surface roughness, polymer type and metal surface treatment to the bond strength between metal and polymer. ASTM D3164M and D4896 were use to determine parameters and interpret results. ASTM D2093 and D2651 were used to prepare metal and polymer surfaces prior to the adhesion. The bond strength was calculated as the failure load divided by the fracture surface area. A schematic representation of the sample is shown in Figure 1.

Six samples of each case were tested in tensile load with a Mechanical Testing System (MTS Systems Corp., Eden Prairie, MN, USA) under a displacement rate of 1.3 mm/s until failure (see Figure 2). To analyze the effect of roughness, steel metal samples were ground to 600, 400, 240 and 120 grit finishes and bonded to PP with a 600 grit surface finish. An average roughness was obtained for each case using a contact profilometer, Hommel tester T500. Once the optimum roughness was found, steel specimens were tested to bond with different polymers, PPMA, soft TPU and phenol formaldehyde glycidyl ether resin with carbon nano fullerenes (CNT epoxy). Once the polymer with the highest bond strength was found, steel specimens with plasma treatment, silicon coating (Si-steel) and amorphous hydrogenated carbon coating (a-C:H-steel), were tested to evaluate the metal surface modification. Table 2 shows the variables for the different cases in the study.

2.4 Plasma Treatment on Steel Surface

Surface modification and coating were explored using a proprietary amorphous, hydrogenated carbon coating vessel from Plasma Electronic, GmbH [15]. In particular,

the vessel utilized a silicon-based undercoating to improve the adherence of an a-C:H coating. The deposition method is Plasma Activated Chemical Vapor Deposition (PACVD). Under a controlled low atmosphere of reaction gasses, the vessel induces a voltage bias of approximately 500 volts. The steel to be coated is in contact with the cathode target and an even, stable, high energy plasma of reaction elements is formed on the entire cathode surface. The kinetics of the plasma allows Chemical Vapor Deposition (CVD) to occur at much lower temperatures. The properties of the coating vary based on the reaction gas used and other processing parameters. The temperature of the process is 200ºC; in consequence, no thermal impact is expected on the material. Some processing parameters are showed in Table 3 and a schematic representation of the process is showed in Figure 3.

The typical processing parameters were set to deposit a 0.5μm adhesive layer of silicon, silicon carbide, and carbon via a tetramethyl silane reaction gas. The process then transitions the partial pressure of the adhesive layer gas with the top layer gas under constant pressure. The top layer is deposited via methane gas to a total thickness of 2.0 μm. The process was modified to yield some samples with only the adhesive silicon-rich layer and tested along side typically processed, fully coated samples and uncoated samples. Previous research [8, 16, 17-20] showed the reactivity of silicon to be favorable in making reactive groups that would adhere to the iron as well as the polymer matrix material; therefore, the adhesive layer was investigated separate from the complete carbon coating.

3. RESULTS & DISCUSSION

3.1 Molecular Characterization

3.1.1 Functional Polar Groups in Polymers

Fourier Transform Infrared Spectroscopy (FTIR) was used to analyze the composition of the thermoplastics used in the study. Because chemical bonds absorb infrared energy at specific frequencies (or wavelengths), specific functional groups of the polymer are determined by the spectral locations of their IR absorptions (peaks).

Figure 4 compares the FTIR spectra of neat PP and modified PP with maleic anhydride (PPMA). The below spectra shows four new absortion peaks at 2348, 1638, 997 and 675 cm^{-1}: the first and second ones correspond to C=O carbonyl functional group, the third one to C-O stretch anhydride functional group, and the last one to C-H bend alkene functional group. These groups constitute the maleic anhydride molecule (MA) [21]. The MA content in PP-MA was calculated by Equation 1, where A_{997} is the absorbance of the anhydride group at 997 cm^{-1}, d is the thcikness (mm) of the sample, and K is a constant (= 0.25) detected by calibratrion of the known MAH content of PPMA polymer.

$$\text{MA wt\%} = K (A_{997}/d) = 0.25 (0.07/2) = 0.875 \text{ wt \%} \qquad \text{Eq. (1)}$$

Figure 5 compares the FTIR spectra for two types of TPU - soft TPU and hard TPU with the purpose of explaining why TPU enhances good adhesion to the steel surface. Thus, at 3298, 1528 and 1504 cm^{-1}, -NH amide functional group is observed. Carbonyl groups from ester –C=O are located at 1727 and 1698 cm^{-1}; functional carbons of

aromatic rings –C=C are found at the range of 1600-1475 cm^{-1}; and, finally, at 2341 cm^{-1} is the peak of isocyanate functional group –N=C=O. All the described peaks are active sites able to react with the steel surface due to the polarity and the double bonds [22-23]. The intensity of the –CH alkane peaks and –C=O carbonyl peaks at 2919-2848 and 1727-1698 cm^{-1} determine the amount of crystalline and amorphous regions in the polyurethane and generates the difference between soft TPU and hard TPU. For soft TPU, the higher content of amorphous regions correlates with the higher intensity of the peaks mentioned above.

3.1.2 Metal Coating Characterization

EDS/SEM is employed to qualitatively characterize the modified surface of steel by the Plasma Activated Chemical Vapor Deposition treatment (PACVD). Figure 6 shows the steel as as-received material before treatment. The spectrum reveals only iron (Fe) peaks from steel and the topography of the surface has a roughness value, R_z, of 1.92 μm. Three-dimensional surface profiles of coated steels with the amorphous hydrogenated carbon (a-C:H) and silicon (Si) are shown in Figures 7(a) and 8(a). The pictures reveal differences in coating thickness and surface roughness. Thus, the Si coating exhibits a roughness of 1.74 μm with 0.5 μm in cross sectional thickness. The a-C:H coating results in a roughness of 2.15 μm with 2.0 μm in cross sectional thickness. Figure 7(b) confirms the presence of SP_3 bonded carbon on the coating layer shown as the first peak in the spectrum. Carbon atoms on the steel surface might create covalent bonds with reactive groups on the polymeric surface. Figure 8(b) shows the composition of the coating on the steel surface revealing the presence of Si as the second peak in the spectrum. The coating

is thin as mentioned above; therefore, the spectrum obtained by EDS/SEM technique detects also the main component of the steel (iron). Silicon is a useful element for anchoring polymeric layer to a metal substrate [11]. The Si coating contains Si-O bonds that react with hydroxides and hydrocarbon groups to link with the polymeric material.

3.2 Contact Angle & Surface Energy

Adhesion between surfaces to be joined might proceed with the chemical attraction of specific sites. The chemical attraction is due to Van der Waal forces, ionic interactions, or covalent interactions. Consequently, the wettability of the surface by a liquid is an indication to obtain adhesion; however, it may not be a sufficient condition in forming strong interface bonds. To measure wettability, contact angle was determined for different polymers and steel with and without coating treatment; the surface energy was determined for each material. Higher surface energy generates better adhesion to substrates with similar polarity. A contact angle equal to or greater than 80º means that the surface is hydrophobic, so the material might repeal polar substances. In general, polymers are hydrophobic and have low surface energies. Table 4 shows values of surface energy for common materials for both matrices and fibers.

3.2.1 Polymer Surfaces

In general, polymers have low surface energy with contact angles above 80^{o}; a contact angle below this value is an indication that the polymer has been treated to improve its adhesion [26]. An angle close to 110^{o} implies a hydrophobic behavior of the polymer, and an angle close to 70^{o} is related with a hydrophilic polymer [27]. Figure 9 shows the

optical measurements of contact angle for the polymers in the study. As predicted, PP has high contact angle of 84º, followed by PPMA with 79º and soft TPU with 76º. Unexpectedly, the resin with carbon nano fullerenes (CNT) has the highest value from all the polymers with 110º; a possible explanation is given below.

There exists a relationship between the contact angle of the water on the polymer surface and the surface energy of the polymer which can be seen in Figure 10. When the drop of water rest on the polymer surface, the surfaces acting at the interfaces must balance; these forces represent surface tensions acting in the direction of the surfaces. The force between the water droplet and the polymer surface is called wetting tension, γ_c, and is described by the relationship given in Equation 2 [28]:

$$\gamma_c = k_1 \gamma_{GL} - (1-\cos\theta)/ k_2 , \text{ where} \qquad \text{Eq. (2)}$$

γ_c : wetting tension
γ_{GL} : surface tension of the gas-liquid interface = 72 dyne/cm for water
k_1 =0.54 and k_2= 0.4

Figure 11 compares the results of surface energy and contact angle for the four polymers in the study, PP, PPMA, soft TPU and CNT resin. As expected, PP has the lowest surface energy (35 dyne/cm) due to the saturated polymer chain without any polar groups to react. Functionalization of PP is achieved by maleic anhydride to create -CO= reactive polar groups; these polar groups increase wettability of the polymer and consequently adhesion with the metal substrate.

A normal surface energy value for phenolic resin is 47 dyne/cm [1]; thus, the fact that the phenolic resin is functionalized with fullerene particles has a dominant effect on the surface energy decreasing the value to 29 dyne/cm. Despite the large interfacial area of

fullerenes, CNT can easily agglomerate, bundle together and entangle on the resin [29-30], leading to many defect sites and limiting the efficiency to promote adhesion, which can explain the drastical drop in the surface energy of the resin. To corroborate this statement, Figure 12 (a) provides an SEM micrograph showing the cross section of cured CNT-epoxy after failure with small brighter spots that suggest the presence of agglomerates; a closer micrograph Figure 12 (b) reveals the agglomeration of CNTs.

Figure 13 (a-b) illustrates the correlation between contact angle and surface energy to the bond strength measurements between the different thermoplastic polymers and steel. Higher surface at the polymer reveals superior bond strength with steel, which is measured by lap shear strength test. The value of surface energy has direct relationship with the amount of polar groups or reactive ions at the surface of the polymer; thus, PP, which lacks of free radicals in its polymeric chain, has the lowest surface energy. Soft TPU with –NH and –C=O functional groups and PPMA with C=C,-C=O functional groups have similar surface energy close to 38 dyne/cm, which allows the polymer to attach to steel. A surface energy above 36 in polymers is an indication of good adhesion with fibers of different materials (i.e. carbon, glass, Kevlar) [10, 14, 26-27].

Processing conditions also play a role in the surface energy of the polymer. Specimens of PP were fabricated by compression molding under two different pressures, 110 and 550 psi. The contact angle was measured for both specimens (Figure 14); the PP processed at higher pressure has the lower contact angle with a surface energy increased in 16%. These can be explained due to less surface defects giving a smoother surface [31]. As the surface of the polymer is smoother, the contact angle is smaller, which means high wettability and subsequently the possibility for better adhesion.

3.2.2 Steel Coated and Uncoated

Usually, metals have high surface energy, however to increase wettability, surface treatment was employed to impart reactive site for bonding with polymeric materials. Figure 15 shows the contact angle for steel coated and uncoated. Comparing the contact angle of the uncoated steel with Si coated steel and a-C:H coated steel, Si coating provides a surface to steel with lower value for a contact angle of 79º, however the difference between the three cases is almost insignificant (82º, 79º, 80º respectively), increasing the surface energy only by 6% according to Figure 16.

3.3 Lap Shear Strength

Bond strength of polymer-metal adhesion was determined by single lap shear test. The experimental matrix used for the analysis is described above in Table 2 and the results are shown from Figure 17 to Figure 21. Figure 17 shows the effect of mechanical interlocking. The mechanical interaction at the interface is related to the interlocking effect between two surfaces and is significantly influenced by the friction coefficient, matrix stiffness and cohesive bond. In previous research [32], the variables that play a significant role to the mechanical interlocking were friction coefficient with 83.5% of contribution over the matrix stiffness and initial cohesive bond with 3% and 0.5%, respectively. An interaction between the first two contributes to the 13% remaining. Imparting roughness to a surface increases friction coefficient; thus, the mechanism of adhesion occurs when a rough steel surface is brought into contact with the melting (flowing) polymer. The polymer is able to fill the rough surface and create relatively strong mechanical bonds. As the steel surface roughness increases, the bond strength with PP increases.

Figure 18 compares the bond strength of steel with different type of polymers. According to the results, PPMA and TPU bond with similar strength to steel, which confirms the previous analysis of molecular characterization and wettability of these polymers. PPMA exhibits bond strength of 3.18 MPa vs 3.25 MPa for soft TPU. Maleic anhydride modified PP is close to the double value on bond strength compared with neat PP (3.18 vs. 1.47 MPa). The CNT resin has an unexpected low value for bond strength with steel equal to 2.26 MPa; this value could be due to porosity in the resin that generates failure points at the interface.

PAPCVD on the metal surface was used to add specific molecules on the surface that can diffuse into the bulk of the polymer surface and set up a stronger interface. This interface represents the elimination of the joining surface and replaces it with a relatively smooth gradient from the metal to the polymer. Thus, molecules of silicon, hydrogen and carbon could interact with the surface of PPMA. The surface of PPMA offers active radicals of -C=O that interact with the molecules on the steel surface after the plasma treatment. Figure 19 shows the effect of plasma treatment on steel on the bond strength of PPMA. The bond strength is not only a function of the roughness of the steel surface but also of the type of coating on the steel. Silicon coating promotes better adhesion; however, carbon hydrogenated coating decreases the bond strength with PPMA.

Figure 20 illustrates the efficiency of silicon to promote adhesion between organic (polymers) and inorganic materials (metals); in this case, the bond strength between steel and PPMA increases from 2.06 MPa to 3.03 MPa, approximately 50% stronger than the steel without silicon coating. In contrast to that, the hydrogenated carbon coating produces the opposite effect, thus the bond strength with steel becomes weaker from 2.06

MPa to 1.33 MPa, decreasing 35% in strength. According to Mishra [16], the general structure for the silicon reactive group is XnSiR4-n, where R is an organo functional group chosen for its compatibility with the organic overlayer and X is a hydrolyzable group that eventually forms a metal-siloxane bond (Si-O-metal). On the other hand, despite the reactivity of carbon to bond with polymeric chains, the a-C:H coating on steel failed to increase bond strength between the metal and the polymer surface. This could be explained to the saturation of carbon with hydrogen or oxygen on the steel surface. No quantification of these elements was determined in the molecular characterization.

According to Wolf [1], surface energy of the matrix material heavily influences the composite surface tension and consequently the adhesion between matrix/fiber. Figure 21 shows the effect of treatment to the matrix material as well as to the fiber material (steel). As can be seen, the matrix treatment doubled the bond strength; and the steel treatment (fiber material) increases the bond strength by a factor of 1.6; then, both matrix and fiber are affective to increase adhesion at the interface.

3.4 Adhesion Cohesion Studies

The failure after tensile load for the single lap shear test occurred under two different modes: cohesive failure, where debonding occurred in the molecules of the polymer, and adhesive failure, where debonding occurred at the interface between the polymer and the steel surface. Figure 22 shows both types of failures obtained during the test. A cohesive failure indicates a stronger bond at the interface, which is a desirable condition to reach superior properties in a composite such as interlaminar shear strength and delamination resistance. Figure 23 shows the percentage of cohesive failures having a direct relation-

ship with the strength of the interfacial bond. As the cohesive failure rate increases, the bond strength increases for most of the polymers in the study, with the exception of soft TPU. The bond failure between soft TPU and steel is 100% adhesive. Despite the type of failure, the bond strength of soft TPU is relatively high, which makes predicting the failure mechanism particularly difficult.

4. CONCLUSIONS

Functionalization of polymers has been analyzed in this work. PP one of the most used polymers due to its low cost, good mechanical properties and easy processing can be modified with maleic anhydride to add polar functional groups and improve adhesion with steel. Thermoplastic polyurethane is also a good option to generate adhesion with metal surfaces due to the high content of polar groups that increases wettability of the polymer, even though the mechanical properties are lower. Adversely, epoxy with fullerenes failed in the purpose of increasing adhesion mainly due to the presence of surface voids during the curing process.

Silicon surface coating provides better adhesive properties between metal-to-polymer surfaces. Specifically, this technique appears to be an effective and efficient method to promote better adhesion between steel and PPMA. However, experiments show no correlation between surface energy and bond strength for this type of surface treatment; in fact, for coated steel, wetting tension on the steel surface is not an indication of potentially better adhesion. It is possible that diffusivity is the mechanism of adhesion between coated steel and PPMA.

A correlation between contact angle in the type of polymer and bond strength was found to be directly proportional, which indicates that polar groups on the polymer surface dominate the adhesion with steel and can be predicted by the value of contact angle. Also, for the polymers in the study, the effect of wettability dominates the ability to adhere on steel.

ACKNOWLEDGEMENT

Partial support provided by Tank Automotive Research Command (TARDEC), and the Department of Energy (DOE) Graduate Automotive Technology Education (GATE) is gratefully acknowledged.

REFERENCES

[1] Wolf R.A, Enercon Industries Corporation. Improving adhesion performance between low surface tension composite and dissimilar substrates. ANTEC (2006).

[2] Jang B. Advanced Polymer Composites: Principles and Applications. ASM international, Chap 3 (1994).

[3] Huang X, Birman V, Nanni A, Tunis G. Properties and potential application of steel reinforced polymer (SRP) and steel reinforced ground (SRG) composites. *Composites: part B*, 36 (2005).

[4] Funasaka T, Ashihara T, Maekawa S, Ohno S. Adhesive ability and solvent solubility of polypropylene-butane co-polymers modified with maleic anhydride. *Adhesion and Adhesives*, 19 (1999).

[5] Dhramarajan N, Datta S. Compatibilized polymer blends of isotactic polypropylene and styrene-maleic anhydride co-polymer. *Polymer*, 36 (1995).

[6] Cai C, Shi Q, Li L, Zhu L, Yin J. Grafting acrylic acid onto polypropylene by reactive extrusion with pre-irradiated PP as initiator. *Radiation Physics and Chemistry*, 15 (2008).

[7] Zhang Z, Liu Y, Huang Y, Liu L, Bao J. The effect of carbon-fiber surface properties on the electron-beam curing of epoxy-resin composites. *Composites Science and Technology*, 27 (2002).

[8] Ishida H, Koenig J.L. FTIR characterization of the reaction at the silane/matrix resin interphase of composite materials. *Colloid and Interface Science*, (1986).

[9] Kim Jang Kyo. Impact and delamination failure of woven fabric composites. *Composite Science and technology*, (2000).

[10] Molitor P, Young T. Adhesives bonding of a titanium alloy to a glass fiber reinforced composite material. *Adhesion & Adhesives*, 22, (2002).

[11] Cerny J, Morscher G. Adhesive bonding of titanium to carbon-carbon composites for heat rejection systems. NASA, Glenn Research Center, (2000).

[12] Itoi M, Yamada Y. et al. Effect of surface treatment of pitch-based carbon fiber on mechanical properties of polyethernitrile composites. *Polymer Composites*, 13, (2004).

[13] Soo-Jin, Byung-Jae. Electrochemically Modified PAN Carbon Fibers and Interfacial Adhesion in Epoxy-resin Composites. *Materials Science Letters*, 18 (1999).

[14] Chen M, Ueta S, Takayanagi M. Improvement of Adhesion of kevlar fiber to poly(methyl methacrylate). *Polymer*, 20 (1994).

[15] Plasma-Electronic GmbH. http://www.plasma-electronic.de/en/index.php

[16] Mishra S, Weimer J. A Comparative analysis of trimethylmethoxy and trimethylchloro silanes bonding on copper surfaces. *Vacuum Science & Technology A,* 13 (1995).

[17] Kumar Devendra et al. Microwave atmospheric pressure plasma for surface treatment and reactive coating on steel surfaces. *Surface & Coatings Technology*, 201 (2006).

[18] Evans Ryan et al. The effects of structure, composition, and chemical bonding on the mechanical properties of Si/a-C:H thin films. *Surface and Coatings Technology,* 157 (2002).

[19] Tsutomu Kaneko et al. FTIR analysis of Si-a-C:H films grown by plasma enhanced CVD. *Crystal Growth,* 275 (2005).

[20] Peelamedu Ramesh et al. Microwave atmospheric pressure plasma for surface treatment and reactive coating on steel surfaces. *Surface & Coatings Technology,* 201 (2006).

[21] Wang Z, Hong H, Chung C. Synthesis of maleic anhydride grafted polypropylene with high molecular weight using Borane/O_2 radical initiator and commercial PP polymers. *Macromolecules,* 38 (2005).

[22] Eceiza A et al. Thermoplastic polyurethane elastomers based on polycarbonatediols with different soft segments molecular weight and chemical structure: mechanical and thermal properties. *Polymer Engineering and Science,* 1 (2008).

[23] Kaji Atsushi et al. C-NMR study of anomalous linkages in polyurethane. *Polymer Science Part B: Polymer Physics,* 30 (2003).

[24] Solid surface energy data (SFE) for common polymers. Retrieved from http://www.surfacetension.de/,solid-surface-energy.html. (2007).

[25] Diversified Enterprises, Solid surfaces energies. Retrieved from http://www.accudynetest.com/ surface_energy_materials.html. (2006).

[26] ASTM D546-04 Standard test method for Corona-treated polymer films using water contact angle measurements. (2008).

[27] Chan Ick, Hoon Eui Jeong, Sung Hoon Lee, Hye Sung Cho, Kahp Suh .Wetting transition and optimal design for microstructured surfaces with hydrophobic and hydrophilic materials. *Colloid and Interface Science,* 336 (2009).

[28] Blishteyn M. Wetting tension measurements on corona treated polymer films. *TAPPI,* 78 (1995).

[29] Changchun Wang et al. Polymers containing fullerene or carbon nanotube structures. *Progress in Polymer Science,* 29 (2004).

[30] Qian D, Dickey E. C, Andrews R, Rantell T. Load transfer and deformation mechanisms in carbon nanotube-polystyrene composites. *Applied Physics Letters,* 76 (2000).

[31] Sung Yi et al. Bonding strengths at plastic encapsulate-gold-plated copper lead frame interface. *Microelectronics Reliability,* 40 (2000).

[32] Ochoa-Putman C and Vaidya U. Interfacial shear strength in a metal-thermoplastic composite. *Polymers,* (2009).

Table 1. Materials used in this investigation with select properties.

Material	Description	Melting Temperature	Tensile Strength	Density
Thermoplastic Polyurethane	Hard TPU - Pearlthane D11T75_merquinsa Polycaporlactone-copolyester based TPU, used for injection molding	388 - 406ºF 198 - 208^{o}C	50 MPa 7250 psi	1.23 g/cc
Thermoplastic Polyurethane	Soft TPU- Pearlthane D11T85E_merquinsa Extrusion applications as films and pipes	352 - 370ºF 178 - 188^{o}C	40 MPa 5080 psi	1.16 g/cc
PA6	Nylene-Custom Resins 401D. Injection molding applications	450 - 469ºF 235 - 243^{o}C	79 MPa 11600 psi	1.14 g/cc
PP	Common PP for extrusion compression molding BP	Flow 88^{o}C - 190ºF T_m 162 ^{o}C -324ºF	26 Mpa 5370 psi	0.88-0.92 g/cc
PP-MA	Dow PM613 -Maleic Anhydride Modified Polypropylene	Flow 138 ^{o}C - 280ºF T_m 160 ^{o}C - 320ºF	24 MPa 3480 psi	0.910 g/cc
Nano fullerene epoxy resin	Carbon nano fullerene functionalized in phenol formaldehyde glycidyl ether resin	T_g 140 ^{o}C - 284ºF	45 MPa 6600 psi	1.17 g/cc
Steel	Cold rolled low carbon steel (AISI/SAE1018)	1500 ^{o}C – 2732ºF	370 MPa 53 Psi	7.87 g/cc

Table 2. Variables considered while studying metal thermoplastic bonding for a single lap shear test

Specimen Specifications	Test A	Specimen Specifications	Test B
Roughness (μm)	0.27	Roughness (μm)	0.31
Steel gritted to	600	Steel gritted to	400
Adhesive gritted to 600	PP	Adhesive gritted to 600	PP
Laps	Steel	Laps	Steel
Area of adhesion	0.75x2 in	Area of adhesion	0.75x2 in
Thickness of adhesive	1 mm	Thickness of adhesive	1 mm
Specimen Specifications	Test C	Specimen Specifications	Test D
Roughness (μm)	2.7	Roughness (μm)	4.23
Steel gritted to	240	Steel gritted to	120
Adhesive gritted to 600	PP	Adhesive gritted to 600	PP
Laps	Steel	Laps	Steel
Area of adhesion	0.75x2 in	Area of adhesion	0.75x2 in
Thickness of adhesive	1 mm	Thickness of adhesive	1 mm
Specimen Specifications	Test E	Specimen Specifications	Test F
Roughness (μm)	4.23	Roughness (μm)	4.23
Steel gritted to	120	Steel gritted to	120
Adhesive gritted to 600	PP-MA	Adhesive gritted to 600	Soft TPU
Laps	Steel	Laps	Steel
Area of adhesion	0.75x2 in	Area of adhesion	0.75x2 in
Thickness of adhesive	1 mm	Thickness of adhesive	1 mm
Specimen Specifications	Test G	Specimen Specifications	Test H
Roughness (μm)	4.23	Roughness (μm)	1.92
Steel gritted to	120	Steel coated	No coated
Adhesive gritted to 600	Epoxy	Adhesive gritted to 600	PP-MA
Laps	Steel	Laps	
Area of adhesion	0.75x2 in	Area of adhesion	
Thickness of adhesive	1 mm	Thickness of adhesive	
Specimen Specifications	Test I	Specimen Specifications	Test J
Roughness (μm)	1.74	Roughness (μm)	2.15
Steel coated	Si	Steel coated	a:CH
Adhesive gritted to 600	PP-MA	Adhesive gritted to 600	PP-MA
Laps	Steel	Laps	Steel
Area of adhesion	0.5x1 in	Area of adhesion	0.5x1 in
Thickness of adhesive	1 mm	Thickness of adhesive	1 mm
Specimen Specifications	Test K	Specimen Specifications	Test L
Roughness (μm)	0.27	Roughness (μm)	2.70
Steel gritted to	600	Steel gritted to	240
Adhesive gritted to 600	PP-MA	Adhesive gritted to 600	PP-MA
Laps	Steel	Laps	Steel
Area of adhesion	0.5x1 in	Area of adhesion	0.5x1 in
Thickness of adhesive	1 mm	Thickness of adhesive	1 mm

Table 3. Steel surface treatment parameters

Treatment Parameters	Type of Surface Treatment	
Coating Layer	Silicon,Silicon Carbide	Alpha graphite and SP3 Carbon, Hydrogen
Gas used	Si(CH3)4	CH_4/H_2
Temperature	200ºC	200ºC
Pressure	~150 mbar	~150 mbar
Power level	500V	500V
Pulse width	60ms	60ms
Pre-treat roughness	2.11	1.74
Post-treat roughness	1.74	2.15
thickness	0.5μm	1.0μm

Table 4. Surface energies for common reinforcing and matrix materials [1, 24-25]

Reinforcements	Surface Energy (dynes/cm)	Matrices	Surface Energy (dynes/cm)
Carbon (PAN)	29	Polypropylene *	35
Carbon (Graphite)	32	Polyethylene	31
Glass	40	Nylon-11	33
Kevlar	27	Nylon-6	42
Steel*	35	Epoxy	47
		PET	43
		ABS	42
		PEEK	34

*values obtained in this study

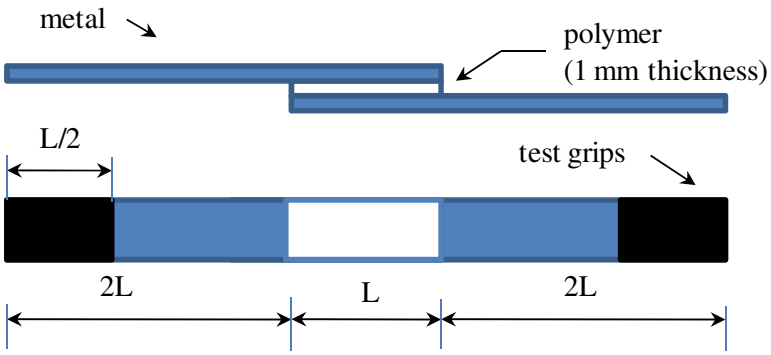

Fig. 1. Schematic representation of the shear lap test specimen

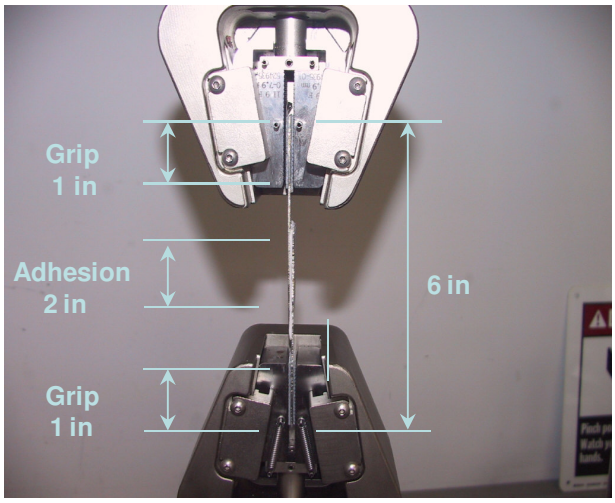

Fig. 2. Lap shear specimen on the test frame

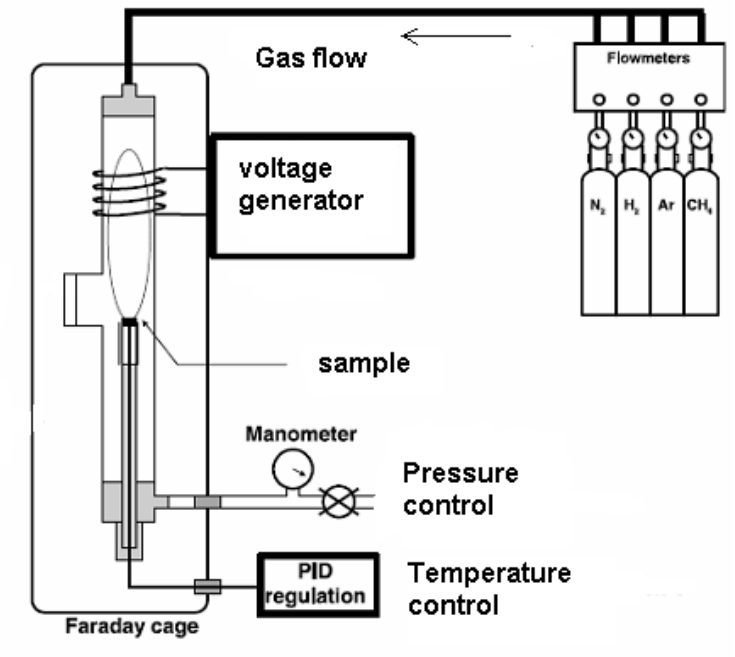

Fig 3. Schematic representation of an ion plasma process

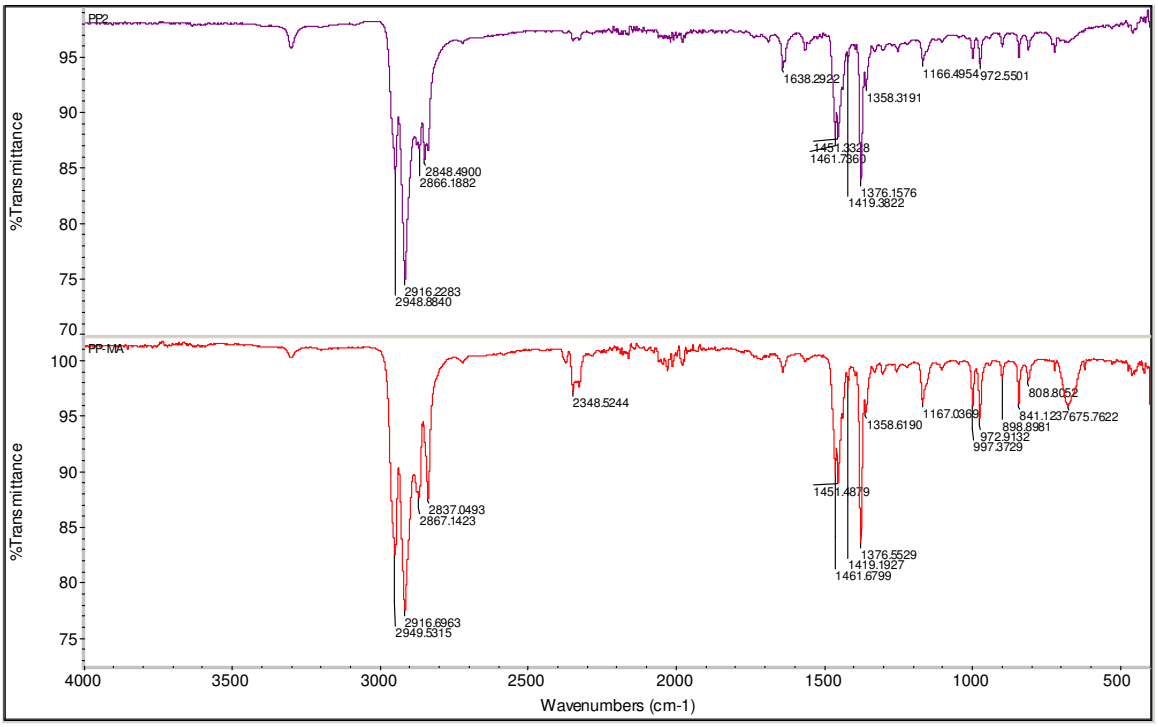

Fig. 4. Fourier Transfor Infrared Spectroscopy (FTIR) spectra of PP (top) and maleic anhydride PP (bottom)

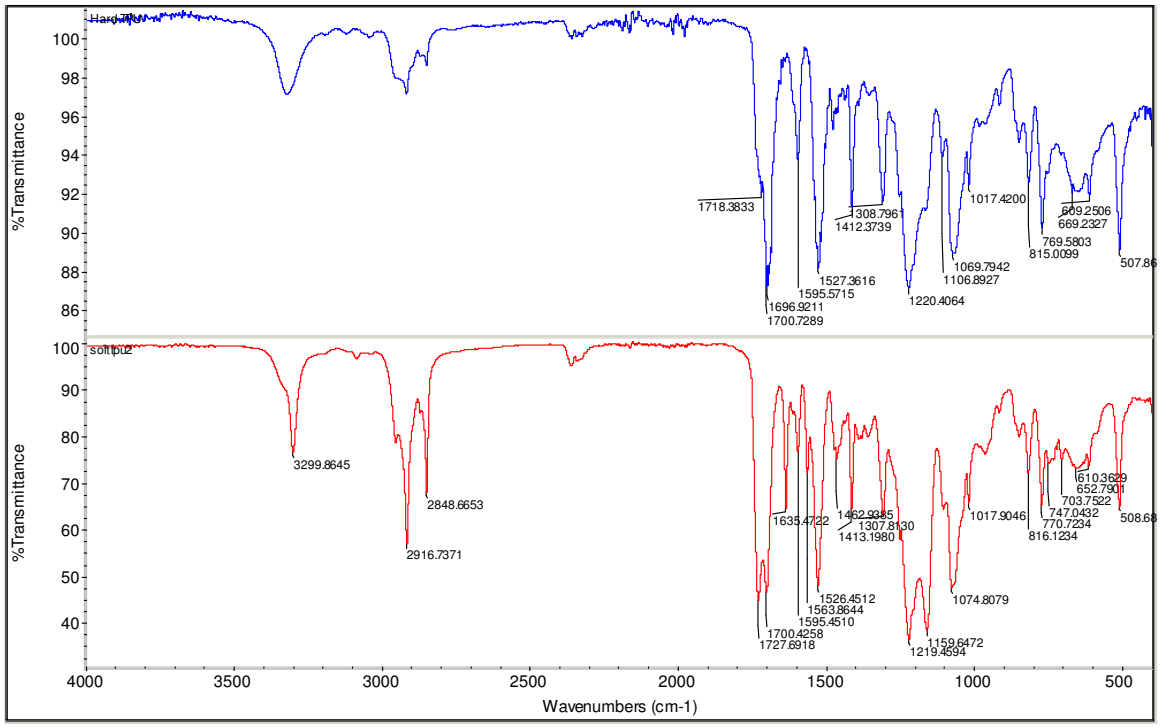

Fig. 5. FTIR spectra for hard (top) and soft (bottom) TPU

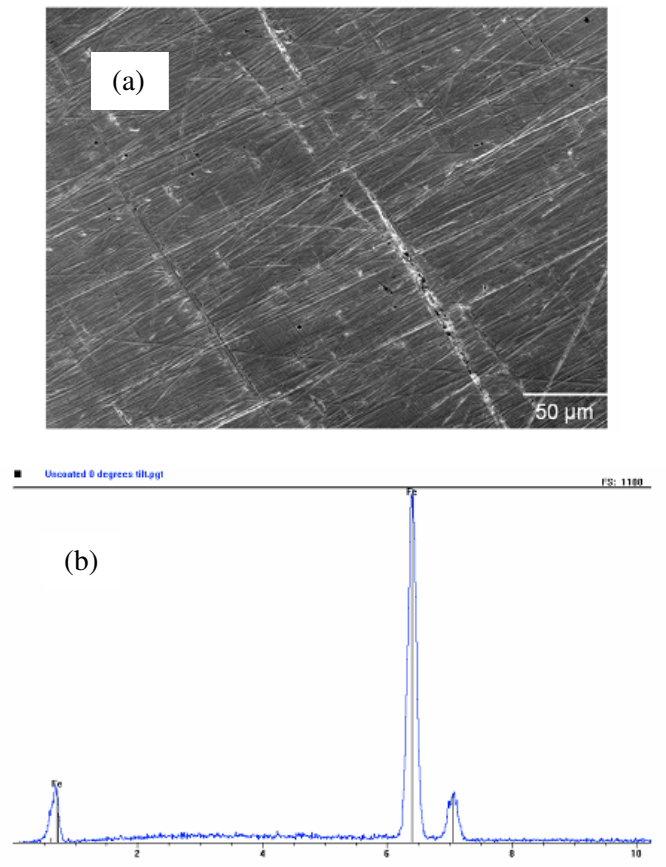

Fig. 6. (a) SEM image of uncoated steel 500X magnification.
(b) Energy dispersive X-ray spectrum from uncoated steel

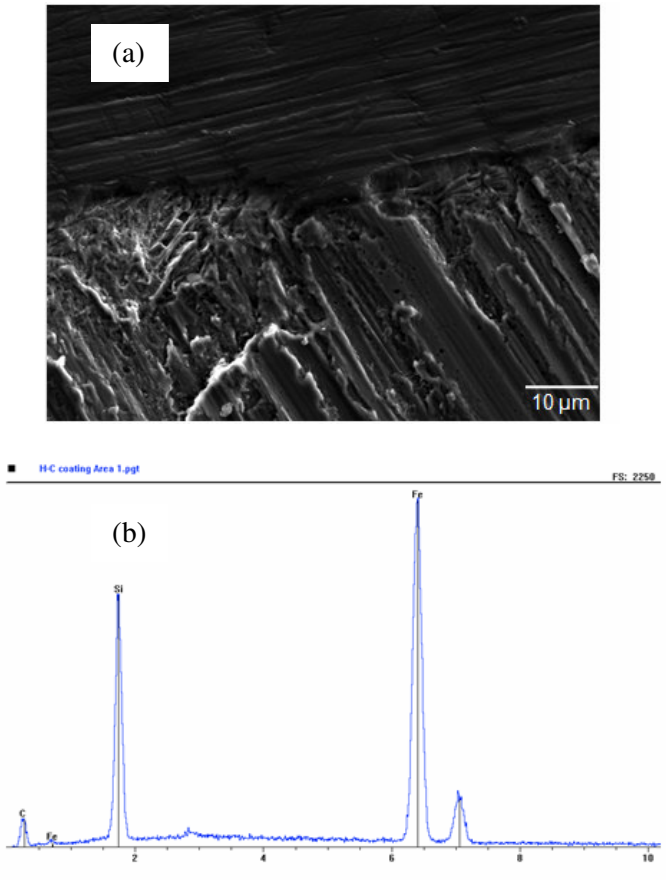

Fig. 7. (a) SEM image of a-C:H coated steel at 2000X magnification.
(b) Energy dispersive X-ray spectrum for a-C:H coated steel

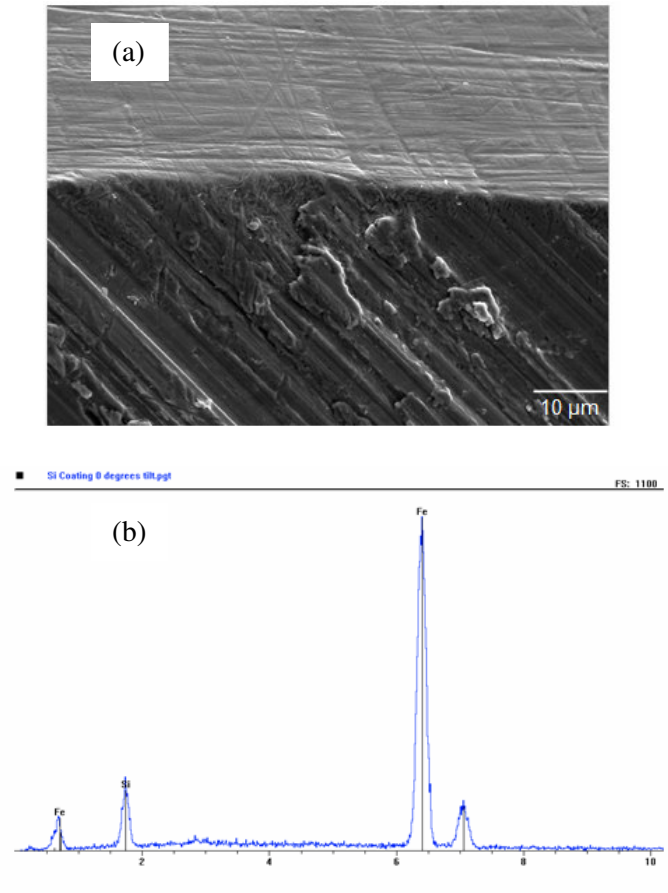

Fig. 8. (a) SEM image of Si coated steel at 2000X magnification.
(b) Energy dispersive X-ray spectrum from Si coated steel

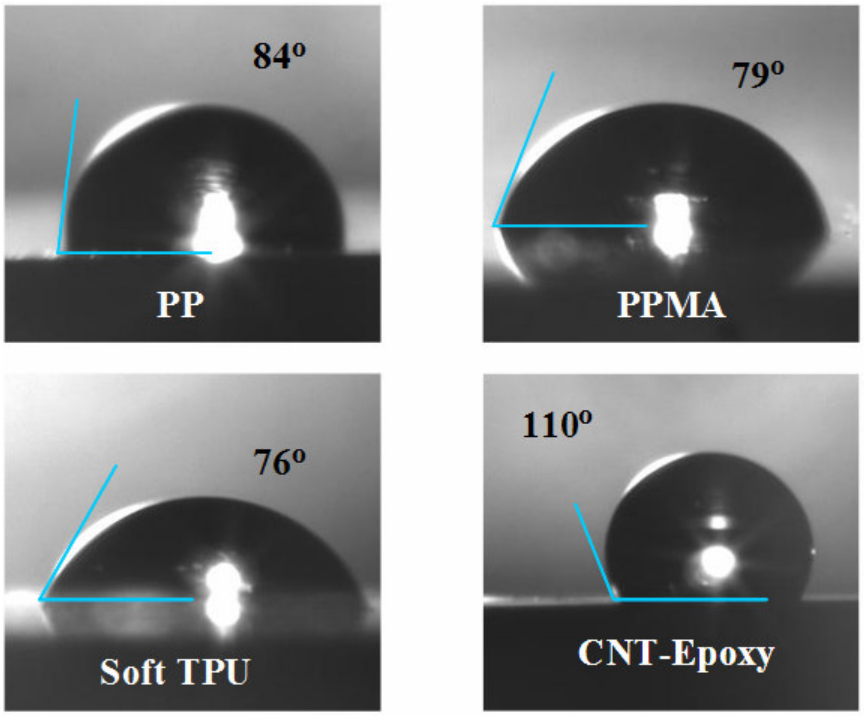

Fig. 9. Droplets of distillated water on polymer surfaces for measuring contact angle

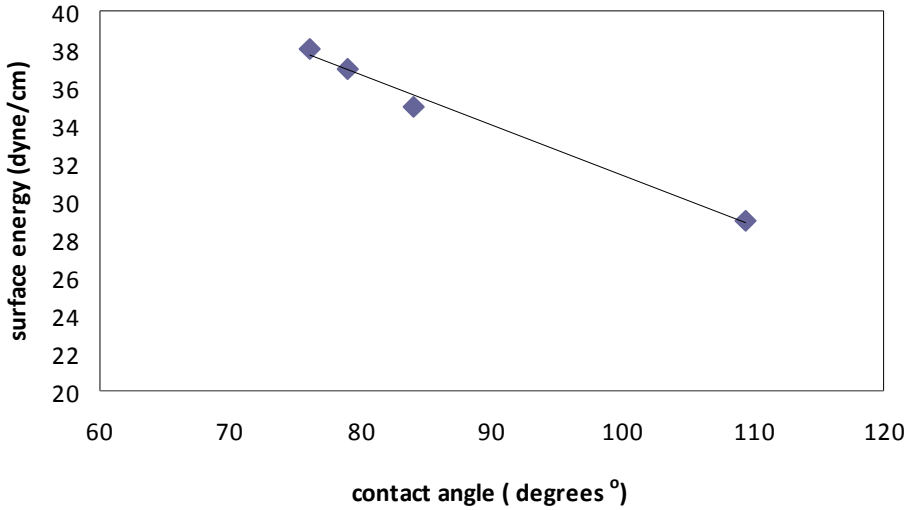

Fig. 10. Relationship between contact angle and surface energy for a thermoplastic polymer

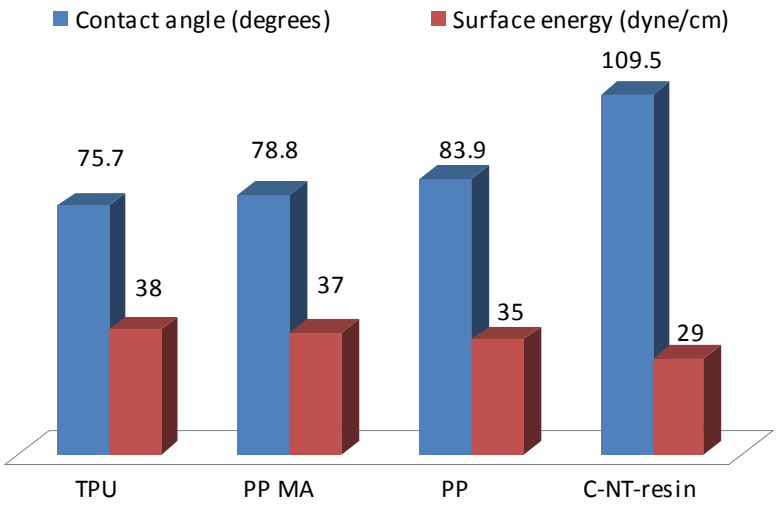

Fig. 11. Contact angle and surface energy for different polymer types.

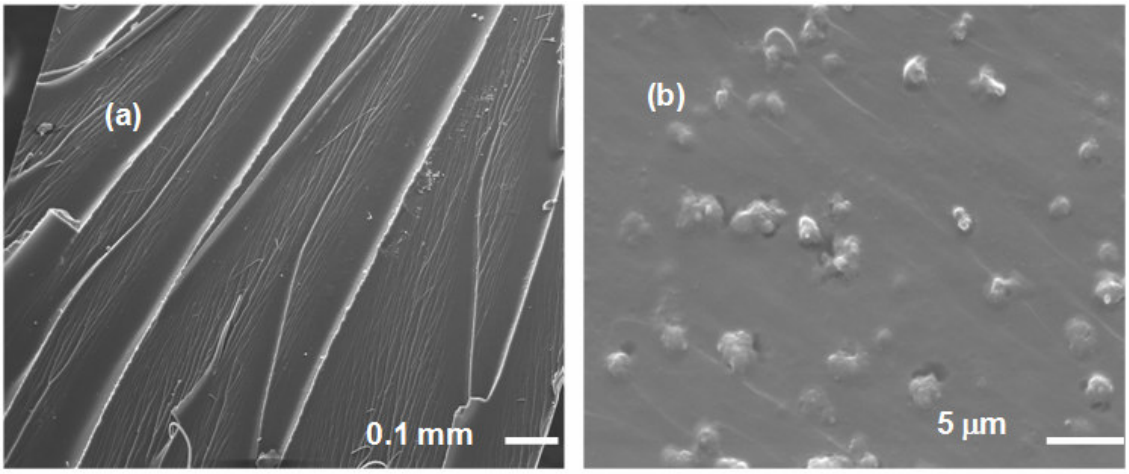

Fig. 12. SEM micrograph of CNT epoxy surface (a) 200 X (b) 6200X

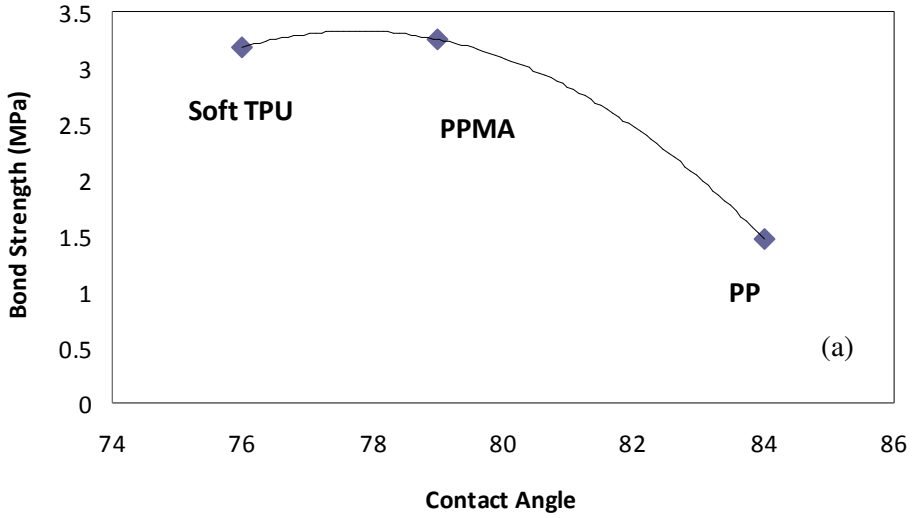

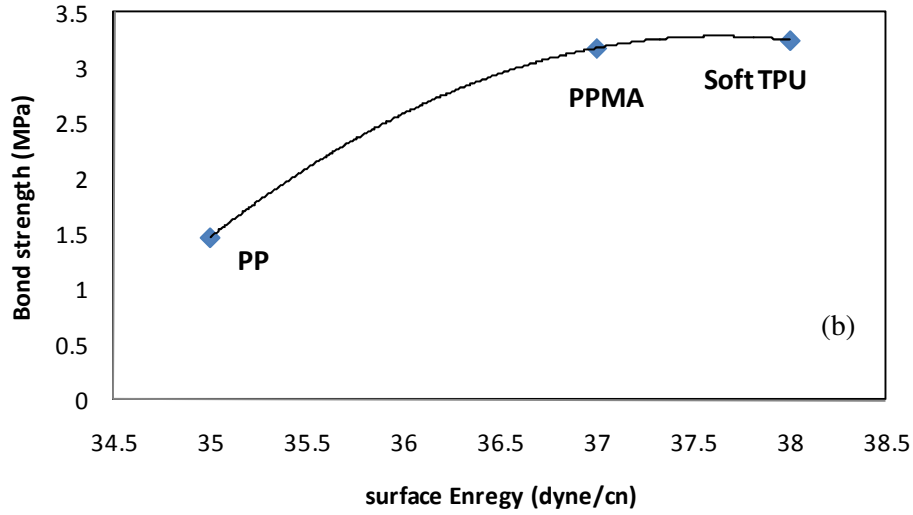

Fig. 13. (a) Correlation between contact angle and bond strength with steel for thermoplastic polymers. (b) Correlation between surface energy and bond strength with steel for different thermoplastic polymers.

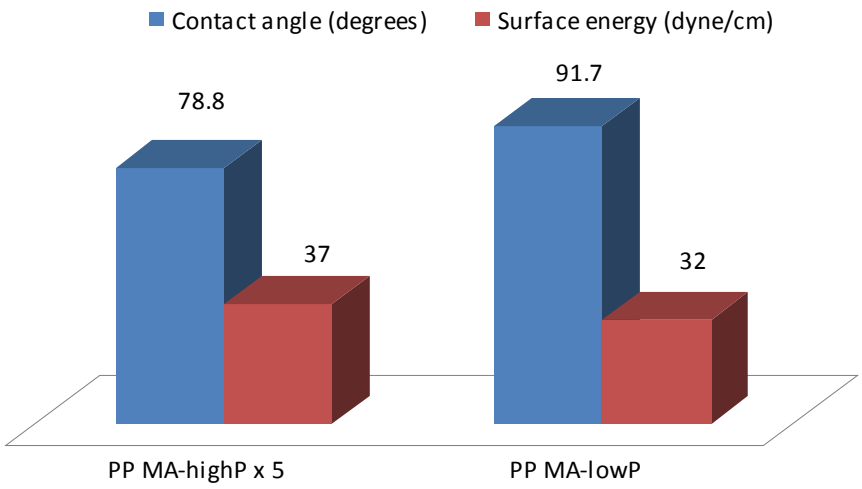

Fig. 14. Effect of consolidation pressure on the contact angle for PP.

.

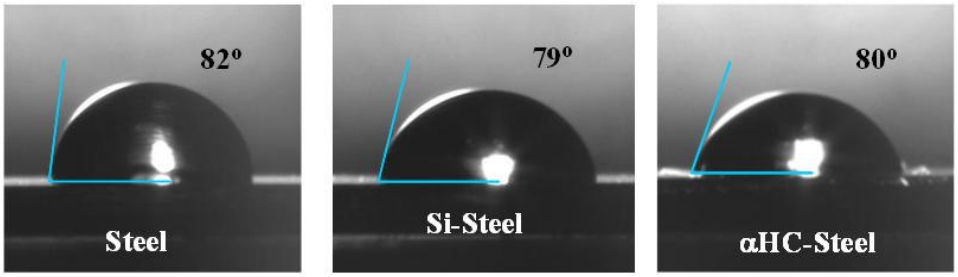

Fig. 15. Droplets of distillated water on treated and non-treated steel surfaces for measuring contact angle.

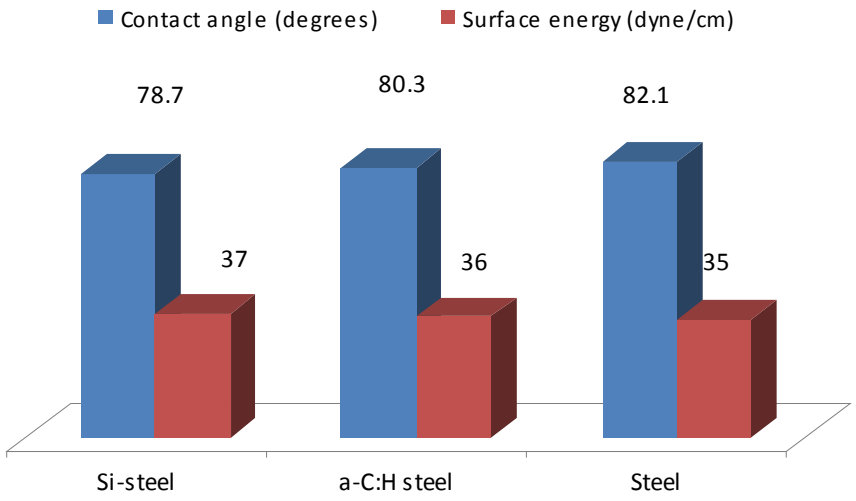

Fig. 16. Contact angle and surface energy for plasma-treated and non-treated steel.

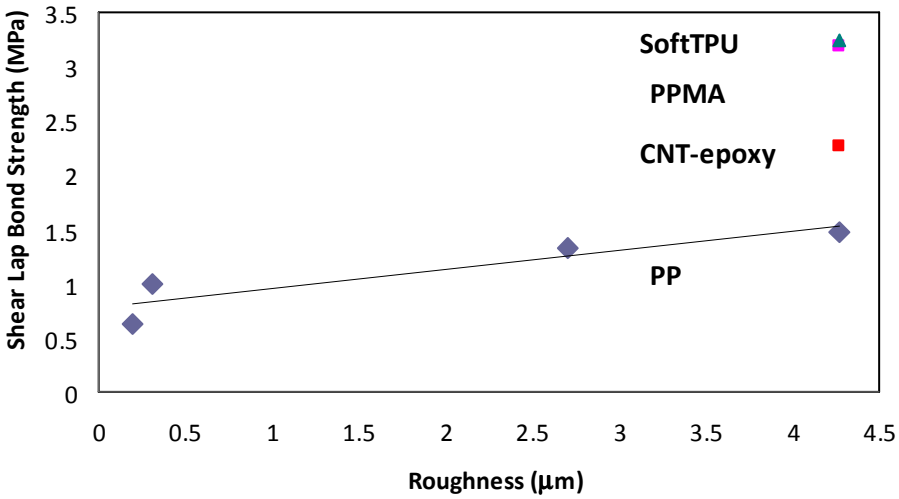

Fig. 17. Effect of roughness on the lap shear strength.

.

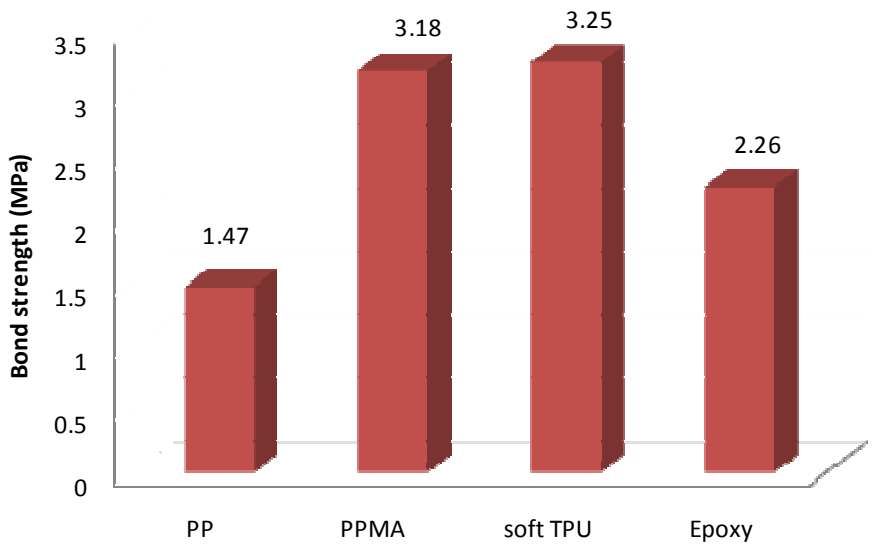

Fig. 18. Effect of the type of polymer on the interface bond strength.

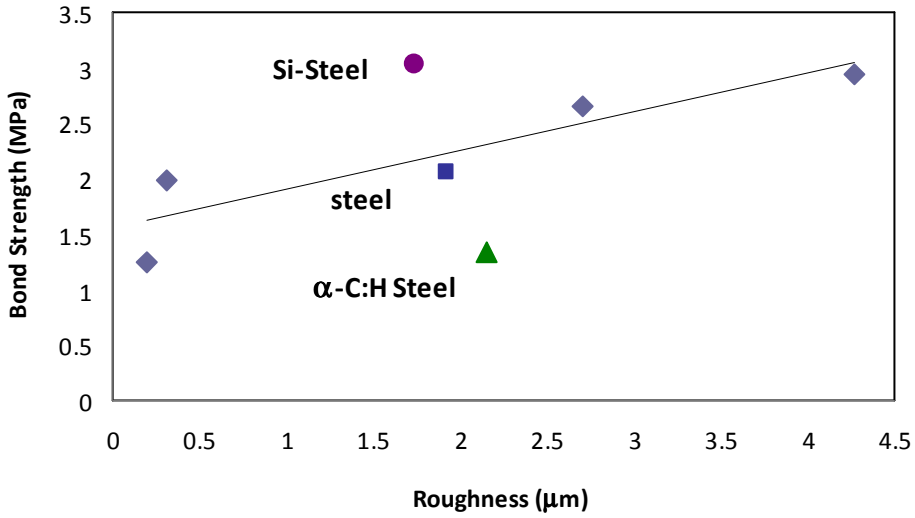

Fig. 19. Effect of plasma treatment on steel to the lap shear bond strength with PP-MA.

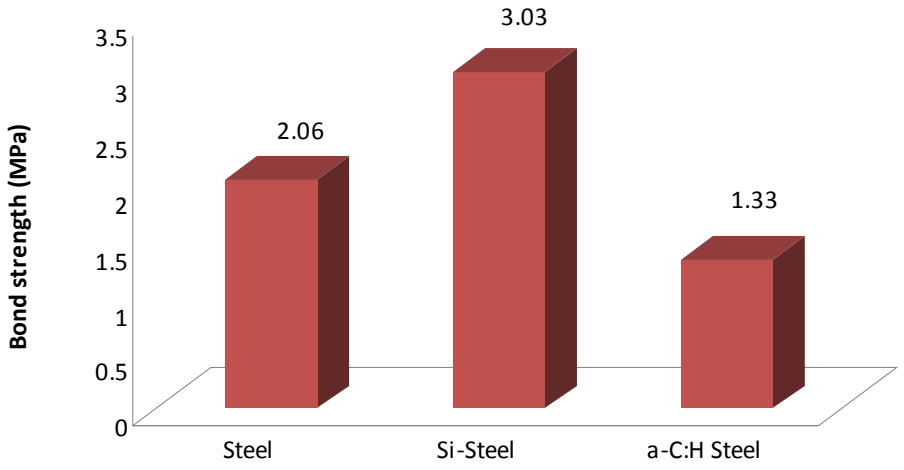

Fig. 20. Effect of coating on steel to the bond strength at the polymer-steel interface using PP-MA as the polymer with plasma-treated and non-treated steel.

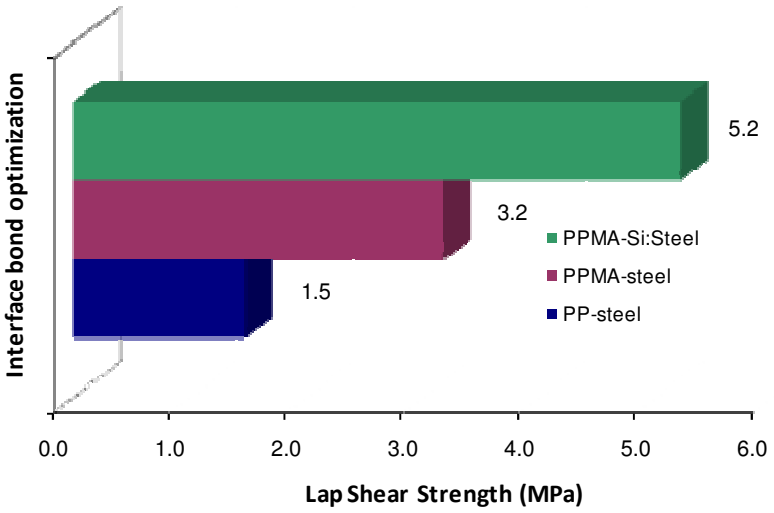

Fig. 21. Correlation between surface and interface bond strength between PP and steel.

Fig. 22. Types of failure at the interface of metal-to-thermoplastic polymer surface.

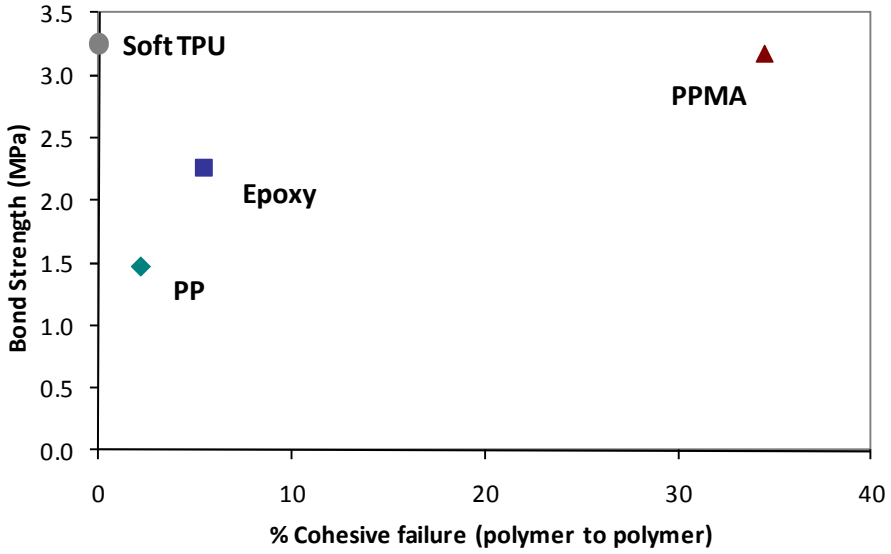

Fig. 23. Effect of cohesive failure on the bond strength at the interface between uncoated metal to thermoplastic polymer.

NUMERICAL ANALYSIS OF THERMAL STRESSES IN METAL-THERMOPLASTIC COMPOSITE

CAROL OCHOA PUTMAN, UDAY K. VAIDYA

In preparation for Journal of Reinforced Plastics and Composites

Format adapted for dissertation

ABSTRACT

A material system comprising a thermoplastic composite with metal cords is considered in this study. Metal/thermoplastic composites provide possibilities as structures for protection and enhanced damage tolerance. The thermal stresses in a metal thermoplastic composite are determined using finite element method (FEM). The analysis takes into consideration the difference in coefficients of thermal expansion between the fiber and the matrix in a steel cord thermoplastic composite and its effect during the cool down from processing temperature to room temperature. As temperature changes during cooling down, thermal stresses are induced at the matrix-fiber interface. Since both the fiber and matrix are dissimilar materials, the fiber-matrix interface constitutes the weak link in the progression of the composite failure. Understanding how the interfacial strength is affected by the residual thermal stresses enables predicting the interfacial strength limit and furthermore the design of a composite to provide improved mechanical performance.

Key words: interface analysis, meta-thermoplastic composite, thermal stresses, FEA.

1. INTRODUCTION

Metal-thermoplastic composites are interesting materials for structural, automotive, aerospace and military applications. The growing demand for high-performance thermoplastic composites has been challenged by the usual problem of a lack of adhesion between the fiber and the matrix. It has been recognized that the mechanical performance of a composite is strongly affected by the fiber-matrix interface bonding as well as the bulk properties of the constituent materials. Interface bonding depends on a number of factors such as matrix morphology, fiber surface condition, mismatch of fiber matrix stiffness, reactive functionalities and thermal residual stresses [5-7].

Residual stresses at the interface are generated by thermal gradients due to the mismatch in Coefficient of Thermal Expansion (CTE) between the reinforcement fiber and the matrix. The objective of the present study is to develop a Finite Element Model (FEM) to gain insight into the effect of temperature-induced stresses at the interface of a metal cord embedded in a polymeric matrix.

Numerous models have been studied to understand the effect of CTE in the composite to generate stress concentrations due to non-linear distribution of thermal strains and stresses between fiber and matrix [4-7]. FEM studies have also been conducted to estimate the residual stresses developed as a result of thermal loads [6]. Jamshidi [8] studied the nylon cord/rubber interface at elevated temperatures. He concluded that increase in temperature causes bond breakage at the interface of nylon cord with rubber compound and also established an optimal temperature and time of curing to achieve the maximum adhesive strength. Rosso [9] implemented FEM to analyze the effect of thermal stresses in a carbon fiber composite under tensile load. In this approach, the material was treated

as linear elastic with temperature dependent properties. The location of high stress concentration was found at the outer edge at the interface between fiber and matrix. Klett and coworkers [10] developed an accurate FEM to predict thermal conductivity parallel and transverse to the fiber axis of unidirectional pitch-based C/C composites. Their model incorporated fiber morphology, matrix morphology, fiber/matrix bonding and random distribution of fibers and defects. Kwon [4] used FEM to compute thermal stresses at the fiber-matrix of a thermoplastic fiber reinforced composite. The author extended a generalized continuum mechanics model for a thermoelastoplastic deformation of fiber and matrix. Stresses at the micromechanical scale are computed from FEM. Two geometric models were evaluated: a unidirectional strip with no boundary constraint, and a homogeneous and isotropic plate with a center hole and constrained edges. Both solutions agreed well with the experimental data. Lou and Desjardin [5] used a FEM to solve the thermal and mechanical equations for a two-dimensional clamped glass/phenolic composite beam subjected to thermal radiative heating. The results showed that the decomposition of the resin and char create local stress concentrations across the heated face. The origin of these stresses was attributed to thermal expansion and contraction across the face and the generation of local high pore gas pressure from resin decomposition. Peterson and coworkers [6] used FEM to determine the internal stress state due to differences in the CTE of carbon/epoxy composite during the curing process. The influence of fiber spacing (or fiber volume fraction) was addressed in this study.

Benveniste [11] and Hasselman [12-13] developed a theory to describe the effective thermal conductivity of the composite with thermal contact at constituent interfaces. The theory applies for continuous matrix composites containing dilute volume fractions of

uniaxial coated cylindrically orthotropic fibers with interfacial thermal barriers at the fiber-coating and coating matrix interfaces.

Based on Benveniste's [11] and Hasselman's [12-13] theories, Chao & Chen [14] developed an analytical solution for a stress field in a three-phase composite cylinder (Figure 1). From this solution, a three-phase boundary problem with perfect interface can be transformed into a two phase problem with imperfect interface by making the interface thickness zero. The solution applies for three coaxial cylindrical layers with arbitrary radii and different material properties. The three-phase composite cylinder represents an embedded fiber-matrix interface characterizing mechanical and thermal mechanisms induced by the interface. This work concluded that the interfacial shear stresses increase with the difference of modulus between fiber and matrix. The maximum stress resulted at the highest temperatures of the interface; and, as expected, the stress increases with the difference in coefficient of thermal expansion of the constituents.

Figure 1 shows a schematic representation of the model used by Benveniste [11], Hasselman [12-13], Chao & Chen [14] to predict the temperature and stress fields for a coaxial cylindrical fiber/matrix composite as a function of the properties of the interface layer, where S represents stress, K is the thermal conduictivity and ΔT is the thermal gradient. The sub-indices f, i, and m represent fiber, interface and matrix, respectively.

As an extension of the models mentioned above [11-14], this study develops a transient thermal analysis using FEA to examine the interface effect on a metal-thermoplastic composite. The FEA is developed at two scales: one at a micro scale and the other at a macro scale. The micro scale model considers the effect of interface bond strength, mismatch in coefficients of thermal expansion, thermal conductivities and stiffness to predict

the temperature gradient and thermal stresses and strains along the interface of a cylindrical cord embedded in a polymeric matrix. The macro scale model focuses on temperature gradients across the interface and generation of thermal stresses consistent with a cool-down process. Additionally, this model uses a coupled thermal-mechanical load to evaluate the effect of residual thermal stresses on the mechanical performance of the composite. This is accomplished by simulating a three-point-bend test with the induced thermal stresses. Both models consider surface-to-surface contact elements along the interface to study the effect of weak, medium and strong bonding between cord and matrix on the generation of thermal stresses. The FEA results in a non-linear thermal strain distribution in the polymeric matrix around the metal cord. Physical parameters, such as the difference in coefficient of thermal expansion and thermal conductivity as well as the bond strength, are evaluated to predict residual stresses along the matrix-cord interface.

2. METHODOLOGY

The influence of thermal stresses at the interface is investigated by FEM. First, a quad-symmetrical cord/matrix model is used at a micromechanical scale to describe the generation of thermal stresses as a function of bonding type at the interface; strong, medium and weak interfaces are analyzed to generate thermal stresses. Second, a model of a metal-thermoplastic composite is used to analyze the influence of temperature to predict thermal stresses and the limiting bond strength that establishes continuity of the interface between the two phases of the steel cord and thermoplastic PP matrix.

2.1 Element Type, Mesh and Contact Algorithm.

For both models, bulk materials, steel and polymer were built using 3D elements in ANSYS 8.0 (SOLID185) with 8 nodes and three degrees of freedom each. The mesh was mapped as hexagonal elements as can be seen in Figure 2 for a quad-symmetrical model. The properties of constituent elements are listed in Table 1 and 2. For the interface, the CONTA174 element was used; this element has 8 degrees of freedom and is used to define surface-to-surface contact. The interface is generated as rigid-to-flexible contact. The contact surface is associated with the polymeric matrix and the target surface with the steel cord.

The definition of initial contact was an important aspect of building the finite element model. For both the three-point bend flexure specimen and the quad-symmetrical cord/matrix, the Penalty method (KEYOPT (2) =1 ANSYS 11.0) was used as the contact algorithm to set the contact properties. This method uses a contact "spring" to establish a relationship between the two contact surfaces with a contact stiffness k. The amount of penetration between the contact and target surfaces depends on the normal stiffness, and the amount of slip in sticking contact depends on tangential stiffness. Higher stiffness values decrease the amount of penetration/slip. Hence, the model considers high stiffness to produce small penetration slip but low enough to obtain adequate convergence. To define the contact stiffness and the allowable penetration, the model considers normal penalty stiffness, penetration tolerance factor, static dynamic ratio, and contact opening stiffness. To determine the contact detection, the model uses Gaussian integration in which the contact surface (polymer) is constrained against penetration into the target surface (steel). However, the target surface, in principle, can penetrate into the contact surface.

2.2 Modeling Interfacial Stresses

Both models were built to capture the behavior at the interface between the steel reinforcement and the polymeric matrix. The models focus on the generation of thermal stresses for a perfect, rough and weak bond at the interface as well as its effect on flexural load response for a three-point bend.

For the metal cord/thermoplastic matrix model shown in Figure 3, one face of the cord is heated to a temperature of 423 K while the rest of the body exhibits a lower initial temperature of 363 K. As heat is transferred from the cord to the polymeric matrix, the polymer is expected to expand. However, since it is constrained by the steel cord, stress is generated at the cord/matrix interface due to differences in thermal expansion coefficients.

For the case of three-point bend model shown in Figure 4, both outside surfaces are cooled to 363 K while the rest of the body is at 423 K. Similar to the previous model, temperature gradients are calculated as thermal loads in a structural environment to generate thermal stresses. As a second step in the structural environment, a transverse force of 500 N is applied to the top surface while the bottom constraints in the three-point bend test. The purpose of the model is to investigate the effect of thermal stresses to the failure of the composite based on the three types of interface discussed in our previous work [15]. The generation of thermal stresses will influence the limiting bond strength at the interface of the metal-thermoplastic composite.

3. RESULTS AND DISCUSSION

For both macro and micro scale models in the study, the FEA investigates thermal strains and thermal stresses generated as result of the heating and cooling down process. Thermal stresses are calculated as a function of the non-uniform temperature distributions between the steel cord reinforcement and the thermoplastic matrix. The model uses a non-linear finite element method based on thermal conductivity in a composite with a thermal barrier at the cord/matrix interface to simulate an imperfect interface (i.e partially bonded) as well as perfectly bonded. The gradient of temperature through the composite generates internal thermal stresses. The present models are limited to thermal elastic stress distributions in the constituents; thus, they neglect the material non-linear behavior, considering only the elastic zone.

3.1 Thermal Stresses – Micro scale Analysis of the Cord/Matrix Model

The FEA for the micro scale analysis uses a quad symmetrical model of a steel cord embedded in PP matrix using material properties listed in Table 3. This model was developed to evaluate the state of stresses between a single steel cord and the thermoplastic matrix.

The majority of the residual stresses are generated during cool down to room temperature due to CTE mismatch and the difference in stiffness between the constituents of the metal-thermoplastic composite [9]. The stresses are predicted considering the materials as linear elastic with temperature dependence.

Figure 5 shows the temperature distribution as function of the type of interface: (a) for a weak interface or partially bonded, (b) for a medium interface bond or partially

bonded, where the roughness of surface plays significant role, and (c) for a strong interface bond or perfectly bonded. As can be seen in Figure 5, as the bonding at the interface becomes stronger from partially bonded to perfectly bonded, the conductivity increases. For case (a), the temperature at the interface reaches 390 K while the perfect interface reaches 416 K in the same amount of time.

Figure 6 shows total deformation of the steel surface, PP surface and thermal stresses at the interface for a medium interface bond (defined as partially bonded with significant surface roughness). Due to the boundary conditions, the stress level decreases symmetrically through the z-(depth) direction. The non-uniform deformation at the surface of matrix and cord results in non-uniform thermal stresses along the interface as dependence on the temperature gradient distribution during the heat transfer process. A maximum deformation of 0.29 mm occurs on the polymer surface while only 0.012 mm of deformation is encountered by the cord surface; this difference in deformation is due to the difference in CTE and the stiffness of the constituent materials which consequently generate thermal strains in the matrix as shown in Figure 7.

As can be seen in Figure 7, the interface establishes a region with a higher value of thermal expansion (0.29 mm) and decreases in a radial direction through the matrix (0.03 mm). The presence of reinforcement (steel) with an expansion coefficient less than that of the matrix (PP) (Table 3) imposes a mechanical constraint on the matrix that impedes the matrix to expand, creating a critical region for thermal stresses (93 MPa).

Considering a perfectly bonded interface, Figure 8 shows the variation of thermal stresses and temperature as a function of time during the heating-up process. The heat is applied to one face of the cord and the temperature of the cord exhibits a constant value

of 423 K with time due to the high thermal conductivity of steel. The temperature of the matrix increases from 365 to 395 K during a total time of 17 minutes. Temperature at surfaces of both steel reinforcement and PP matrix increases gradually, and that reduces the gap between them as a function of time, as can be seen in Figure 8, with the cord temperature and the matrix temperature at the interface. As the gradient of temperature between contact surfaces (matrix/reinforcement) decreases, the thermal stress at the interface decreases as well. As the temperature of the cord approaches the temperature of the matrix, a minimum value of thermal stress remains at the interface (28 MPa). This thermal stress corresponds to the residual stress that remains at the interface assuming a strong interface bond between the constituents.

In addition to the temperature gradient and mismatch in coefficients of thermal expansion and stiffness [16], thermal stresses are a function of interface adhesion between the matrix and fiber [7, 17]. To analyze the effect of the interface bond the previous model was tailored to weak, medium and strong interfacial bond and then used to determine thermal stresses as a function of bond type. Figure 9 illustrates thermal stresses tend to decrease as the interface bond becomes stronger. These results suggest that a stronger interface favors a uniform temperature distribution, avoiding the stress concentrations along an imperfect interface. As can be seen in Figure 10, the estimated value of thermal stress remaining at the interface for a strong bond reaches a minimum value of 25 MPa, in contrast to a weak interface bond where the residual thermal stress increases to 230 MPa; the intermediate case for a medium interface bond has a residual thermal stresses of 68 MPa. According to this, the interaction between matrix and cord establishes a significant difference in the generation of thermal stresses.

Figure 11 describes the dependency of thermal stresses as function of thermal gradient at the interface. For a high thermal gradient, there are proportionally higher thermal stresses. A difference in temperature at the contact surface of constituents (fiber/matrix) of $8^{o}F$ generates thermal stresses of up to 6 MPa, while a difference in temperature of $4^{o}F$ generates lesser thermal stresses of up to 0.5 MPa. As the coefficient of thermal expansion and thermal conductivity of contact surfaces become similar, the generation of thermal stresses can be reduced. Thermal stresses as described by Chawla [16] reach a maximum peak at the interface and contribute to the initiation of failure as will be described in the coupled thermal/structural analysis for the macro scale model. Thermal stresses generated at the interface dominate over internal stresses generated in the matrix or the cord.

3.2 Thermal Analysis – Macro scale

The mismatch in CTE of the fiber and matrix results in thermal stresses in the composite. The determination of the temperature distribution through the metal-thermoplastic composite at the macro scale was the first step in evaluating the generation of thermal stresses in the composite.

Figure 12 shows temperature increases with time for the constituents of the metal-thermoplastic composite as well as the composite as a whole. To consider the cooling process, a specimen was preheated to 425K and cooled with an applied temperature of 365 K to the top and the bottom (Figure 13). As expected the temperature for bulk steel reduces faster with time due to the high thermal conductivity (60.5 W/m K) of the material as shown in Table 4. On the other hand, the thermal conductivity of PP is very low

(0.12 W/ m K), so PP acts as an insulating material where the transfer of heat is very slow. The temperature of the composite drops at a rate of 0.75 ^{0}C/min; this is faster than the cooling rate of neat PP (0.3 ^{0}C/min). Even with this difference, the shape of the cooling curve for PP and the composite follows similar tendencies compared with the steel reinforcement material, see Figure 12. This is explained by the constraint of the PP dominating the conductivity of the composite due to its isolating properties. As expected, the temperature of steel decreases linearly with time. The tendency of the cord temperature agrees with the behavior of a material with high thermal conductivity; the temperature of the polymer and the composite drop slower following the tendency of a thermo-insulating material.

The temperature distribution in the composite is shown in Figure 13. As a result, a temperature of 363 K is attained by the matrix after 20 min of cooling, despite the cord reinforcement still at 423 K. This leads to a non-uniform temperature gradient through the composite, favoring the generation of thermal stresses. Figure 14 shows the heat transfer in the longitudinal fiber direction is 3 times faster than that in the transverse direction, where the cord reinforcement layer acts as a heat dissipation barrier due to the surrounding material.

The difference in thermal properties between the cord reinforcement layer and thermoplastic matrix results in non-uniform temperature distribution. Consequently, a non-uniform thermal strain distribution arises (Figure 15), causing considerable thermal stresses at the interface (Figure 16). Thus, the total deformation reaches 0.31 mm at the interface between the steel cord layer and the PP layer leading to thermal stresses at the interface of 28 MPa.

3.3 Thermal /Structural Analysis: Thermal and Mechanical Load

This analysis investigates the failure of the metal-thermoplastic composite subjected to thermal load (internal thermal stresses) and mechanical load (3-point bend load) as a function of the type of bond at the interface, i.e. weak, medium and strong. This numerical analysis complements previous research which focused exclusively on mechanical bonding [15]. The dimensions in the model, points of loading and constraints correspond to the actual dimensions are same as the model used in this previous work [15]. The contact parameters to define weak, medium and strong interfaces are also explained in detail in Reference [15].

This analysis implements a sequentially coupled analysis [18] where the input of one analysis depends on the results from another analysis using thermal and structural fields. First, to obtain thermal stresses, a temperature field introduces thermal strains in the first structural field. Also, in a second structural field, both thermal stresses and an external transverse load is applied in the model to obtain flexural strength of the metal-thermoplastic composite as can bee seen in Figure 17. All fields use the same geometry with independent loads, constraints and elements.

The FEA results show that maximum interfacial stress is reached along a line at the center of the beam with its maximum value at the mid-point as illustrated in Figure 18. For a 500 N load in three-point loading configuration, the maximum stress generated at the bottom interface is 439 MPa, 526 MPa and 739 MPa for strong, medium and weak interface bond, respectively. The bottom mid-point between reinforcement and matrix carries the highest stress along the contact area, beyond which the materials begins to fail.

Furthermore, the stronger the interface, the lower the stress generated between reinforcement and matrix according to the values mentioned above. A stronger interface allows adequate load transfer through the thickness of the composite to avoid failure by delamination, see Figure 18(a), while a weaker interface limits the transfer of loads through the thickness, leading to failure along the interface as seen in Figure 18(c).

The FEM in Figure 18(a) captures the load transfer through the thickness and width; and, as expected, the areas close to the constraint witness higher stresses. The matrix, which is the softer material, undergoes larger deformation (0.31 mm) than the steel layer (0.12 mm). The difference in stiffness between both components renders the interface weak and consequently leads to onset of failure. Figure 19 illustrates the crack along the bottom interface and through the support span to corroborate the results from FEM.

The stress to failure of the three cases of the interface was predicted from the model and displayed in Figure 20 considering interface thermal stresses. It also compares the results obtained in the absence of thermal stresses. Thus, the failure load, considering thermal stresses for the strong interface (or perfect bonded) case, is predicted to be approximately twice the experimental value (171 MPa from the FEM versus 74 MPa from the experiment). The strong interface case is an idealized case, and unrealistic since a perfectly bonded interface is not easy to produce. In the second case of a medium interface, i.e. where the possibility of sliding between contact surfaces is allowed but opening of the interfaces is restricted, the failure load is closer to the experimental case (134 MPa from the model versus 74 MPa from the experiment). The third case considers sliding and delamination or opening between surfaces. Delamination between surfaces is not desired

because further load transfer cannot occur. In this case, the failure load is predicted at 67 MPa which is in closer agreement with the experiment.

Therefore, by FEA, it was possible to estimate the limiting strength of the metal thermoplastic-composite. In addition, Figure 20 stipulates that residual thermal stresses have large impact on the failure of the composite with a weaker interface.

4.CONCLUSIONS

This work provides a method to determine thermal stresses at the interface of a metal-thermoplastic composite and evaluate the interaction between the fiber and the matrix. Specifically, it analyzes the effect of the bond strength between fiber and matrix on the generation of thermal stresses and predicts the limit bond strength of the composite considering mechanical and thermal loads.

As the bond between matrix and fiber becomes weaker, the effect of thermal stresses becomes pronounced on the strength of the composite. Consequently, thermal stresses should be considered to determine the limited interfacial strength for a composite with non-perfect interface.

Numerical approaches of macro and micro scales of a metal-thermoplastic composite investigate the generation and effect of thermal stresses on the interfacial bond strength. The study was limited to elastic stress distribution. According to the FEM, thermal stresses arose as a result of non-uniform temperature distribution through the interface between matrix and reinforcement material.

The micro scale model shows that a weak interface worsens thermal conductivity between matrix and cord, favoring the generation of thermal stresses. The macro scale

model has been correlated to experimental results of a 3-point-bend load test of a metal-thermopalstic composite. The results show that a weak bond strength between steel cords and PP matrix has a pronounced effect on the generation of thermal stresses during fabrication.

The macro scale model predicts that the heat transfer in the longitudinal direction of the reinforcement is 3 times faster than that in the transverse direction, where the cord reinforcement acts as a heat dissipation barrier to the surrounding material. The composite is predicted to be a thermal isolating material.

ACKNOWLEDGEMENT

Partial support provided by Tank Automotive Research Command (TARDEC) and Department of Energy (DOE) Graduate Automotive Technology Education (GATE) is gratefully acknowledged.

REFERENCES

[1] Ochoa-Putman C, Vaidya U. Interfacial Shear Strength in a Metal-Thermoplastic Composite. *Composites* (2009).

[2] Ochoa-Putman C, Vaidya U. Mechanisms of Interfacial adhesion in metal-polymer composites – Effect of chemical treatment. *Composites* (2009).

[3]Gao Shang-Lin, Kim Jang-Kyo. Cooling rate influences in carbon fiber/PEEK composites. Part 1: Crystallinity and interface adhesion. *Composites; Part A,* 31 (2000).

[4] Kwon YW. Finite element analysis of thermoplastic stresses in composites. *European Journal of Mechanical Engineering,* 37 (1992).

[5] Luo C, Desjardin P. Thermo-mechanical damage modeling of a glass–phenolic composite material. *Composites Science and Technology,* 67 (2007).

[6] Peterson E. The effect of moisture, low temperature and low temperature thermal cycling on the strength and stiffness of unidirectional carbon/epoxy laminates. North Dakota State University, (2004).

[7] Kemal Apalak et al. Thermal non-linear stresses in an adhesively bonded and laser-spot welded single-lap joint during laser-metal interaction. *Materials Processing Technology* 142 (2003).

[8] Jamshidi M, Afshar F, Mohammadi N, Pourmahdia S. Study on cord/rubber interface at elevated temperatures by H-pull test method. *Applied Surface Science,* (2005).

[9] Rosso P, Varadi K. FE macro/micro analysis of thermal residual stresses and failure behavior under transverse tensile load of VE/CF-fiber bundle composites. *Composites Science and Technology,* 66 (2006).

[10] Klett JW, Ervin VJ, Edie DD. Finite-element modeling of heat transfer in carbon/carbon composites. *Composites Science and Technology*, 59 (1999).

[11] Benveniste, Y. and T Miloh. The effective thermal conductivity of composites with interfacial thermal contact at constituent interfaces. *International Journal of Engineering and Science,* 24 (1986).

[12] Hasselman D.P.H, Johnson L.F. Effective thermal conductivity of composites with interfacial thermal barrier resistance. *Composite Materials,* 21 (1987).

[13] Hasselman D.P.H, Donaldson K, Lu Y. Thermal conductivity of uniaxial-coated cylindrically orthotropic fiber-reinforced composite with thermal barriers. *Composite Materials,* 29 (1995).

[14] Chao C, Chen S, and Shen T. And exact solution for thermal stresses in a three-phase composite cylinder under uniform heat flow. *International Journal of Solids and Structures,* 44 (2007).

[15] Ochoa-Putman C, Vaidya U. Numerical model to predict the limiting bond strength in a metal-thermoplastic composite. SAMPE (2008).

[16] Chawla K. Composites materials Science and Engineering. Second Ed, New York, Springer (2001).

[17] Esparragoza I.E, Levy C, Caudill N.E. Thermal stresses in a single elastic fiber embedded in an infinite matrix. *International Journal of Applied Mechaniscs and Engineering,* 11 (2006).

[18] Ansys Coupled-Field Guide. ANSYS 10.0 version, (2005).

Table 1. Features of the finite elements for bulk materials, PP and steel.

Parameter	Matrix	Cord
Material	Polypropylene	Steel
Element type	Solid-8-node SOLID185 (3-D structural solid) SOLID70 (3-D thermal solid)	Solid-8-node SOLID185 (3-D structural solid) SOLID70 (3-D thermal solid)
Meshing	Hexagonal mapped	Hexagonal mapped

Table 2. Features of the finite element for interface definition.

Parameter	Contact	Target
Component	Polypropylene surface	Steel Surface
Contact type	Flexible	Rigid
Element type	CONTA174	TARGE170
Contact features	Penalty method in contact algorithm, penetration tolerance factor, Gaussian interaction for contact definition	

Table 3. Thermal properties used for thermal-micro scale stress analysis.

Material	Conductivity (W/m K)	CTE (1/K)	E modulus (Pa)	Poisson ratio
Steel cord	60.5	$12x10^{-6}$	$200x10^{9}$	0.3
Polypropylene	0.12	$185x10^{-6}$	$2x10^{9}$	0.4

Table 4. Thermal properties used for heat transfer analysis.

Material	Conductivity (W/m K)	Specific heat (KJ/kg K)	Density (kg/m^3)
Steel cord	60.5	0.49	7870
Polypropylene	0.12	2.9	910

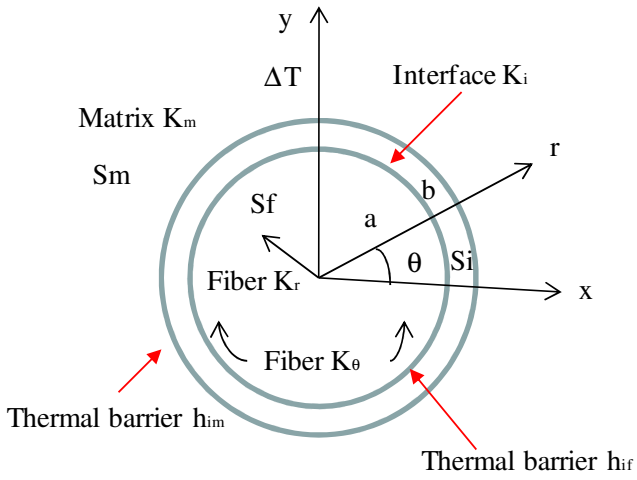

Fig. 1. Schematic representation of the cross-section of the cord surrounded by matrix.

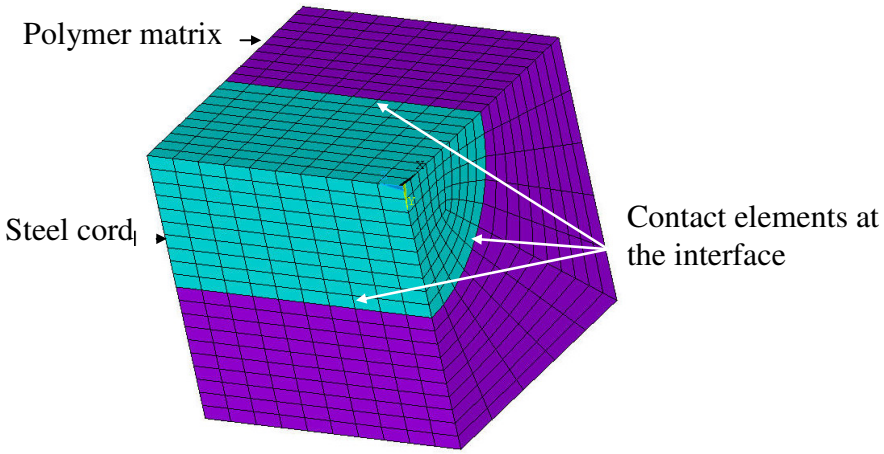

Fig. 2. Quad-symmetrical cord/matrix model used for the micro scale analysis.

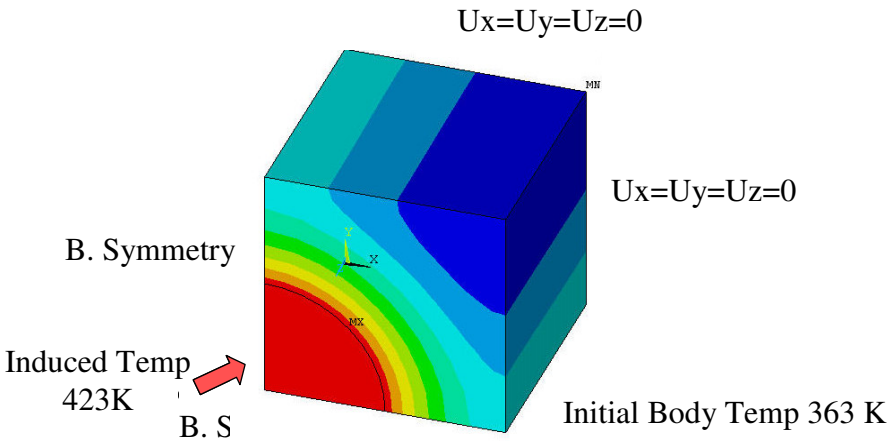

Fig. 3. Thermal and mechanical loads and constraints on the quad-symmetrical cord/matrix model.

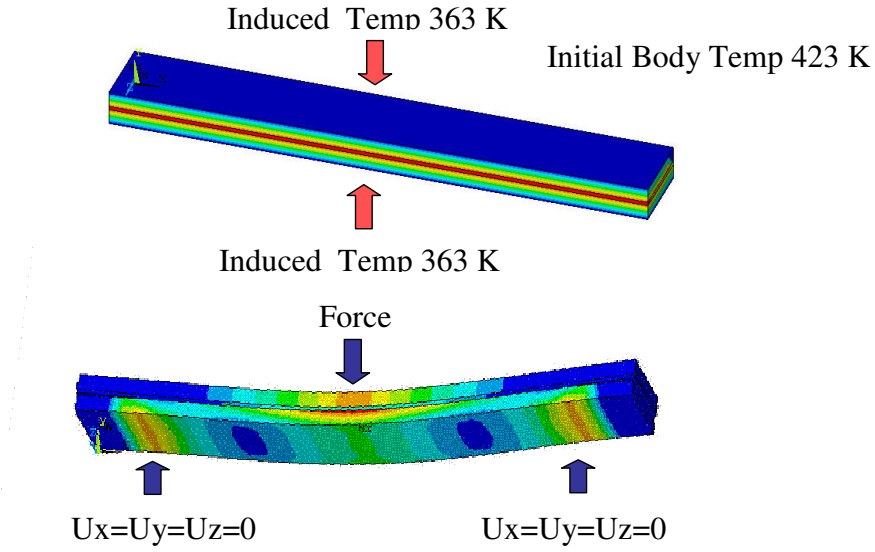

Fig. 4. Thermal and mechanical loads and constraints on the 3-point bend flexure model.

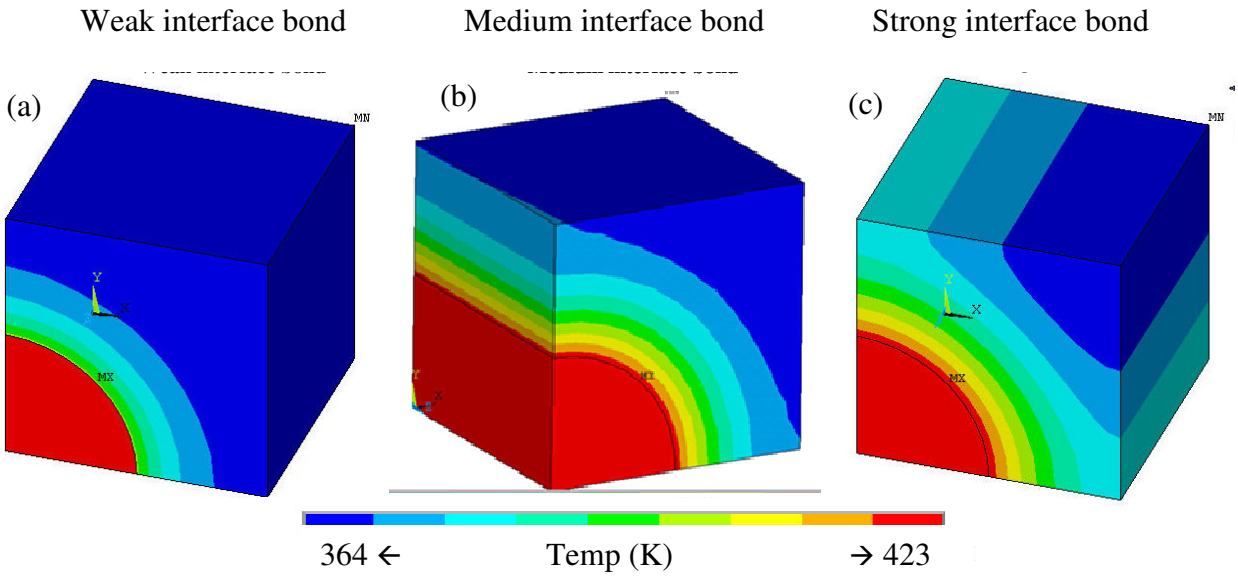

Fig. 5. Temperature profiles for steel cord embedded in PP matrix as a function of the type of interfacial bond. (a) Weak interface bond; (b) medium interface bond, and (c) strong interface bond.

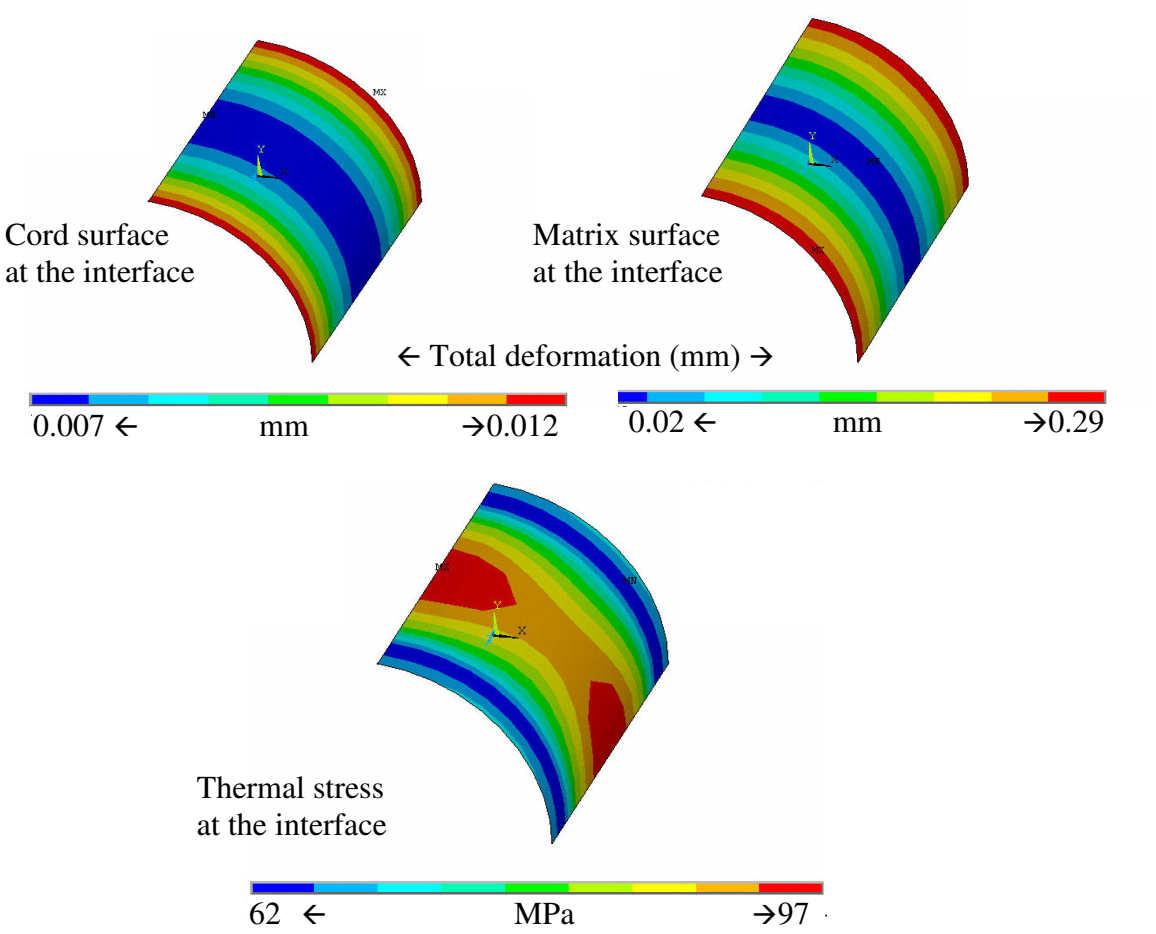

Fig. 6. Deformation and stress at the interface between steel cord and the PP matrix for a medium interface bond. (a) Deformation distribution at the cord surface, (b) deformation distribution at the matrix surface, and (c) thermal stresses at the interface.

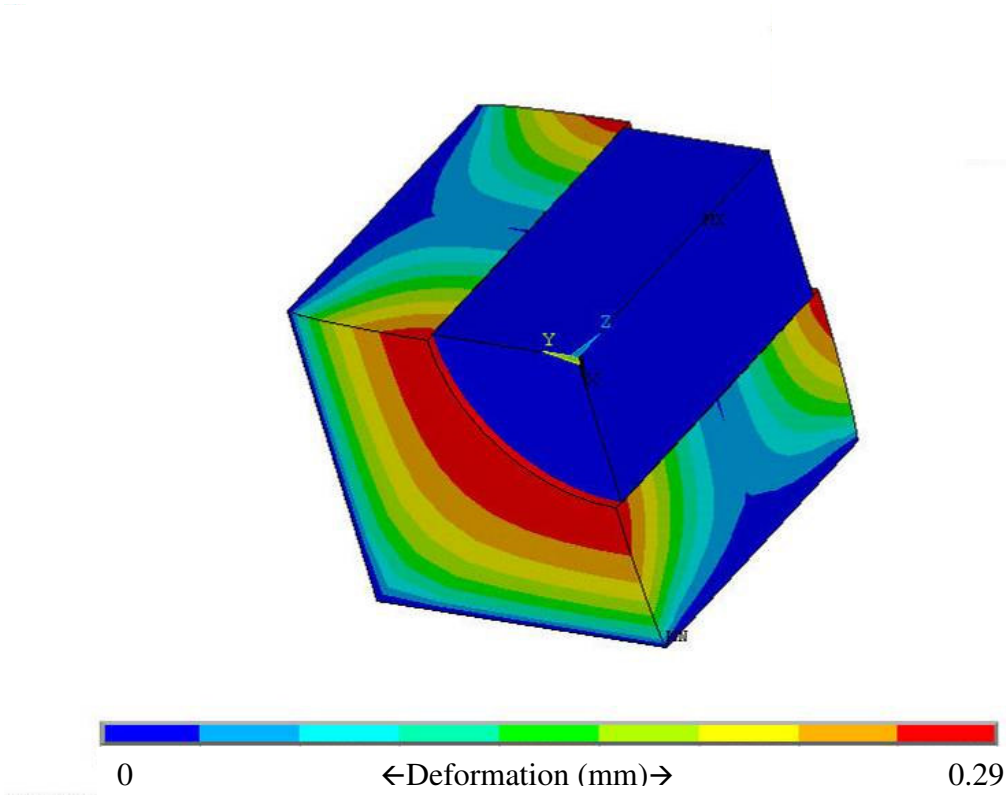

Fig. 7. Profile of matrix deformation due to thermal expansion for a steel cord embedded in PP matrix for a medium interface bond.

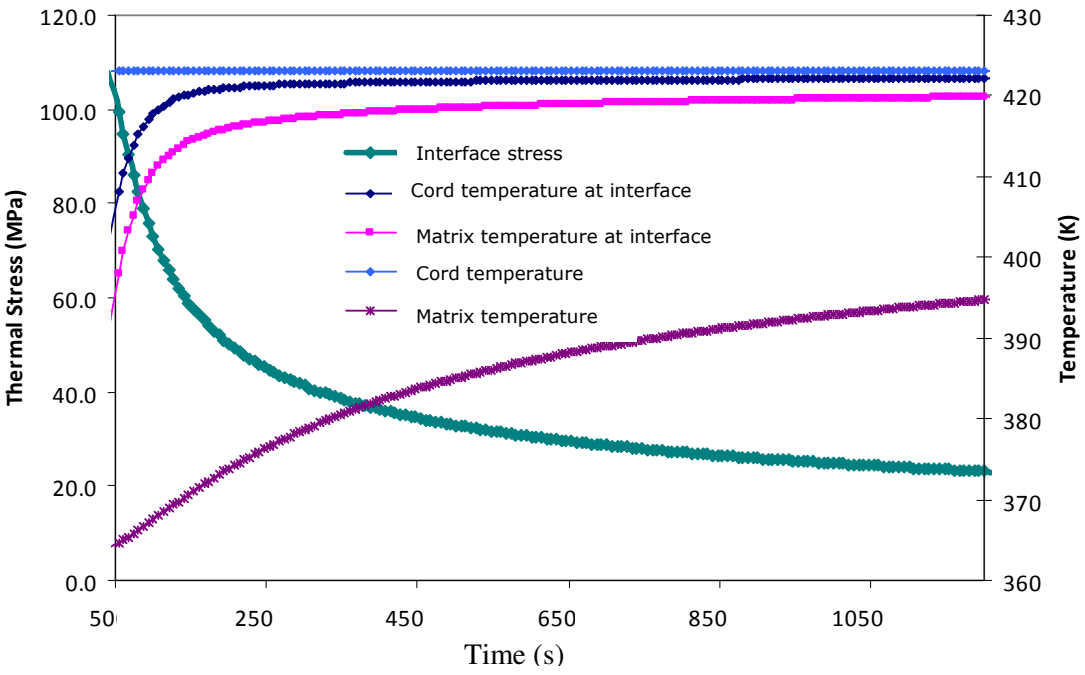

Fig 8. Thermal stresses and temperature as a function of time for a composite (steel cord/PP matrix) considering a strong bond interface.

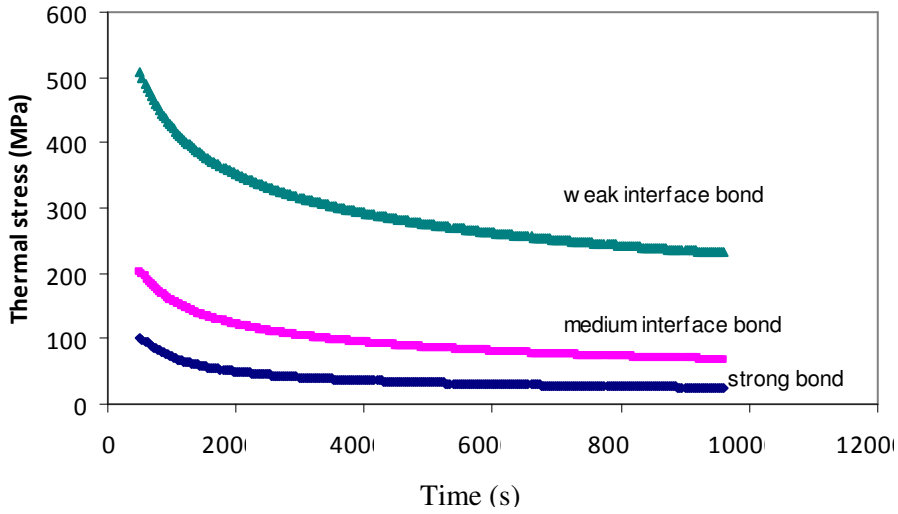

Fig. 9. Thermal stress profile as a function of the bond strength at the interface between steel cord and PP matrix.

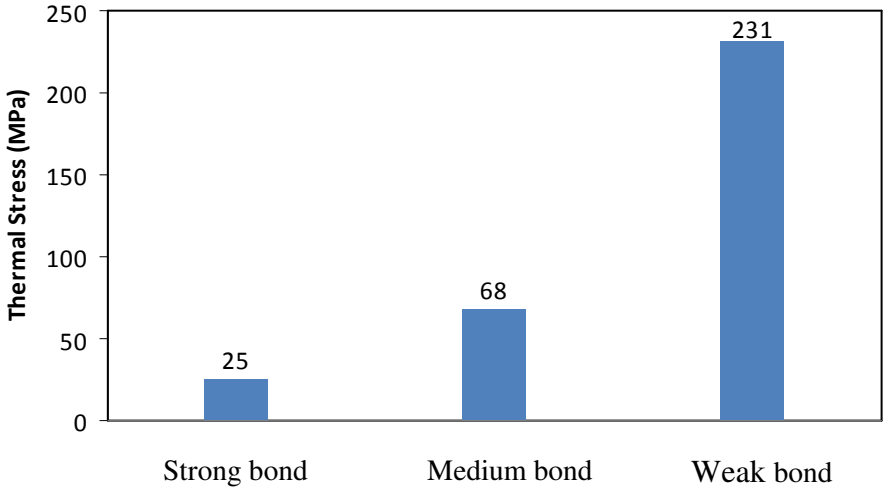

Fig. 10. Thermal stress at the interface as function of strong, medium and weak bond.

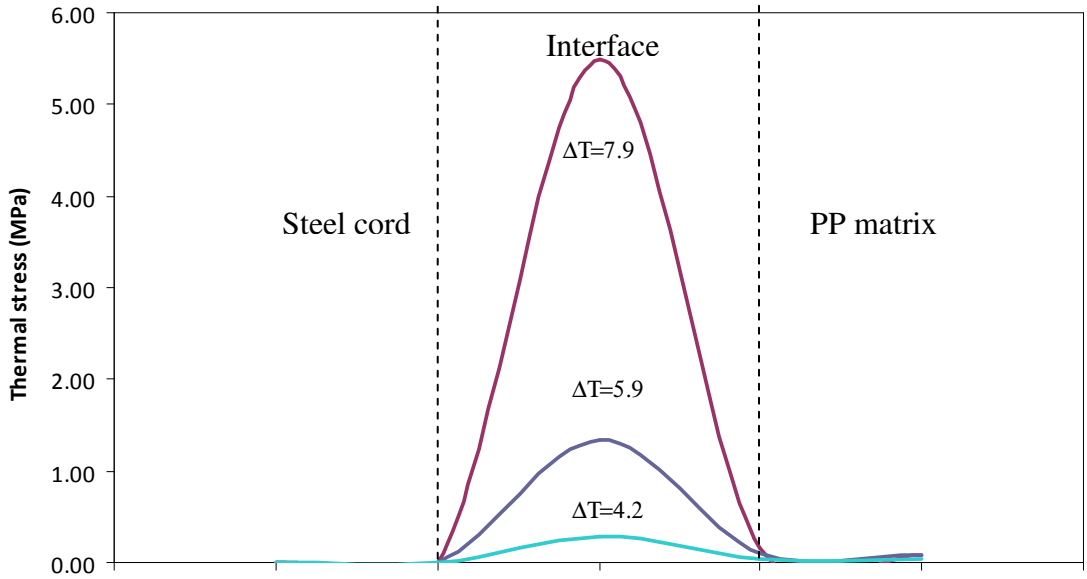

Fig 11. Thermal stresses for a perfect interface as a function of the temperature gradient of the matrix/cord interface.

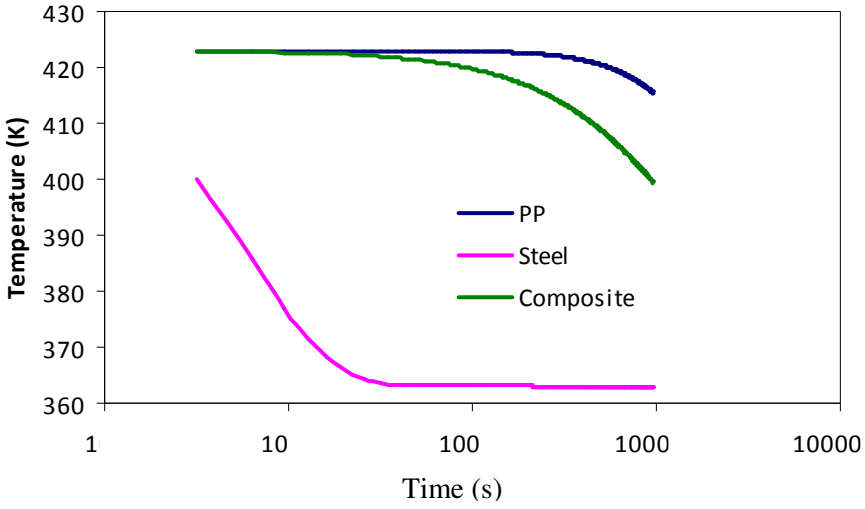

Fig 12. Thermal conductivity for steel, PP and metal-thermoplastic composite specimens.

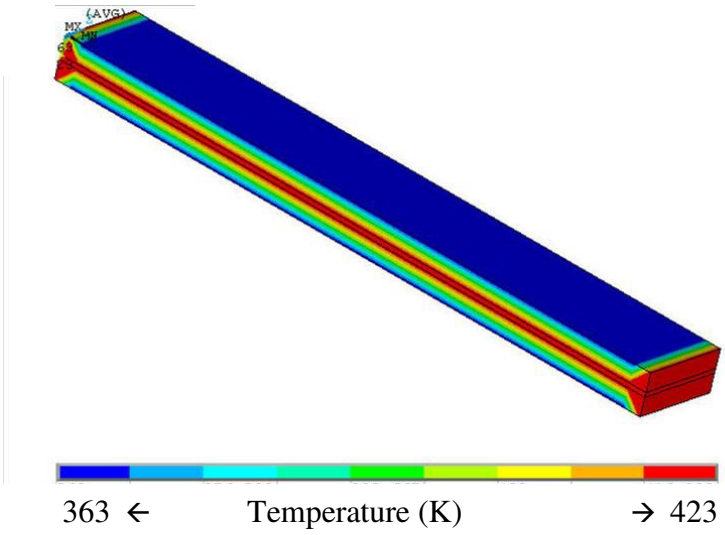

Fig. 13. Temperature profile of a PP-steel composite specimen.

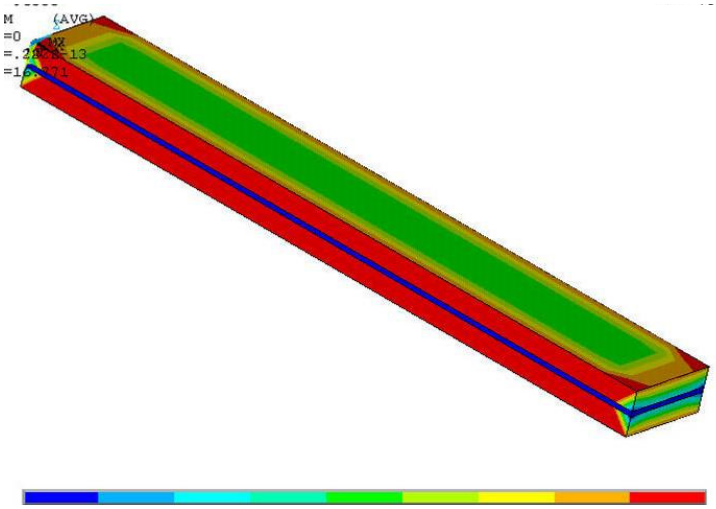

Fig 14. Heat transfer for the PP-steel macro scale model.

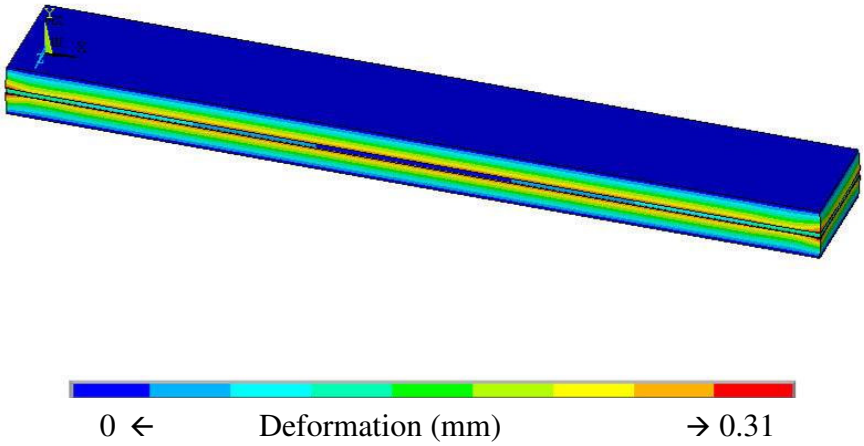

Fig 15. Total deformation after cooling down from 423 K to 365 K for a steel-thermoplastic composite.

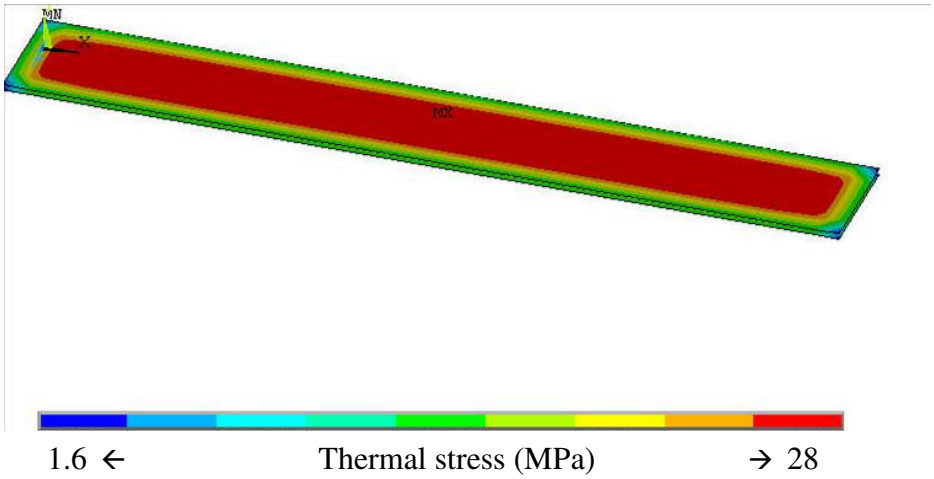

Fig 16. Thermal stresses at the interface after cooling down from 423 K to 365 K for a steel-thermoplastic composite.

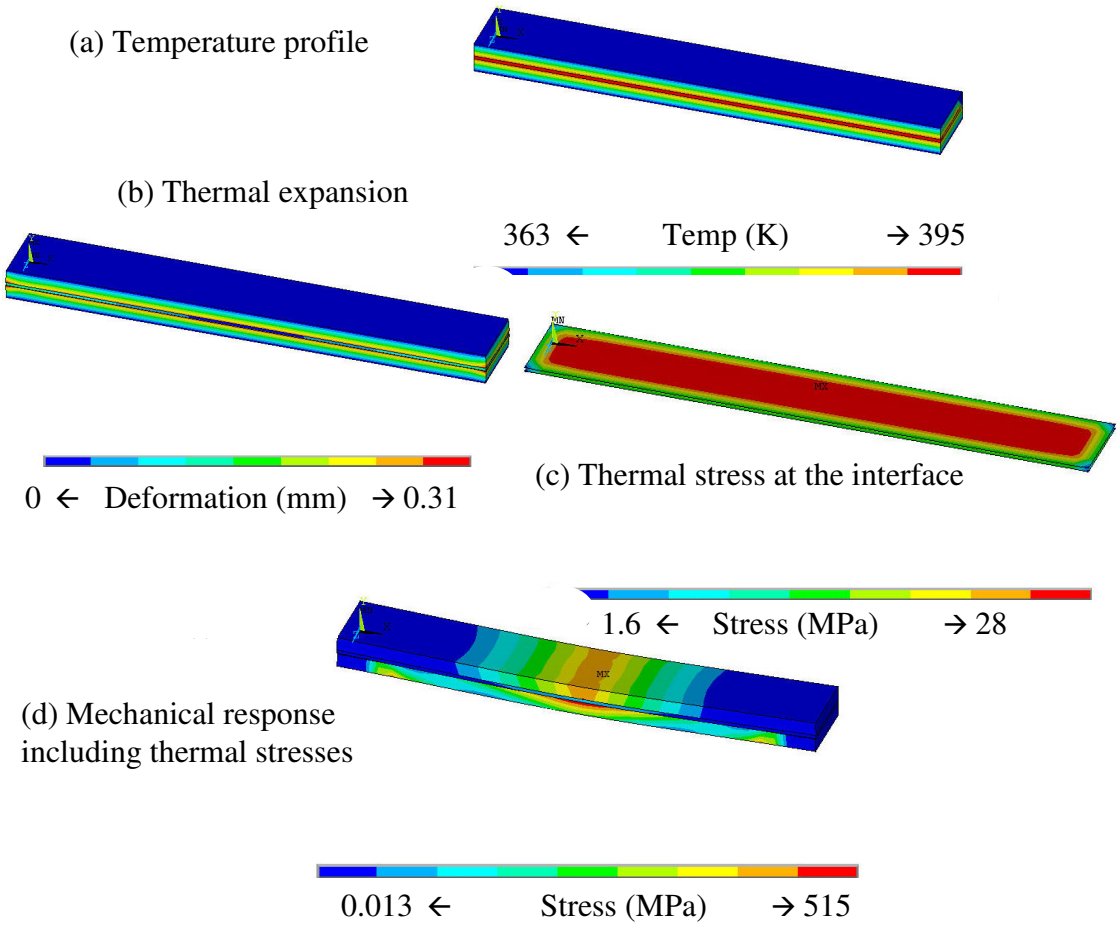

Fig 17. Coupled thermal/structural analysis for metal-thermoplastic composite: (a) First environment (thermal) to predict temperature distribution. (b) and (c) Second environment (structural) to release thermal stresses; and (d) Third environment (structural) to predict flexural strength of the composite.

(a)

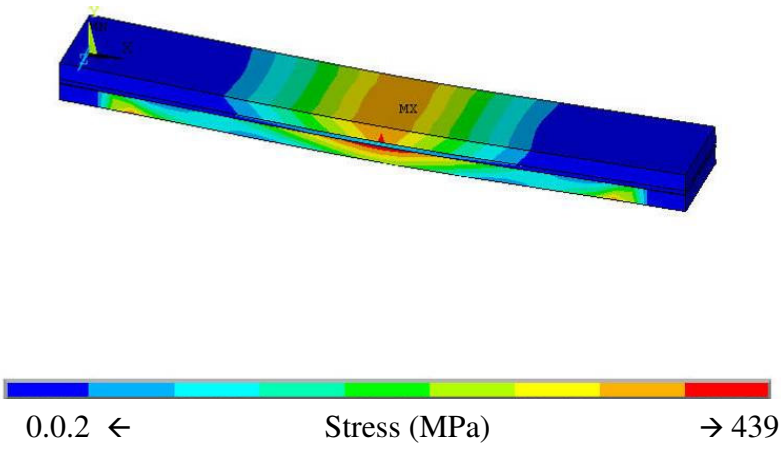

(b)

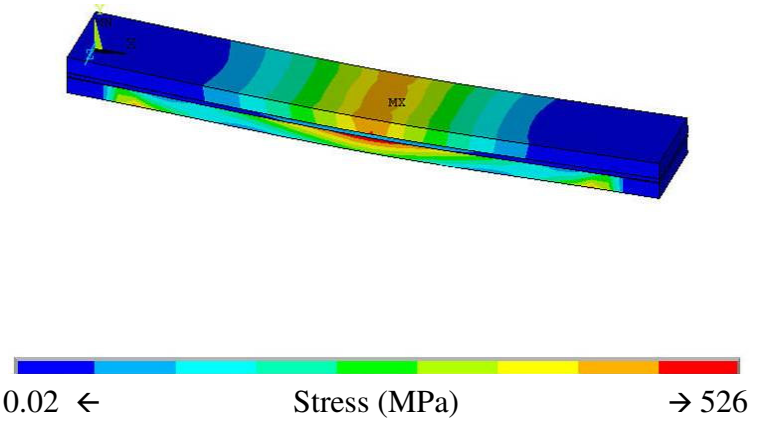

(c)

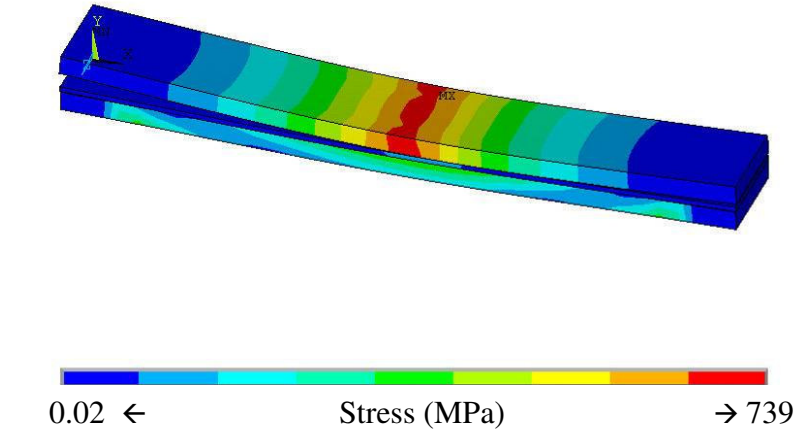

Fig 18. Coupled thermal/structural analysis for a metal-thermoplastic composite for a 3-point flexure loading case. (a) strong interface (b) medium interface, and (c) weak interface

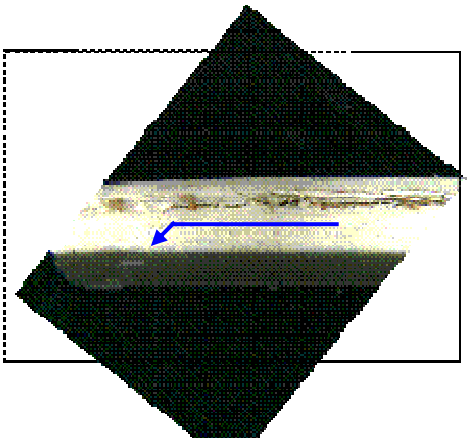

Fig 19. Crack propagation along the interface for steel reinforced PP matrix.

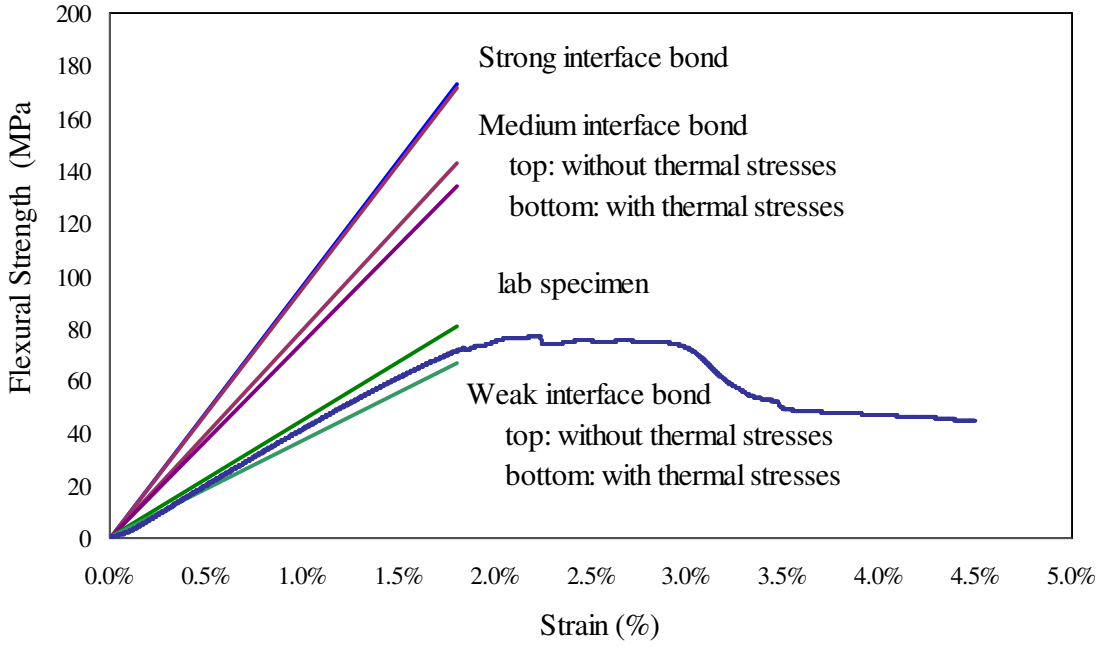

Fig 20. Stress-strain curves for three cases of the interface obtained by FEA and experimental flexural loading

OVERALL CONCLUSIONS

The interfacial strength between a steel cord and a thermoplastic polymer is significantly influenced by the friction coefficient, matrix stiffness and cohesive bond. The interfacial shear strength between steel cords and thermoplastic polymers is guided by several contributing factors of which approximately 83% was attributed to the friction coefficient, 3% to matrix stiffness, and only 0.5% due to the initial cohesive bond. The interaction between friction coefficient and matrix stiffness plays a significant role with 13% of contribution. No significant interaction between other parameters and the cohesive bond strength was observed.

The experimental studies indicated that PP on steel showed the lowest coefficient of friction, followed by PA6, hard TPU and soft TPU. Similar correlation was observed for the cohesive bond. Thus, an optimum value of interfacial shear strength was obtained for soft TPU with steel cords. The value of interfacial shear strength correlates directly to the friction coefficient; thus, the increase in value of dynamic friction coefficient from 0.3 to 0.5 increases the value of interfacial shear strength almost four times.

Finite element analysis (FEA) is an effective tool to simulate contact problems by the implementation of a frictional model. This approach is based on the simple case of Coulomb friction law to describe the mechanical bonding isolated from other interactions. The FEA captures the peak load for the pull-out process. Both experimental and numerical values are close enough with a discrepancy less than 10%. The debonding load

to pull-out the steel cord from PP is 140 N from experimental measurements versus 150 N for the FEA; for PA6, it is 270 N versus 310 N and for TPU 650 N versus 750 N.

FEM captures the load transfer through the thickness and width accurately; and, as expected, the areas close to the constraint witness higher stresses. The matrix which is the softer material undergoes higher deformation than the steel layer. The difference in stiffness between both components renders the interface weak and consequently leads to onset of failure. The failure load for the strong interface (or fully bonded) case is predicted to be approximately more than two times the experimental value (180 MPa from the FEM versus 74 MPa from the experiment).

The perfect interface case is an idealized case, since the friction coefficient is taken to be equal to 1. In the second case, a rough interface, i.e. where the possibility of sliding between contact surfaces is allowed, but opening of the interfaces is restricted; the friction coefficient (μ) is taken as 0.5. Here the failure load is closer to the experimental case (119 MPa from the model versus 74 MPa from the experiment). The third case considers both opening of surfaces and sliding between surfaces. Opening between elements is not desired because further load transfer cannot occur. In this case, the failure load is predicted at 96 MPa which is in closer agreement to the experiment.

The load obtained from the experiment is approximately lower by 20% than predicted by the FE model for the weak interface. Based on the model, it can be predicted that the flexural strength of the steel-PP specimen can be improved by approximately 40% by varying the interface friction coefficient between the steel and PP from a weak (μ=0.3) to rough (μ=0.5) interface. This suggests that by providing increased surface

roughness to the steel, the friction coefficient would increase resulting in a higher degree of interfacial bonding between the steel and the PP.

Functionalization of polymers has been analyzed in this work. PP is one of the most used polymers due to its low cost, good mechanical properties, easy processing and additionally, it can be modified with maleic anhydride to add polar functional groups and improve adhesion with steel. Thermoplastic polyurethane is also a good option to generate adhesion with metal surfaces due to the high content of polar groups that increases wettability of the polymer, even though the mechanical properties are lower. Adversely, epoxy with fullerenes failed in the purpose of increasing adhesion mainly due to the presence of surface voids during the curing process.

Silicon surface coating provides better adhesive properties between metal-to-polymer surfaces. Specifically, this technique appears to be an effective and efficient method to promote better adhesion between steel and PPMA. However, experiments show no correlation between surface energy and bond strength for this type of surface treatment; in fact for coated steel, wetting tension on the steel surface is not an indication of potentially better adhesion. It is possible that diffusivity is the mechanism of adhesion between coated steel and PPMA.

A correlation between contact angle in the type of polymer and bond strength was found to be directly proportional, which indicates that polar groups on the polymer surface dominate the adhesion with steel and can be predicted by the value of contact angle. Also, for the polymers in the study, the effect of wettability dominates the ability to adhere on steel.

FEA provides an efficient method to determine thermal stresses at the interface of a metal-thermoplastic composite and evaluate the interaction between the fiber and the matrix. Specifically, it analyzes the effect of the bond strength between fiber and matrix on the generation of thermal stresses and predicts the limit bond strength of the composite considering mechanical and thermal loads.

As the bond between matrix and fiber becomes weaker, the effect of thermal stresses becomes pronounced on the strength of the composite. Consequently, thermal stresses should be considered to determine the limited interfacial strength for a composite with non-perfect interface.

Numerical approaches of macro and micro scales of a metal-thermoplastic composite investigate the generation and effect of thermal stresses on the interfacial bond strength. The study was limited to elastic stress distribution. According to the FEM, thermal stresses arose as a result of non-uniform temperature distribution through the interface between matrix and reinforcement material. A weak interface worsens thermal conductivity between matrix and cord, favoring the generation of thermal stresses.

FEM has been correlated to experimental results of a 3-point-bend load test of a metal-thermoplastic composite. The results show that a weak bond strength between steel cords and PP matrix has a pronounced effect on the generation of thermal stresses during fabrication.

FEM predicts that the heat transfer in the longitudinal direction of the reinforcement is 3 times faster than that in the transverse direction, where the cord reinforcement acts as a heat dissipation barrier to the surrounding material. The composite is predicted to be a thermal isolating material.

LIST OF REFERENCES

1. Gao Shang-Lin, Kim Jang-Kyo. Cooling rate influences in carbon fiber/PEEK composites. Part1: Cristallinity and interface adhesion. *Composites Part A,* 31 (2000).

2. Kocak S, Pidavarti V. Three-dimensional micromechanical modeling of cord-rubber composites. *Mechanics of Composites Materials and Structures,* 7 (2000).

3. Ebbott T.G. An application of finite element-based fracture mechanics analysis to cord-rubber structures. *Tire Science and Technology,* 24 (1996).

4. Huang X, Birman V, Nanni A, and Tunis G. Properties and potential application of steel reinforced polymer (SRP) and steel reinforced ground (SRG) composites. *Composites Part B,* 36 (2005)

5. Lopez A, Galati N, Alkhrdaji T, Nanni A. Strengthening of a reinforced concrete bridge with externally bonded steel reinforced concrete bridge with externally bonded steel reinforced polymer. *Composites Part B,* 12 (2006).

6. Lucien Patrick M. The experimental behavior of steel fiber reinforced polymer retrofit measures. University of Pittsburg, (2006).

7. Casadei P, Nanni A, Alkhrdaji T, Thomas J. Performance of Double –T-prestresses concrete beams strengthened with steel reinforced polymer. ACI special publication, SP-230-44 (2005).

8. Csadei P, Nanni A. and Ibell T. Development and validation of steel reinforced polymer for strengthening of transportation infrastructures. University of Missouri-Rolla Center for infrastructure engineering studies, UTC R94, (2005).

9. Casadei P, Nanni A. Steel reinforced polymer: an innovative and promising material for strengthening the infrastructures. *Composites*, 21 (1995).

10. Sun T, Jih C.J. Quasi static modeling of delamination crack propagation in laminates subjected to low velocity impact. *Composites Science and Technology,* 54, (1995).

11. Srinisavan K. et al. Characterization of damage modes in impacted thermoset and thermoplastic composites. *Reinforced Plastics and Composites,* 11 (1992).

12. Cerny J, Morscher G. Adhesive bonding of titanium to carbon-carbon composites for heat rejection systems. NASA, Glenn Research Center, (2000).

13. Chawla K. Composites materials. Science and Engineering. Second Ed. New York, Springer, (2001).

14. Funasaka T, Ashihara T, Maekawa S, Ohno S. Adhesive ability and solvent solubility of polypropylene-butane co-polymers modified with maleic anhydride. *Adhesion and Adhesives,* 19 (1999).

15. Jang B. Advanced Polymer Composites: Principles and Applications. ASM international, Chap 3, (1994).

16. Kocak S, Pidavarti, V. Three-dimensional micromechanical modeling of cord-rubber composites. *Mechanics of Composite Materials and Structures,* 7 (2000).

17. Meo M, Achard F, Grassi M. Finite element modeling of bringing micro-mechanics in through-thickness reinforced composite laminates. *Composite Structures,* 71 (2005).

18. Zhang Xi, Liu Hong-Yuan, Mai Yui-Wing, Diao Xiao-Xue. On steady-state fiber pull-out I: The stress field. *Composites Science and Technology,* 59 (1999).

19. Liu Hong-Yuan, Zhang Xi, Mai Yiu-Wing, Diao Xiao-Xue. On steady-state pull-out II: Computer simulation. *Composites Science and Technology,* 59 (1999).

20. Hutchinson J, Jensen H. Models of fiber debonding and pullout in brittle composites with friction. *Mechanics of Materials,* 9 (1990).

21. Pidaparti R, May W. Prediction of cord-rubber composite properties using a micromechanical model. Recent advances in structural mechanics. ASME, (1994).

22. Pidaparti R. Analysis of cord-rubber composite laminates under combined tension and torsion loading. *Composites Part B,* 28B (1997).

23. Jang Kyo Kim, Yiu Wing Mai. Engineered Interfaces in Fiber Reinforced Composites. First Ed, New York, Elsevier Science, (1998).

24. Dhramarajan N. Datta S. Compatibilized polymer blends of isotactic polypropylene and styrene-maleic anhydride co-polymer. *Polymer,* 36 (1995).

25. Cai Chuanlun, Shi Qiang, Li Lili, Zhu Lianchao, Yin Jinghua. Grafting acrylic acid onto polypropylene by reactive extrusion with pre-irradiated PP as initiator. *Radiation Physics and Chemistry,* 22 (2008).

26. Zhang Z, Liu Y, Huang Y, Liu L, Bao J. The effect of carbon-fiber surface properties on the electron-beam curing of epoxy-resin composites. *Composites Science and Technology,* 31 (2002).

27. Ishida H and Koenig J.L. FTIR characterization of the reaction at the slane/matrix resin interphase of composite materials. *Colloid and Interface Science,* 12 (1986).

28. Kim Jang Kyo. Impact and delamination failure of woven fabric composites. *Composite Science and Technology,* 18 (2000).

29. Molitor P, Young T. Adhesives bonding of a titanium alloy to a glass fiber reinforced composite material. *International Journal of Adhesion & Adhesives,* 22 (2002).

30. Paproth A, Wolter K, Deltschew R. Adhesion of polymer/metal bonds for molded interconnect devices (MID). 28th Int. Spring Seminar on Electronics Technology, (2005).

31. Swapan K. Metal Filled Polymers: Properties and Applications. *Plastics Engineering,* 11 (1986).

32. Carotenuto G, La Peruta G, Nicolais L. Letter to the editor, *Sensors and Actuators: Part B,* 114 (2006).

33. Castello X, Estefen S. Limit strength and reeling effects of sandwich pipes with bonded layers. *International Journal of Mechanical Sciences*, 49 (2007).

34. Causa A.G, Borowczak M, Huang Y. Some observations on the testing methodology of cord-rubber composites: a review. *Progress in Rubber and Plastics Technology,* 4 (1997).

35. Ramani K, Moriarty B. Thermoplastic bonding to metals via injection molding for macro-composite manufacture. *Polymer Engineering and Science,* 38 (1998).

36. Suresh S, Needleman A. Symposium on Interfacial Phenomena in Composites: Processing, Characterization, and Mechanical Properties, RI, Newport, (1988).

37. Eiss N, Hanchi J. Stick–slip friction in dissimilar polymer pairs used in automobile interiors. *Tribology International*, 31 (1998).

38. Ghorieshi J, Sharma A, Lopresti M, Ghorieshi M. Temperature Measurement at the Polymer-Metal Contact: A Tribometer Design, Proceedings of the ASEE New England Section 2006 Annual Conference, (2006).

39. ANSYS Contact Technology Guide. ANSYS 10.0 version, (2005).

40. Solid surface energy data (SFE) for common polymers. Retrieved from http://www.surface-tension.de/,solid-surface-energy.htm, (2007).

41. Diversifie Enterprise, Solid surfaces energies. Retrieved from http://www.accudynetest.com/ surface_energy_materials.html. (2005).

42. Fiel, Chappell, Mckillip. Tire cord to rubber adhesion using amide structures. Ashland Chemical Company. R& D division, (1974).

43. Steward R, Goodshio V, Guild F. Investigation and demonstration of the durability of air plasma pre-treatment on polypropylene automotive bumpers. *Adhesion and Adhesives,* 25 (2005).

44. Jamshidi M, Afshar F, Mohammadi N, Pourmahdia S. Study on cord/rubber interface at elevated temperatures by H-pull test method. *Applied Surface Science,* 12 (2005).

45. Rosso P, Varadi K. FE macro/micro analysis of thermal residual stresses and failure behavior under transverse tensile load of VE/CF- fiber bundle composites. *Composites Science and Technology,* 66 (2006).

46. Ishida H, Kumar G. Molecular characterization of composites interfaces. *Polymer Science and Technology,* 31 (1985).

47. Mat Web. Material properties. Retrieved from http:// www.matweb.com. (2006).

48. Montgomery Douglas C. Design and Analysis of Experiments. 5th Edition, Ney York, Prentice Hall, (2001).